BROADLY TUNABLE ULTRASHORT PULSE GENERATION WITH MODE-LOCKED SEMICONDUCTOR LASERS

By

MICHAEL JOSEPH BRENNAN, B. Sc.

A Thesis
Submitted to the School of Graduate Studies
in Partial Fulfilment of the Requirements
for the Degree
Doctor of Philosophy

McMaster University

MODE-LOCKED ASYMMETRIC QUANTUM WELL SEMICONDUCTOR LASERS

DOCTOR OF PHILOSOPHY (2004) McMaster University

(Engineering Physics) Hamilton, Ontario

TITLE: Broadly Tunable Ultrashort Pulse Generation with Mode-Locked Semiconductor Lasers

AUTHOR: Michael Joseph Brennan, B. Sc. Physics (University of Windsor)

SUPERVISORS: Dr. H. K. Haugen and Dr. P. Mascher

NUMBER OF PAGES: xix, 143

Abstract

Wavelength tunable ultrashort pulses are generated with mode-locked InGaAs/GaAs semiconductor lasers mounted in an external cavity. A broad tuning range is achieved through the use of an asymmetric quantum well (AQW) structure in the active region of the devices. Furthermore, the incorporation of a bend in the waveguide of the devices results in a broadband, low modal reflectivity. This allows the lasers to be mode-locked in a compact, linear external cavity. Passive mode-locking of dual asymmetric quantum well devices have produced pulses 2 to 5 ps in duration, tunable from 954 nm to 1015 nm. Compression of the pulses using a modified grating pair compressor has yielded optical pulses as short as 510 fs. Similar devices based on a triple asymmetric quantum well active region are capable of producing pulses 2 to 11 ps in duration under passive mode-locking, tunable from 942 nm to 1017 nm. Preliminary work with long wavelength InGaAs/GaAs lasers has resulted in pulses 2 to 5 ps in duration with average output powers ranging from 750 μW to 1.8 mW. Pulse compression yields pulses as short as 570 fs.

The synchronization of a passively mode-locked semiconductor laser to a mode-locked Ti:Sapphire laser, using an all-optical synchronization method, is studied. The parameter space is explored in order to determine the operating conditions that yield optimal synchronization of the two lasers. Good qualitative agreement is obtained between a simple theoretical model of the synchronization process and the corresponding experimental measurements. It is also shown that the synchronization of the mode-locked semiconductor laser with a femtosecond laser provides an additional means by which the mode-locked semiconductor laser can be characterized.

Acknowledgments

Many people have contributed to this work and deserve thanks. Initial work on the project was performed by Steve Wallace as part of his Ph. D. research prior to my arrival at McMaster University. I owe special thanks Steve for the knowledge and skills he passed on to me during my first two years at Mac. As Steve was preparing to leave the group, Joel Milgram joined the group. I owe thanks to Joel for many hours of technical discussion, assistance and entertainment. Upon completion of his Masters degree, Joel was promptly replaced by Andrew Budz. Andrew deserves thanks for his work as a summer student, as well as for the many hours of technical discussions, assistance and entertainment as a graduate student. I also owe thanks to all other members (and former members) of the research group including Andrzej Borowiec, Henry Tiedje, Travis Crawford, Paul Dube, Ben Doyle and Andrew Logan. They have contributed through many hours of technical discussions, assistance and/or entertainment. In addition, I would like to thank all of the above named people for their friendship during my stay at McMaster.

I would like to thank my supervisors, Harold Haugen and Peter Mascher, for taking me on as a graduate student. In particular, Harold's commitment and dedication to the project has allowed it to progress to the point where it is at today. I could not have asked for better supervisors. I would also like to thank Brad Robinson for the growth of all of the laser structures used in this work. The various agencies, which have funded this research through scholarships or grants, deserve thanks, including the Natural Science and Engineering Research Council (NSERC), the Ontario Graduate Scholarships in Science and Technology (OGSST) programme, the Canadian Institute for Photonics Innovations and McMaster University.

I would like to thank my parents, my brother and my sister, for their love and support through out my academic years. They have encouraged me to achieve and strive for success.

And last, but not least, I would like to thank my wife Kim and my son Ethan. Kim has steadily supported me and encouraged me through out my graduate studies. She has always been there for me and is the love of my life. Our son Ethan came into our lives two years ago. Since his arrival, my outlook on life has changed. This thesis may have been completed much sooner if I wasn't in such a rush to get home each day to see him.

Table of Contents

List of Figures

List of Tables

Chapter 1 Introduction

1.1 Outline

This section provides a brief outline of the content covered within this thesis. The first chapter (this chapter), provides the motivation behind this work, as well as a brief review of the literature relevant to mode-locking, and wavelength tunable mode-locked semiconductor diode laser sources.

Theory relevant to mode-locking of semiconductor diode lasers is discussed in Chapter 2. Short pulse generation using the gain switching and Q-switching techniques are briefly covered. The methods of mode-locking and external cavity mode-locking with semiconductor diode lasers are discussed.

Chapter 3 outlines the considerations involved in designing a semiconductor laser for the generation of broadly tunable ultrashort pulses. The use of an asymmetric quantum well active region to achieve a broad gain bandwidth is discussed. Each of the laser structures used throughout this work is described in detail. The final portion of the chapter is devoted to a discussion on how to achieve a low facet modal reflectivity for external cavity operation. Particular emphasis is placed upon the use of anti-reflection coatings and on a novel bent-waveguide device design.

The experimental results achieved by mode-locking the semiconductor lasers are presented in Chapter 4. The initial discussion is centred on preliminary results obtained by mode-locking conventional two-contact, symmetric quantum well, semiconductor lasers in an external cavity. Next, the results obtained with the dual and triple asymmetric quantum well devices are presented. To the best of the author's knowledge, these results represent the largest tuning range ever achieved with a passive (and hybrid) mode-locked semiconductor laser. Mode-locking results obtained with the long wavelength InGaAs/GaAs lasers follow. These results represent the first demonstration of mode-locking with an electrically pumped, long wavelength edge emitting InGaAs/GaAs laser. The chapter concludes with a discussion of the effects of modifying the repetition rate of the mode-locked laser, as well as a brief presentation of the results obtained via monolithic mode-locking with select devices.

In Chapter 5, the synchronization of the external cavity mode-locked semiconductor laser with a mode-locked Ti:Sapphire laser is discussed. Synchronization of the lasers is interesting from many perspectives, including the possibility of using the system as an additional diagnostic tool for pulse characterization. The method of synchronization as well as a description of the results obtained are outlined. A simple model describing the synchronization mechanism is presented in the last section of the chapter. The experiments used to test the validity of the model agree qualitatively with the simulated results.

The last chapter summarizes the key results presented in this thesis and outlines future work. Some of the results presented in this thesis can also be found in the reference list provided in Appendix A.

1.2 Motivation

The motivation behind this work is the development of a compact, tunable, ultrafast semiconductor laser source. A semiconductor laser source satisfying the above requirements would be attractive for a number of applications. In particular, such a system would be a desirable replacement for solid-state crystal lasers and gas lasers in applications requiring modest pulse durations and energies. A semiconductor laser source has advantages in that it can be made more compact, is more reliable and can be made cheaper than other laser sources.

One application for which the lasers under development would be suitable for is that of two-photon fluorescence spectroscopy (TPFS). Two-photon fluorescence spectroscopy is the process by which light from a laser source is used to excite a fluorescent dye via two-photon absorption. Since the interaction is nonlinear, a short-pulse laser is typically utilized. The advantages of TPFS over its single photon counterpart are numerous [1-5]. TPFS offers improved spatial resolution, reduced photo-bleaching and easy discrimination between pump wavelength and signal wavelength. Ultrafast solid-state lasers are currently the systems of choice for TPFS due to their short pulse duration (100 fs or less) and large average power (hundreds of milliwatts). The main negative aspect with regards to using these systems for TPFS is their substantial cost. The development of a suitable *all-semiconductor* source for low power TPFS applications would be advantageous for reasons already stated. Making the source wavelength tunable would provide access to a wide variety of dyes, as well as additional means by which to discriminate against experimental artifacts in the signal data. A number of dyes have broad absorption bands that fall within the range of 450 nm to 550 nm [6], requiring lasers that operate within the 900 nm to 1100 nm wavelength range for TPFS.

Another application of relevance is the use of mode-locked long wavelength ($\lambda \sim$ 1075-1085 nm) InGaAs/GaAs lasers as a seed source for short pulse amplification in ytterbium-doped fibre amplifiers. While direct short pulse generation from an ytterbium-doped fibre laser has been demonstrated [78-10], complex cavities are required to manage the dispersion in the system. Using a mode-locked semiconductor laser as a seed source would allow for a simple cavity design and the ability to achieve high, and variable, repetition rates.

With these applications in mind, broadly tunable InGaAs/GaAs lasers operating between 940 nm and 1020 nm, as well as longer wavelength InGaAs/GaAs lasers operating in the vicinity of 1070 nm were fabricated. A large tuning range is achieved by using an asymmetric quantum well (AQW) structure. An AQW structure contains quantum wells of different thickness or of different composition. The different quantum wells have different transition energies, resulting in a broadened gain bandwidth for the laser structure. Ultrashort pulses are obtained by passive and hybrid mode-locking of the aforementioned devices in external cavities.

Since some of the applications discussed require higher average output powers than that typically achieved with a mode-locked semiconductor laser, amplification of the ultrashort pulses is required. The focus of this work is on the development of tunable, mode-locked semiconductor lasers, while the development of suitable semiconductor optical amplifiers has been left to other members of the research group.

1.3 Requirements for two-photon fluorescence spectroscopy

Since one of the target applications for the development of tunable, short-pulse semiconductor laser sources is TPFS, it is useful to estimate the operating parameters required for such an application. Consider that in a TPFS measurement, as an approximation, the number of photons n absorbed per fluorophore per second is proportional to [4],

$$n \propto \frac{p^2}{\tau f} \tag{1.1}$$

where p is the average power of the laser, τ is the pulse duration and f is the repetition rate of the laser. This equation can be used, along with data from the literature, to obtain an estimate on the output power, pulse duration and repetition rate required by a mode-locked semiconductor laser to achieve adequate signal levels in a TPFS experiment.

In work by Lago *et al.* [1], two-photon-induced fluorescence from biological markers was generated with a dye laser emitting pulses 2 ps in duration at a repetition rate of 7.6 MHz, for powers ranging from 5 to 70 mW (after fibre coupling). Now consider a semiconductor laser source with properties identical to that of the dye laser used by Lago, with the exception of pulse duration, average power and repetition rate. The ratio of n_{diode}/n_{dye} is plotted in Figure 1-1 for different pulse durations as a function of average power. The data in the figure was generated using a repetition rate of 500 MHz for the semiconductor laser, and an average power of 10 mW for the dye laser.

In examining Figure 1-1, it can be seen that for typical mode-locked semiconductor laser pulses having a duration of a few picoseconds, an average power between 80 and 100 mW is required in order to generate the same amount of signal as that generated by the dye laser. For sub-picosecond pulses, an average power between 40 and 60 mW is required.

The ratio of the number of photons absorbed per fluorophore per second for the semiconductor laser to that of a Ti:Sapphire laser is plotted in Figure 1-2 and Figure 1-3. A repetition rate of 80 MHz and a pulse duration of 100 fs is assumed for the Ti:Sapphire laser in both figures, while average powers of 10 mW and 100 mW are used in Figure 1-2 and Figure 1-3, respectively.

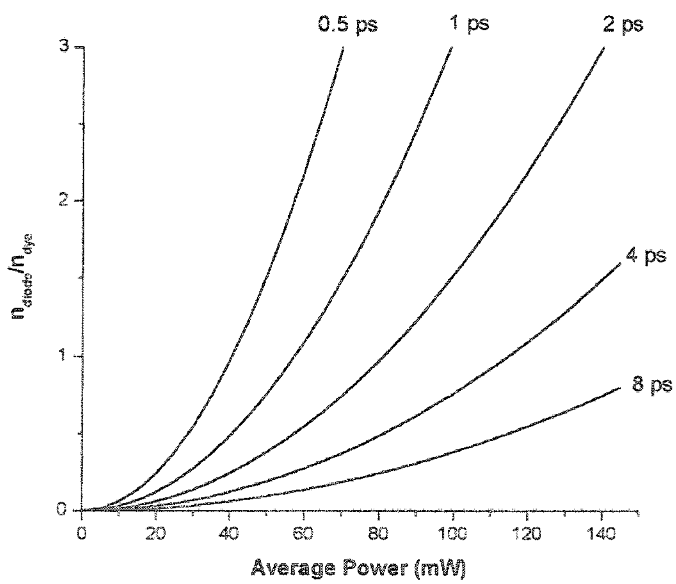

Figure 1-1: n_{diode}/n_{dye} as a function of average power for the semiconductor laser source. A repetition rate of 500 MHz is assumed for the semiconductor laser and an average power of 10 mW is used for the dye laser. The ratio is shown for semiconductor laser pulse durations ranging from 0.5 ps to 8 ps.

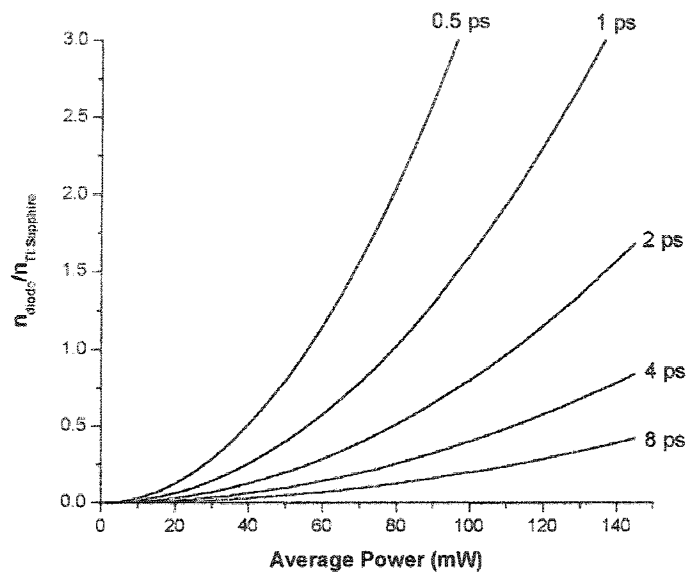

Figure 1-2: $n_{diode}/n_{Ti:sapphire}$ as a function of average power for the semiconductor laser source. A repetition rate of 500 MHz is assumed for the semiconductor laser and an average power of 10 mW is used for the Ti:Sapphire laser. The ratio is shown for semiconductor laser pulse durations ranging from 0.5 ps to 8 ps.

For the case of low average power pulses from the Ti:Sapphire laser, average powers ranging from 60 mW to 100+ mW are required in order to generate the same amount of signal, depending upon the duration of the semiconductor laser pulse. For the 100 mW average power pulses from the Ti:Sapphire laser, signal collection times between 10 and 100 times longer are required to generate the same signal with the semiconductor laser. This may or may not be a suitable trade-off depending upon the nature of the experiment. Also, depending upon the output of the semiconductor laser, a smaller spot size may be achievable with the Ti:Sapphire laser, which will increase the demands on the output power of the semiconductor laser source.

Mode-locked semiconductor lasers typically have average output powers in the 1-2 mW range and pulses a few picoseconds in duration. It is estimated that following post-amplification with a semiconductor optical amplifier (SOA) and post-compression with an external compressor, a mode-locked semiconductor laser is capable of generating signal levels sufficiently large to be useful for low power TPFS applications.

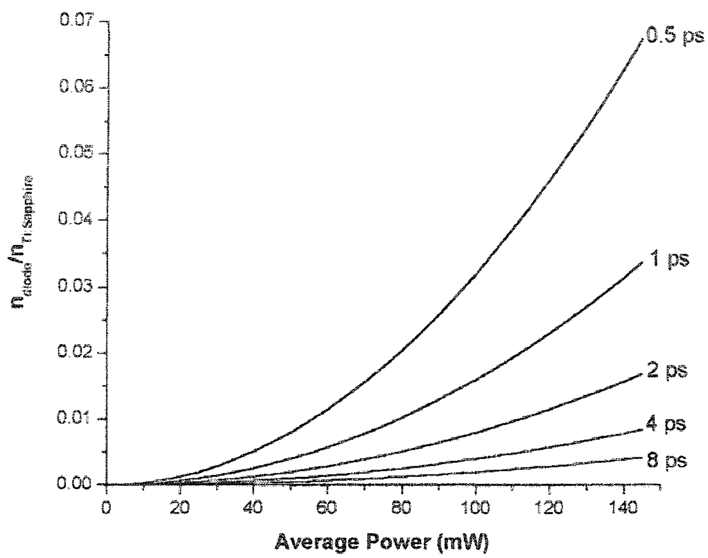

Figure 1-3: $n_{diode}/n_{Ti:Sapphire}$ as a function of average power for the semiconductor laser source. A repetition rate of 500 MHz is assumed for the semiconductor laser and an average power of 100 mW is used for the Ti:Sapphire laser. The ratio is shown for semiconductor laser pulse durations ranging from 0.5 ps to 8 ps.

1.4 Mode-locked semiconductor laser literature review

The study of mode-locked semiconductor lasers has been a field of intense research for several decades. This section discusses experimental work related to active, passive and hybrid mode-locking of semiconductor lasers, as well as the development of wavelength tunable, mode-locked semiconductor lasers.

1.4.1 Active mode-locking

Early reports on active mode-locking with semiconductor lasers were made by Ho *et al.* [11] and by Glasser [12] using GaAs based lasers mounted in external cavities. The lasers were uncoated and the external cavities consisted of a spherical mirror positioned a few centimetres from the laser facet. Pulses with duration between 18 and 20 ps were reported at repetition rates in the vicinity of 2 to 3 GHz. Holbrook *et al.* generated the first bandwidth-limited pulses from an actively mode-locked laser [13]. An angled stripe laser mounted in a 40 cm long external cavity produced pulses 16 ps in duration with a time-bandwidth product of 0.36. Early work by van der Ziel [14] studied in detail the dependence of the pulse width on external parameters. Pulses 5.3 ps in duration were observed under optimized conditions.

Applications of anti-reflection (AR) coatings to the laser facets allowed Olsson and Tang [15] to generate 6 to 8 ps pulses at a repetition rate of 250 MHz from an actively mode-locked, linear external cavity laser. Both facets were AR coated, requiring the need for feedback at both ends of the device. Mounting the device in a ring cavity configuration produced pulses 16 ps in duration.

Sub-picosecond pulse generation from actively mode-locked semiconductor lasers have been reported by a number of groups. Corzine *et al.* generated 580 fs pulses at a wavelength of 1.3 μm from an actively mode-locked GaInAsP semiconductor laser [16]. The AR-coated laser was mounted in an external cavity consisting of a mirror and a Fabry-Perot etalon, operating at a repetition rate of 1.6 GHz. Takada *et al.* have reported on the generation of 550 fs pulses from an actively mode-locked monolithic multiple-quantum-well laser (MQW) integrated with a MQW electro-absorption modulator [17]. The laser operated at a wavelength of 1.59 μm and an optical fibre was used to compress the pulses.

Delfyett *et al.* achieved high power pulses by amplifying the output of an actively mode-locked laser with a semiconductor optical amplifier (SOA) [18]. Pulses 15 ps in duration with peak power over 3 W operating at a wavelength of approximately 830 nm were obtained. The pulses were generated by active mode-locking an angled stripe semiconductor laser mounted in an external cavity with an identical device used as an SOA.

While the above discussion is far from complete, it does provide a summary of the range of outputs achievable with an actively mode-locked semiconductor laser. The interested reader is referred to references [19] and [20] for a more complete account of experimental active mode-locking research.

1.4.2 Passive and hybrid mode-locking

The first study of passively mode-locked semiconductor lasers was performed with devices containing uncontrollable saturable absorbers [21]. The devices were aged to the point where the lasing threshold increased by more than 10%. The dark line defects incurred during the aging process act as a saturable absorber. Such devices mounted in an external cavity generated pulses 5 ps in duration at a repetition rate of 850 MHz. Yokoyama *et al.* [22] employed a similar technique to generate saturable absorption and were able to generate pulses 580 fs in duration at a repetition rate of 6.6 GHz. The main drawback of this technique is that the obtained results are not reproducible and that the devices are prone to failure.

One method to introduce a controllable saturable absorbing region into the laser device is by proton bombardment or ion implantation. Proton bombardment was used by van der Ziel *et al.* to introduce regions of saturable absorption within their lasers [23-25]. Mounted in external cavities, these devices were capable of generating bursts of 650 fs pulses at a repetition rate of 1 GHz.

Another method by which a saturable absorber can be introduced into the device is by fabricating multiple-contact diode lasers. Operating one of the sections below its transparency point can induce saturable absorption. Harder *et al.* were the first to demonstrate this technique and reported on the generation of 35 ps pulses from a two-section laser mounted in a linear external cavity [26]. This method of incorporating a saturable absorber monolithically is often used in the fabrication of lasers for monolithic mode-locking [27, 28]. A review of short pulse generation using multi-segment mode-locked semiconductor lasers can be found in reference [29].

Silberberg *et al.* achieved passive mode-locking of semiconductor diode lasers by using a GaAs/GaAlAs multiple-quantum-well sample attached to a mirror to act as a saturable absorber in an external resonator [30]. A steady train of 1.6 ps pulses at repetition rates varying from 500 to 1000 MHz was achievable.

Early studies of hybrid mode-locking used cavity arrangements containing two optically coupled diode lasers [31, 32]. One of the diodes acted as a saturable absorber by operating it below its transparency point while the gain of the other diode was modulated at the cavity round trip time. Bandwidth-limited optical pulses ranging from 25 - 30 ps were successfully generated with this configuration. The average output power from the oscillator was 1 mW.

Delfyett *et al.* have presented a number of results with regards to high-power ultrashort pulse generation using mode-locked semiconductor lasers [18, 33, 34]. The lasers were mounted in an external cavity consisting of a MQW saturable absorbing mirror and amplified with a semiconductor optical amplifier. Pulses 5 ps in duration were generated under hybrid mode-locking conditions and compressed to 460 fs using a double pass grating pair compressor. Cubic phase compensation with a deformable mirror further compressed the pulses to 290 fs. Using a modified MQW saturable absorbing mirror in which the width of the quantum wells was varied, pulses 200 fs in duration were achieved post-compression.

A number of other groups have successfully generated sub-picosecond pulses under passive and hybrid mode-locking [35-39]. A more complete account regarding passive and hybrid mode-locking experiments can be found in reference [40].

1.4.3 Wavelength tunable, mode-locked semiconductor lasers

As previously discussed, broadband wavelength tuning of pulses from mode-locked semiconductor lasers is desirable from an application standpoint. Most of the work reported to date on wavelength tunable mode-locked semiconductor lasers has involved tuning of actively mode-locked devices. Since the number of publications is limited, details of each will be provided below.

Early work was performed by Chen *et al.*, in which they actively mode-locked Brewster-angled diodes to generate 9.5 ps pulses tunable over 15 nm centred around 840 nm [41]. Tuning was achieved by using an external cavity that incorporated either a Fabry-Perot etalon or a diffraction grating. Similar results were obtained with both cavity configurations. Epler *et al.* achieved a slightly larger tuning range by actively mode-locking a coupled-stripe quantum-well laser in an external cavity [42]. Pulses 50 ps in duration with a peak power of 265 mW were tunable from 729 nm to 747 nm at a repetition rate of 1.27 GHz. At wavelengths similar to Chen *et al.*, Serenyi *et al.* reported a tuning range from 802 to 835 nm with an actively mode-locked GaAs/AlGaAs laser [43]. The laser diode was mounted in an external cavity with a narrowband interference filter being used for wavelength tuning. Pulses ranging from 26 ps at 835 nm down to 12 ps at 802 nm were generated by the system.

A number of groups have reported results on wavelength tuning of actively mode-locked semiconductor lasers at wavelengths of interest to the telecommunications community. Hou *et al.* achieved a 60 nm tuning range (1260 nm to 1320 nm) with an actively mode-locked semiconductor laser mounted in a grating external cavity [44]. Pulses 10 to 15 ps in duration with an average output power of 100 μW were generated at a 1 GHz repetition rate. Compression with a 7.5 km length of fibre resulted in pulses 4 to 6 ps in duration. Wiesenfeld *et al.* obtained similar results using an identical system with the exception that a modified grating-pair compressor was used in place of a fibre [45]. Bird *et al.* used a packaged actively mode-locked semiconductor laser to achieve a 40 nm tuning range centred either at 1.3 μm or 1.55 μm [46]. Transform-limited pulses 20 ps in duration were generated with a grating external cavity at repetition rates variable from 2 to 8 GHz. The largest tuning range in this wavelength regime was achieved by Hofmann *et al.* [47]. Pulses 30 ps in duration with an average output power of 100 μW were generated at a repetition rate of 300 MHz, tunable over 155 nm (1448 to 1563 nm). A final report was made by Akimoto *et al.* in which a tuning range of 52 nm (1535 to 1587) was presented [48]. Wavelength tuning was achieved by rotating a disk-shaped interference filter situated inside the external cavity. Pulses ranging from 18 to 39 ps in duration were generated at a repetition rate of 8 GHz.

There have only been, to the best of the author's knowledge, two reports on wavelength tuning of passively mode-locked semiconductor lasers. The first is by Wu *et al.* in which they achieved a small tuning range of 8.8 nm by temperature tuning a monolithic passively mode-locked semiconductor laser [49]. Nearly transform limited pulses ranging from 1.2 to 3 ps were generated in the wavelength range of 1528.4 nm to 1537.2 nm. The second publication is by Schrans *et al.* in which they report a wavelength tuning range of 26 nm with a passively mode-locked two section multiple quantum well laser [50]. A linear cavity with feedback from a diffraction grating was used to generate pulses 4.5 ps in duration tunable from 829 to 855 nm. Post-compression with a grating-pair compressor yielded pulses as short as 260 fs [51].

The only report on mode-locking with an asymmetric quantum well active region was made by Lee and Lin [52]. An angled-stripe laser was actively mode-locked in a ring cavity to produce pulses 13-21 ps in duration tunable from 795 to 857 nm. The laser operated at a repetition rate of 295.3 MHz with an average output power of 2 mW. The reported results are summarized in Table 1-1.

Table 1-1: Summary of the tuning ranges and pulse durations reported for tunable, mode-locked semiconductor lasers. Note: In the column titled *Typical Pulse Duration*, brackets around an entry indicate that a pulse compressor was used to achieve that particular pulse duration.

ML Method	Tuning Range (nm)	Centre Wavelength (nm)	Repetition Rate	Typical Pulse Duration (ps)	Reference
Active	15	840	326 MHz	9.5	41
Active	18	738	1.27 GHz	50	42
Active	33	819	N/A	12 to 26	43
Active	60	1290	1 GHz	10 to 15 (4 to 6)	44, 45
Active	40	1300 or 1550	2 to 8 GHz	20	46
Passive	8.8	1532.8	80 GHz	1.2 to 3	49
Passive	26	842	561 MHz	4.5 (0.26)	50, 51
Active	115	1505	300 MHz	30	47
Active	52	1561	8 GHz	18 to 39	48
Active	62	826	295 MHz	13 to 21	52

1.5 Project contributors

All of the results presented in this thesis have been obtained directly through the author's efforts. This includes the laser structure design and device fabrication (photolithography, etching, SiO_2 deposition, metallizing, cleaving, AR coatings), writing data acquisition and control software, setting up and performing the experiments, and analyzing the data. However, a number of individuals have also contributed time and effort towards the project. The contributions of each of these individuals are outlined below.

- The laser structures were grown by Brad Robinson using the molecular beam epitaxy (MBE) facility at McMaster University. Brad Robinson has also contributed to a number of technical discussions regarding laser structure design.
- Steve Wallace has made numerous early contributions towards this project while completing his Ph.D. thesis. Initial work on anti-reflection facet coatings, laser design and laser processing were done in collaboration with Steve Wallace. In particular, initial mode-locking results presented in section 4.2.1 were obtained in collaboration with Steve.
- Joel Milgram has collaborated on anti-reflection facet coating deposition, laser design and laser processing while completing research for his Masters' degree. Joel was also involved in the early design stage of the bent-waveguide devices and made the first detailed spatial profile measurements of the lasers. Joel has also contributed to the advancement of short pulse generation in general through his daily involvement in the project. Joel's work focussed on research and development of semiconductor optical amplifiers (SOAs).
- Andrew Budz has collaborated on anti-reflection facet coating deposition, laser design and laser processing while completing research for his Masters', and now more recently, his Ph.D. degree. Andrew has also contributed towards the advancement of short pulse generation in general through his daily involvement in the project. Andrew's work focuses on the research and development of SOAs.
- Some of the early experimental work on the synchronization of the mode-locked semiconductor laser to the mode-locked Ti:Sapphire laser was performed in collaboration with Henry Tiedje. The results presented in section 5.3.2 were obtained in direct collaboration with Henry. Henry has also contributed to numerous technical discussions on synchronization related issues.

Chapter 2 Mode locking – Basic Theory

2.1 *Introduction*

This chapter will provide the background necessary to follow the discussions in the chapters to follow. The first section will discuss the different methods of short pulse generation with an emphasis on mode-locking. Active, passive and hybrid mode-locking are discussed as well as the requirements for mode-locking a semiconductor laser in an external cavity.

2.2 *Short Pulse Generation – Gain Switching and Q-Switching*

The three methods commonly used to generate short optical pulses with semiconductor diode lasers are gain-switching, Q-switching and mode-locking. Each of the methods has advantages and disadvantages, and each method imposes particular requirements upon the semiconductor laser. This first section summarizes the concepts of gain switching and Q-switching.

2.2.1 Gain-Switching

Gain switching is perhaps the simplest method with which to generate short optical pulses with a semiconductor laser. With this method, the gain of the device is rapidly switched on and off to generate short bursts of radiation from the laser. The main advantage of gain-switching is that the process does not require an external cavity, nor does it require any sophisticated fabrication technology. The main disadvantages of this pulse generation technique come in terms of minimum achievable pulse duration and noise. The durations of gain switched pulses are typically much longer than that which can be achieved with other methods. While pulse durations ranging from 310 fs to a few picoseconds have been reported [53-56], all of these results were obtained following compression of the pulses. Typically, the durations of pulses emitted directly from gain-switched lasers lie in the 15 ps range and above [57-64]. The noise on the output of a gain switched laser is large because each optical pulse builds up from spontaneous emission. This leads to intensity fluctuations, noise on the optical spectrum, and pulse-to-pulse timing jitter.

2.2.2 Q-Switching

Q-switching is a pulse generation technique that is widely used in solid state laser systems [65]. However, this technique is not as widely used in semiconductor laser systems as compared with gain switching and mode-locking. The basic principle behind the method is the modulation of the loss within the laser cavity. When the cavity is in a low Q state (high loss), a large population of carriers builds up. When the Q of the cavity is suddenly switched to a low loss state, stimulated emission builds up and rapidly depletes the high carrier density. This results in the generation of a short optical pulse. The loss of the cavity is then increased again, and the process is repeated.

Q-switching of a semiconductor laser can be accomplished monolithically or by coupling the device to an external cavity. External cavity Q-switching methods are straightforward and are similar to those methods used for other types of laser systems. An overview of these methods can be found in references [65, 66]. Q-switching of a monolithic device typically involves some ingenuity in the device design stage. A typical device used for monolithic Q-switching is composed of two or three sections, with one of the sections acting as a modulator. Modulation of the loss is achieved by shifting the band edge of the modulator section via the Franz-Keldysh effect [67] or by the quantum confined Stark effect [68]. Other experimental schemes have also been developed, and the interested reader is referred to references [69, 70].

One of the main advantages of using a Q-switched laser is the capability for high power generation [71]. Picosecond pulses with energies in excess of 100 pJ have been generated. The main disadvantage of Q-switching lies in the device fabrication, the minimum achievable pulse duration and the amount of noise on the pulses. Also, the relatively short spontaneous emission lifetime of a semiconductor laser places additional constraints on the output as compared with a Q-switched solid-state laser system. As discussed previously, special consideration is required for designing a device for monolithic Q-switching. Q-switched semiconductor laser pulses typically measure in the tens of picoseconds [66-71]. Similar to gain switched lasers, each generated pulse builds up from spontaneous emission, resulting in significant amplitude, spectral and timing jitter noise on the pulse.

2.3 *Mode-locking*

Mode-locking is a short pulse generation method which typically generates optical pulses much shorter than that produced by the gain-switching and Q-switching techniques. It is the method upon which the work presented in this thesis has been based, and as such, it will be covered in more detail.

The concept of mode-locking can be easily explained by considering the output of a multimode Fabry-Perot laser in the frequency domain. Given a resonator of length L, the output of the laser consists of series of longitudinal modes separated by $\delta\omega$, with $\delta\omega$ given by,

$$\delta\omega = \frac{\pi c}{n_g L} \tag{1.2}$$

where n_g is the group refractive index and c is the speed of light. The output of the laser consists of the sum of the frequency components that correspond to each of these longitudinal modes and is given by,

$$E(t) = \sum_m A_m e^{i(\omega_0 t + m\delta\omega t + \varphi_m)} + c.c. \tag{1.3}$$

where A_m is the amplitude of the m^{th} mode and φ_m is the phase of the m^{th} mode. In continuous-wave operation of the laser, the relative phases between the longitudinal modes are random. The interesting case to consider is when the modes are forced to maintain a fixed amplitude and phase relationship. That is,

$$\begin{aligned} \varphi_m - \varphi_{m-1} &= \delta\varphi \\ A_m &= A_0 \end{aligned} \tag{1.4}$$

Applying equation (1.3), it can be shown that the resultant electric field is a periodic function of time given by

$$E(t) = A_0 \frac{\sin\left[(M+1)\delta\omega t_1 / 2\right]}{\sin(\delta\omega t_1 / 2)} e^{i\omega_0 t} + c.c. \tag{1.5}$$

where M is the number of locked Fabry-Perot modes and $t_1 = t + \delta\varphi/\delta\omega$. The envelope of $E^2(t)$ for $M = 15$ is shown in Figure 2-1.

As demonstrated by the figure, the output of a mode-locked laser consists of a train of optical pulses with duration (FWHM) inversely proportional to the spectral width ($M\delta\omega$) and a repetition rate equal to the round trip cavity time (T),

$$T = \frac{2\pi}{\delta\omega} \tag{1.6}$$

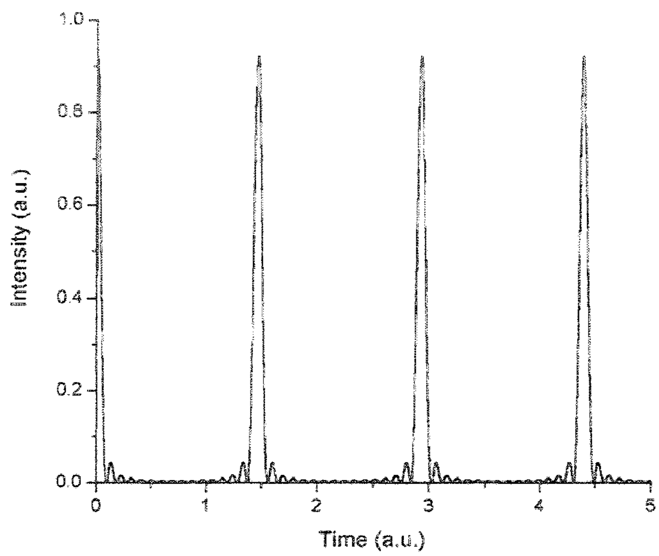

Figure 2-1: Simulation of the output of a mode-locked laser with 15 (*M=15*) completely locked modes.

2.3.1 Methods of Mode-locking Semiconductor Lasers

The commonly used techniques to achieve mode-locking are active, passive and hybrid techniques. The term active mode-locking is used to describe mode-locking achieved by applying an external RF signal to the semiconductor laser for gain/loss modulation. By modulating the laser at the Fabry-Perot mode spacing frequency, sidebands are produced on each Fabry-Perot mode. These sidebands overlap adjacent Fabry-Perot modes, and as a result, the phases are locked by the external modulation. While this seems simple in principle, the small dimensions of a semiconductor laser require very large modulation frequencies for active mode-locking. For a typical semiconductor laser measuring 500 μm in length, the required modulation frequency is approximately 86 GHz. For smaller devices, the required modulation frequency is well into the hundreds of GHz. Modulating a semiconductor laser at such high frequencies is technically challenging. Special considerations have to be made during the design process to reduce the capacitance and resistance of the device. The device also requires proper packaging to minimize RF coupling losses. From a financial standpoint, the equipment necessary for high-frequency modulation is quite costly. An alternative method is to couple the device to an external cavity, effectively reducing the Fabry-Perot mode spacing. While this method substantially reduces the required modulation frequency for active mode-locking, it does impose additional restrictions on the device. External cavity mode-locking is discussed in detail in section 2.3.2.

A semiconductor laser is passively mode-locked if it is mode-locked in the absence of an external modulation source. The necessary element to achieve passive mode-locking is a suitable saturable absorber inside the resonator. A saturable absorber is deemed suitable if the following conditions are met [29, 72, 73]

- the saturation energy of the absorber is less that the saturation energy of the gain medium
- the recovery time of the absorber is faster than that of the gain medium
- the unsaturated gain of the gain medium is greater than the unsaturated loss of the absorber

These three conditions can be interpreted as follows. The first implies that the loss must saturate faster than the gain. Meeting the second condition prevents the build up of amplified spontaneous emission between the pulses and ensures that gain is experienced only within the vicinity of the peak of the pulse. The third condition is necessary in order to allow laser oscillation to build up on start-up. A discussion on suitable saturable absorbers for mode-locking semiconductor lasers follows in section 2.3.3.

The third method employed to mode-lock a semiconductor laser is hybrid mode-locking. The technique is simply a combination of active and passive mode-locking elements, and as such, details have already been provided.

2.3.2 External Cavity Mode-locking

External cavity mode-locking of a semiconductor laser offers a number of advantages over monolithic mode-locking. Some of these advantages are

1. smaller modulation frequencies for active mode-locking
2. the ability to modify the repetition rate
3. broad wavelength tuning

Some of the more commonly used external cavity configurations are shown in Figure 2-2. Wavelength tuning is typically achieved by placing a diffraction grating in the cavity or by using a Fabry-Perot etalon. Translating the feedback element in the cavity varies the repetition rate. In the case of a fibre external cavity, the length of the fibre is fixed, and as such, the repetition rate of the mode-locked laser is not easily modified. Also, since feedback with an external fibre cavity is achieved by using a highly reflective coating on one end of the fibre or by using a fibre with a distributed Bragg reflector (DBR), the operation wavelength of the laser is not easily tuned. A ring cavity configuration is typically used for angled-stripe laser diodes or lasers with anti-reflection coatings applied to both facets. In this case, the ring cavity provides the feedback necessary at both ends of the device.

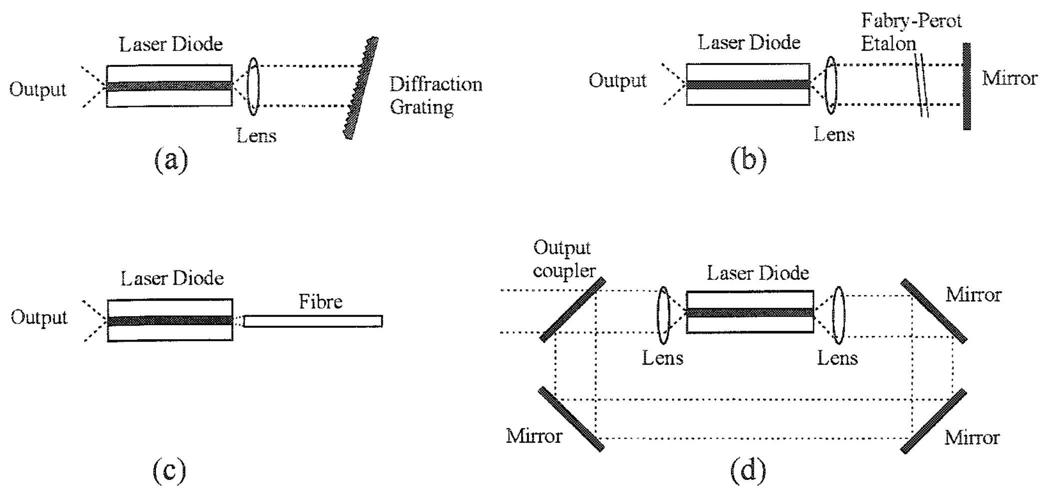

Figure 2-2: Commonly used external cavity configurations of mode-locked semiconductor lasers. a) Linear external cavity with a diffraction grating used for feedback. b) Linear external cavity with a mirror used for feedback and a Fabry-Perot etalon used for wavelength selection. c) External fibre cavity. d) Ring cavity configuration.

While external cavity mode-locking offers numerous advantages over monolithic mode-locking, there are several difficulties which need to be overcome. The first and foremost of these is suppression of the Fabry-Perot modes of the device. In order to suppress the Fabry-Perot modes of the laser chip, the modal reflectivity of the facet coupled to the external cavity must be sufficiently low. Due to the high gain of semiconductor lasers, a modal reflectivity below 10^{-4} is required [74]. If the reflectivity is much higher, the available bandwidth for mode-locking will be limited, and secondary pulses may form. In the case of active mode-locking, simulations have shown that secondary pulses may form even for a facet reflectivity on the order of 10^{-5} [74]. Since one typically wishes to obtain the shortest pulse possible from a given mode-locked source, limiting the available bandwidth is detrimental. There are two main reasons why the formation of secondary pulses is undesirable. The first reason is that it limits the temporal resolution of the system were it to be used in a diagnostic capacity. Secondly, the presence of secondary pulses reduces the amount of gain available for the primary pulse. The most popular methods to reduce the modal reflectivity of a laser facet are through the application of anti-reflection coatings, or by using an angled stripe laser. This particular subject is discussed in further detail in Chapter 3.

2.3.3 Saturable absorbers

The three types of saturable absorbers that are commonly used for passive and hybrid mode-locking of edge emitting semiconductor lasers are saturable absorbers fabricated by ion implantation, saturable absorbers based on multi-section devices and semiconductor saturable absorber mirrors. Associated with each of these saturable absorber types are a number of advantages and disadvantages, both of which are discussed below.

A saturable absorber can be formed in a semiconductor laser by implanting ions into one end of the device. The defects introduced into the semiconductor crystal significantly reduce the carrier lifetime in the semiconductor from the nanosecond time scale down to the picosecond time scale [75]. This technique also allows a saturable absorber to be introduced into devices that have already been fabricated. The main drawbacks of this method are that the saturable absorption is not controllable (once it has been introduced) and that there is risk of incurring damage to the device facet during the implantation process.

The second type of absorber is based on the fabrication of a multi-section device. A section of the device will act as a saturable absorber by operating it below its transparency point. This has the advantage of being able to incorporate a saturable absorber into the device monolithically. As such, this type of absorber can be used to achieve monolithic passive mode-locking of a semiconductor laser. The recovery time of this type of saturable absorber can be as fast as 15 ps [29]. The disadvantage of using this technique is that additional optical losses are introduced into the laser cavity as well as the fact that there are now two or more sections that need to be biased. Also, fabrication requires a specially designed photolithography mask.

The third type of saturable absorbers used is a saturable absorber multiple-quantum-well mirror. For this type of absorber, a multiple-quantum well (MQW) structure is grown and mounted on a mirror, or the structure is grown on a distributed Bragg reflector (DBR). The absorber is then used as a feedback element in an external cavity. The absorber recovery time of this structure is typically measured in nanoseconds. In order for this structure to be a suitable saturable absorber, the absorber must recover faster than the gain. There are several ways by which the absorber recovery time can be decreased. Focussing the laser beam tightly on the absorber causes the absorber recovery time to be dominated by diffusion of carriers out of the excited region. This method has produced recovery times on the order of 400 ps in GaAs/GaAlAs MQW material [30]. An alternative approach is to use proton bombardment of the MQW structure to enhance the carrier recombination rate. This technique has produced recovery times as short as 150 ps in GaAs/GaAlAs MQW material [76]. A third method has been demonstrated in which an InGaAs/GaAs MQW structure has been grown at low-temperature in order to produce a saturable absorber with a 69 ps carrier lifetime [77]. One advantage of the MQW structure is that the room temperature exciton resonances can be used for saturable absorption. These resonances saturate at an optical intensity up to ten times lower than the intensity required to saturate band-to-band transitions [76]. It has also been shown that the nonlinear absorption of the exciton resonance has a fast sub-picosecond relaxation time that can aid in the pulse shaping process of a mode-locked laser [78]. The main disadvantage of this method is that growth of the structures is non-trivial. For example, the multiple-quantum-well saturable absorber mirror used by Silberberg *et al.* consisted of 47 periods of GaAs/InGaAs layers grown on a GaAs substrate [30]. Relying on the exciton resonance for saturable absorption presents a second disadvantage. That is, the laser must operate at the wavelength corresponding to the resonance, which severely restricts the amount of wavelength tuning that can be accomplished with such a system.

2.3.4 Limits on the achievable pulse duration

Based solely on the gain bandwidth of a semiconductor laser, pulse durations on the order of 50 fs should be achievable by mode-locking. If dispersion effects of the device are taken into account, the achievable pulse duration lies in the 100 to 200 fs regime [79]. However, as the results discussed in section 1.4 indicate, these pulse durations are much shorter than that which is typically achieved experimentally. A number of mechanisms interact in determining the pulse duration of a mode-locked semiconductor laser, including [80]:

1. Self-phase modulation – The term self-phase modulation is used to describe the phenomena where the index of refraction of the material is changed by the passage of the optical pulse.
2. Responses of the gain and absorber for passive mode-locking – The gain and absorber have finite bandwidths that limit the achievable pulse duration. Also, changes in the gain due to gain saturation result in changes to the index of refraction described by the Kramers-Kronig relations.
3. Spontaneous emission noise – Spontaneous emission noise results in small, random fluctuations in the gain. This leads to small, random fluctuations in the index of refraction.

4. Bandwidth-limiting factors in the laser cavity – Elements such as diffraction gratings or Fabry-Perot etalons placed inside the laser cavity will limit the bandwidth of the optical pulse.
5. Dispersion – The dispersion of the laser chip, and other elements in the cavity such as lenses will affect the pulse.

The interaction of these various mechanisms results in the generation of pulses from mode-locked semiconductor lasers with durations much larger than that determined by the gain bandwidth alone.

In actively mode-locked semiconductor lasers, dynamic detuning contributes to the limit on the achievable pulse duration [81]. The phenomenon of dynamic detuning originates from the saturation of the gain in a semiconductor laser. As the pulse propagates through the laser, the leading edge of the pulse saturates the gain, causing a reduction in the amount of gain available for the trailing edge of the pulse. In a *steady-state* situation, all points on the pulse waveform should experience the same amount of gain in one round trip around the laser cavity. In order for this to occur, the peak of the pulse detunes from the peak in the gain waveform (recall that the gain is modulated in an actively mode-locked laser) to a position forward in time. As the pulse continues to shift forward in time, the slope of the applied waveform seen by the pulse becomes steeper until is exactly balances the reduction in gain due to gain saturation seen by the trailing edge of the pulse. Since this dynamic detuning mechanism has only one stable solution, it defines the pulse shape, peak power and pulse width for a given set of operating conditions and hence sets a limit on the achievable pulse width. Simulations by Morton et. al. [81] have shown that dynamic detuning sets the limit on the achievable pulse duration (~500 fs for the particular set of operating conditions used) despite neglecting dispersion and using an infinite gain bandwidth in their calculations.

2.3.5 Chirp of mode-locked semiconductor lasers

The generation of ultrashort pulses with semiconductor lasers typically produces picosecond pulses with time-bandwidth products far in excess of the theoretical minimum (see section 1.4.1). The excess bandwidth of the pulse is the result of a chirp imposed on the pulse by some of the mechanisms discussed in the previous section. Sub-picosecond pulses are often attained by compensation of the chirp on the pulse. Knowledge of the chirp is essential in order to perform any type of chirp compensation. It has been observed experimentally that actively mode-locked lasers produce red-chirped pulses while passively mode-locked lasers tend to produce blue-chirped pulses [82]. In a red-chirped (or down-chirped) pulse, the carrier frequency becomes smaller as one progresses from the leading edge of the pulse to the trailing edge of the pulse. In a blue-chirped pulse (or up-chirped) pulse, the carrier frequency becomes larger as one progresses from the leading edge of the pulse to the trailing edge of the pulse. The model developed by Schell *et al.* [82, 83] indicates that this observed tendency in chirp is a result of different magnitudes of the linewidth enhancement factor in the gain and absorber sections of passively mode-locked semiconductor laser. The linewidth enhancement factor (typically denoted as α) is a measure of the coupling between the gain and the refractive index [84, 85], and is defined as

$$\alpha = -\frac{2\pi}{\lambda}\frac{dn/dN}{dg/dN} \qquad (1.7)$$

where dn/dN is a measure of the change in refractive index for a change in free carrier concentration, dg/dN is the differential gain, and λ is the wavelength.

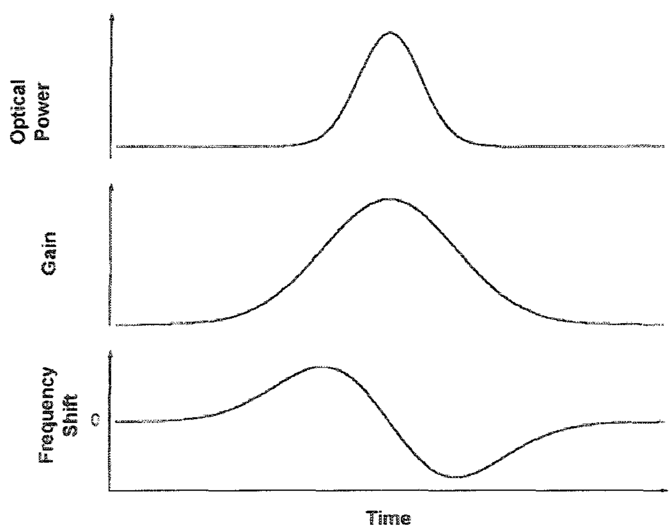

Figure 2-3: Chirp on a mode-locked laser pulse. The figure is based on figure 1b from reference [82]

If $\alpha > 0$, a decrease in gain leads to a corresponding increase in the refractive index. For a mode-locked semiconductor laser, the temporal net gain for one round trip through the laser must have negative curvature with respect to time to ensure that peak of the pulse experiences more gain than the leading and trailing edges. For $\alpha > 0$, it follows that the curvature of the refractive index with respect to time is positive for a single section laser, where α is constant in the laser cavity. Since the shift in optical frequency is proportional to the derivative of the refractive index with respect to time, this results in a chirp on the pulse, as shown in Figure 2-3. The chirp on the pulse will be a red chirp since the carrier frequency is becoming smaller as a function of time on the portion of the pulse where most of the energy is contained.

For a two-section passively mode-locked laser, a red-chirp on the pulse will also be obtained if the linewidth enhancement factors are assumed to be equal in the gain and absorber sections. However, Schell *et al.* show that the α parameters are significantly different in the gain and absorber sections and that for significantly smaller α parameters in the absorber section as compared with the gain section, the pulse will be predominantly blue-chirped.

Chapter 3 Laser Design

As previously stated, the motivation behind this work is the development of a broadly tunable mode-locked semiconductor laser source operating within the wavelength range of 900 and 1100 nm. This goal imposes several requirements on the device:

- broad gain bandwidth in order to achieve a large tuning range
- external cavity operation for wavelength tuning
- multiple-contact design for easy incorporation of a saturable absorber
- GaAs substrate with InGaAs quantum-wells in order to achieve the desired emission wavelength

Each of these issues, along with other considerations, will be discussed in the sections that follow.

3.1 Broad gain bandwidth

It has been shown that a broad gain bandwidth can be achieved through the use of an asymmetric quantum well structure [86-89]. Asymmetric quantum well (AQW) structures are structures that contain quantum wells of different thickness or of different compositions. An illustration of the active region of an AQW structure is shown in Figure 3-1.

Changing the composition or thickness of the quantum well results in a change in the ground state energy level. The main disadvantage in using quantum wells of different thickness to obtain a broad gain bandwidth is that thin wells contribute less gain than thick wells for a given carrier density. In order to have roughly equal contributions to the gain, more thin wells need to be incorporated into the structure than thick wells. As an example, Hamp *et al.* describes an InGaAsP/InP laser structure comprised of two 100 Å wells, two 50 Å wells, and fourteen 40 Å wells [90]. However, a design with this many wells is not feasible with GaAs based lasers incorporating InGaAs quantum wells due to strain considerations. This issue is addressed in section 3.1.1.

Hamp *et al.* [90, 91] and Woodworth *et al.* [92] also show that proper choice of the device length is required to achieve a broadly tunable asymmetric quantum well laser. The length of the laser should be chosen to equal the transition cavity length. Hamp *et al.* have defined the transition cavity length to be the cavity length above which the AQW device initially lases on the low energy wells and below which they initially lase on the high energy wells. Since all of the devices used in this work do not lase in the absence of external feedback (due to suppressed facet modal reflectivity), the concept of the transition cavity length does not apply.

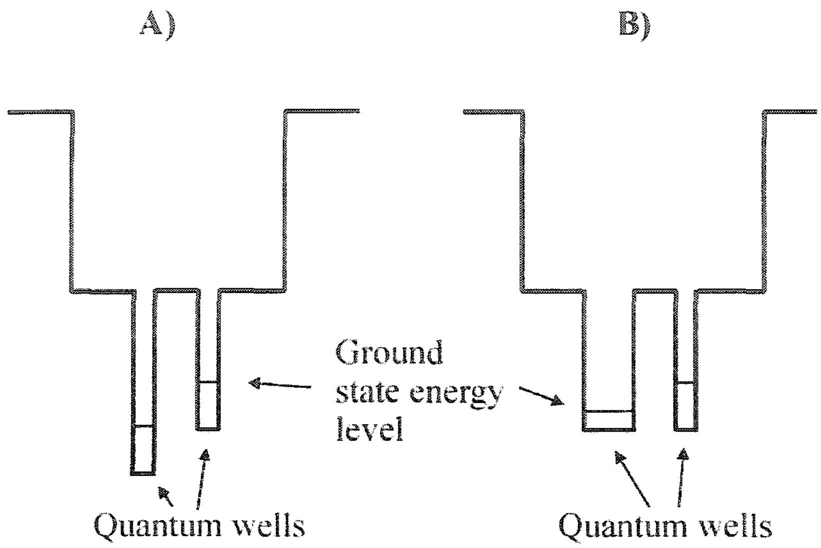

Figure 3-1: Illustration of the conduction band of an AQW structures. A) AQW structure where the composition of the wells has been varied, B) AQW structure where the thickness of the wells has been varied.

3.1.1 Strain considerations

The lattice constant of GaAs and InP is 5.6533 Å and 5.8688 Å, respectively [93]. The lattice constant of $In_xGa_{1-x}As$ is determined by Vegard's law and is given by [93, 94]

$$\begin{aligned} a_{In_xGa_{1-x}As} &= xa_{InP} + (1-x)a_{GaAs} \\ a_{In_xGa_{1-x}As} &= 5.6533 + 0.2155x \end{aligned} \tag{3.1}$$

where a denotes the lattice constant and x denotes the indium content.

Since the lattice constant of GaAs is smaller than that of InP, an epitaxial layer of InGaAs grown on GaAs is compressively strained. While a compressively strained quantum-well is desirable for achieving a low threshold and a high differential gain [95], it limits the number of quantum-wells that can be incorporated into a laser structure. The total thickness of the quantum-wells must be kept below the critical thickness to avoid the formation of crystal defects. The critical thickness of $In_xGa_{1-x}As$ on GaAs can be determined from the model developed by Matthews and Blakeslee [96] and is given by

$$\varepsilon = \frac{a(1-\sigma/4)\left[\ln\left(L_c\sqrt{2}/a\right)+1\right]}{2\sqrt{2}\pi L_c(1+\sigma)} \tag{3.2}$$

where ε is the strain, a is the GaAs lattice constant, σ is Poisson's ratio and L_c is the critical thickness. Experimental data by Fritz *et al.* [97] and Andersson *et al.* [98] agree very well with equation (3.2). The function is plotted below for InGaAs grown on GaAs (Figure 3-2).

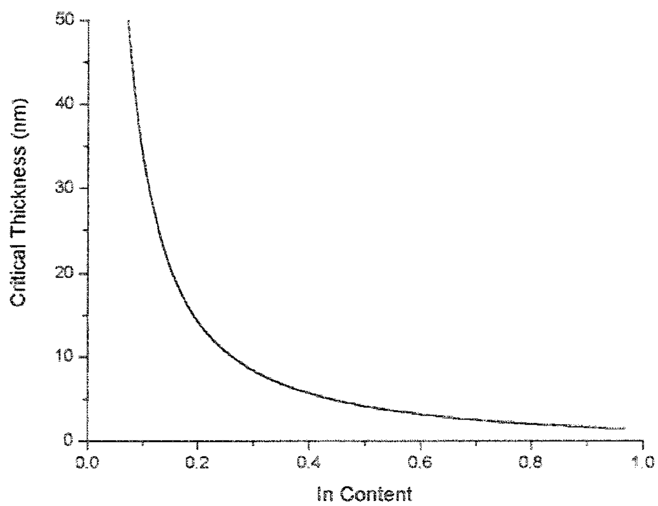

Figure 3-2: Critical thickness versus In content for InGaAs grown on GaAs. See equation (3.2), taken from reference [96].

An InGaAs/GaAs quantum-well laser designed to emit light around 980 nm requires an indium content of approximately 22%. The exact value depends upon the thickness of the quantum-well and the material used for the barrier layer. The critical thickness is 12 nm for this indium concentration. This means that only two 6 nm quantum wells can be incorporated into the laser structure while maintaining good crystal quality. In order to incorporate additional quantum wells, thinner quantum wells need to be used or the quantum wells need to be designed for emission at shorter wavelengths.

For an InGaAs/GaAs quantum-well laser operating at 1075 nm, the indium content is approximately 33%. This corresponds to a critical thickness of just over 7 nm. This limits the design to a single quantum well, which is undesirable from a gain-bandwidth standpoint. A potential solution to this limitation is to include strain-balancing layers in the laser design. Strain balancing can be achieved through the use of GaAsP barriers and has been successfully demonstrated by a number of researchers [99-102]. The effect of growth conditions and strain compensation on indium incorporation in such lasers can be found in reference [103].

3.2 Laser structures

Devices have been fabricated from a number of different laser structures for short pulse generation. In the 980 nm wavelength regime, symmetric quantum well structures, dual asymmetric-quantum-well structures and triple asymmetric quantum well structures have been fabricated. In the 1075-1085 nm wavelength regime, a preliminary structure containing a single quantum well has been fabricated. All of the laser structures incorporate InGaAs quantum-wells grown lattice-matched to GaAs. Details for each of the laser structures follow.

3.2.1 Symmetric quantum well laser structures

Two different types of symmetric quantum well laser structures are used to make devices for operation at a wavelength in the vicinity of 980 nm. The first symmetric quantum well device is shown in Table 3-1. It consists of a 100 nm n-type GaAs buffer layer grown on a GaAs substrate, a 1.3 μm n-type InGaP cladding layer, two 60 Å InGaAs quantum wells surrounded by 100 nm GaAs barriers, and a 1.28 μm p-type InGaP cladding layer and a p-type GaAs contact layer. A 50 Å GaAs etch stop is positioned 180 nm into the p-type InGaP cladding layer.

One feature to take note of in this design is the use of GaAs as the barrier material in the active region. As discussed in reference [104], the use of GaAs in this capacity is non-ideal from two perspectives. First consider the case of electron/hole confinement. For a 980 nm quantum well, the barrier height in the conduction band is on the order of $2.5 \times kT$. This is considered to be weak confinement and will result in poor temperature and power performance. The second case to consider is the optical properties of the structure. The large index contrast between the GaAs barriers and the InGaP cladding results in a tightly confined mode. While this may be desirable to optimize the energy extraction from the gain medium, it results in an undesirably large far-field divergence angle.

Table 3-1: Symmetric QW laser structure with GaAs barriers.

Layer	Material	Thickness
Contact	GaAs	0.2 μm
Cladding	*p* InGaP	1.1 μm
Etch stop	*p* GaAs	5 nm
Cladding	*p* InGaP	0.18 μm
Barrier	GaAs	100 nm
Quantum Well	InGaAs	6 nm
Barrier	GaAs	10 nm
Quantum Well	InGaAs	6 nm
Barrier	GaAs	100 nm
Cladding	*n* InGaP	1.3 μm
Buffer	n^+ GaAs	0.1 μm
Substrate	n^+ GaAs	

Table 3-2 : Symmetric QW laser structure with InGaAsP barriers.

Layer	Material	Thickness
Contact	p^+ GaAs	0.2 μm
Cladding	*p* InGaP	1.1 μm
Etch stop	*p* GaAs	5 nm
Cladding	*p* InGaP	0.18 μm
Barrier	InGaAsP	110 nm
Quantum Well	InGaAs	6 nm
Barrier	InGaAsP	10 nm
Quantum Well	InGaAs	6 nm
Barrier	InGaAsP	110 nm
Cladding	*n* InGaP	1.3 μm
Buffer	n^+ GaAs	0.1 μm
Substrate	n^+ GaAs	

In order to address the issues presented by GaAs barriers, laser structures based on quaternary (InGaAsP) barriers were designed. Use of the quaternary allows the band-gap of the material to be chosen independently of the lattice constant, permitting optimization of the laser structure. The InGaAsP symmetric quantum well laser design is shown in Table 3-2 and consists of a 100 nm n-type GaAs buffer layer grown on a GaAs substrate, a 1.3 μm n-type InGaP cladding layer, two 60 Å InGaAs quantum wells surrounded by InGaAsP barriers, and a

1.28 μm p-type InGaP cladding layer and a p-type GaAs contact layer. A 50 Å GaAs etch stop is positioned 180 nm into the p-type InGaP cladding layer. The InGaAsP band-gap is 1.584 eV.

While the above structure sidesteps some of the issues raised by the use of GaAs barriers, use of this structure presents a new difficulty. The difficulty lies in the growth of the InGaAsP layers. During the growth process, the quaternary material tends to segregate into InAs rich regions and GaP rich regions. In order to alleviate this problem, the material is grown at a low temperature. Lowering the temperature reduces the surface mobility of the adatoms during the growth process, resulting in a more homogenous growth [104]. However, lowering the temperature results in non-ideal growth conditions for the InGaAs quantum-wells. As such, it is expected that a number of defects are present in the quantum-wells.

Devices fabricated from structures incorporating quaternary barriers require very long burn-in times before they begin to operate with efficiencies comparable to devices fabricated from the previous laser structure. The amplified spontaneous emission (ASE) output power for angled-facet devices typically increases by as much as a factor of 100 during a burn-in period in excess of 7 days.

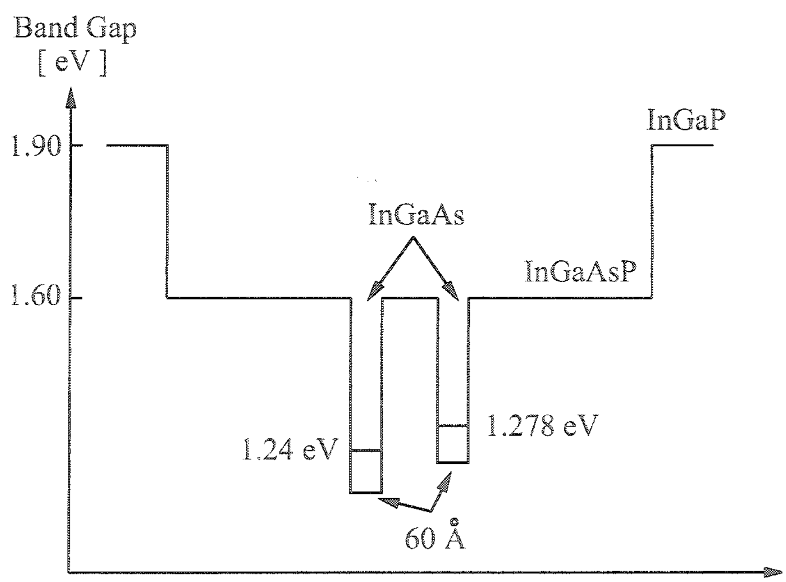

Figure 3-3: Conduction band of the active region for the 2 AQW laser structure.

3.2.2 Dual asymmetric quantum well laser structures

The dual asymmetric quantum well laser structure is identical to the symmetric quantum well structure presented in Table 3-2 with the exception of the composition of the quantum wells. For this structure, the In concentration in each of the wells is varied such that the transition energies of the wells correspond to wavelengths of 960 nm and 990 nm. The conduction band of the active region is shown in Figure 3-3.

3.2.3 Triple asymmetric quantum well laser structures

In an attempt to increase the gain bandwidth beyond that which was achievable with the dual asymmetric quantum well system, a laser structure incorporating three quantum wells was designed. Unfortunately, a number of difficulties were encountered during the design and fabrication process.

Initially, due to concerns regarding the overall strain of the active region, devices were grown using strain-compensating GaAsP barrier layers. The phosphorus concentration in the barriers is approximately 20%. The use of GaAsP barriers presents difficulties in optimizing the design of the waveguide, as the index of refraction of GaAsP lattice-matched to GaAs is not well known. The devices fabricated from this preliminary structure exhibit low thresholds of 7 to 10 mA for 350 μm long devices. However, the devices operate multimode (lateral modes) at currents a few milliamps above threshold. The number of lateral modes varies from 3 to 7 (and beyond in some cases) as the drive current is modified.

Since the exact reason for the multimode operation of the device just described was not discernable, and the use of GaAsP barriers was a *new* variable, a new structure was grown with reduced phosphorus content (approximately 10%). The low threshold current observed in the preliminary structure is maintained in the new structure. While the new devices also exhibit multi-lateral mode operation beyond threshold, the situation is improved over the first design. The new devices operate with a single lateral mode output over a much larger current range as compared with devices fabricated from the earlier design. However, the current range over which single mode output is achievable is insufficient for conducting mode-locking experiments. Device heating is deemed not to be responsible for the multi-lateral mode output since the same multi-mode output is observed when driving the devices with a pulsed-current source. Also, modifying the temperature of the stage upon which the device is mounted has little impact on the onset of the multi-mode behaviour.

The ridge waveguide (see section 3.4) does not provide sufficient confinement to support the large number of modes observed. In fact, the device behaves almost as though the light *did not see* the ridge at all. That is, the device seems to be operating in a gain-guided manner. This notion is supported by observations made with angled-stripe devices. At sufficiently high currents, the devices begin to lase as though the waveguide is not present (Figure 3-4). This is not seen with angled stripe devices fabricated from symmetric QW and dual asymmetric QW material.

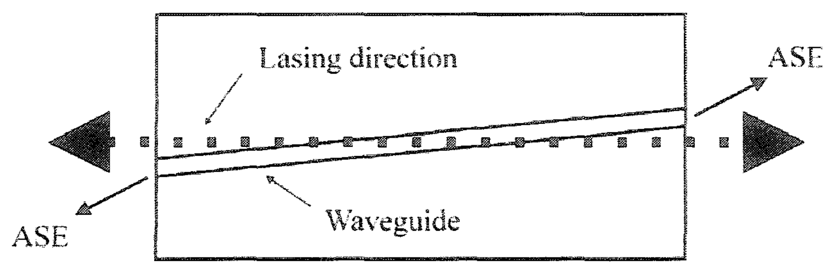

Figure 3-4: Illustration indicating the direction along which the 3 AQW angled strip device is lasing.

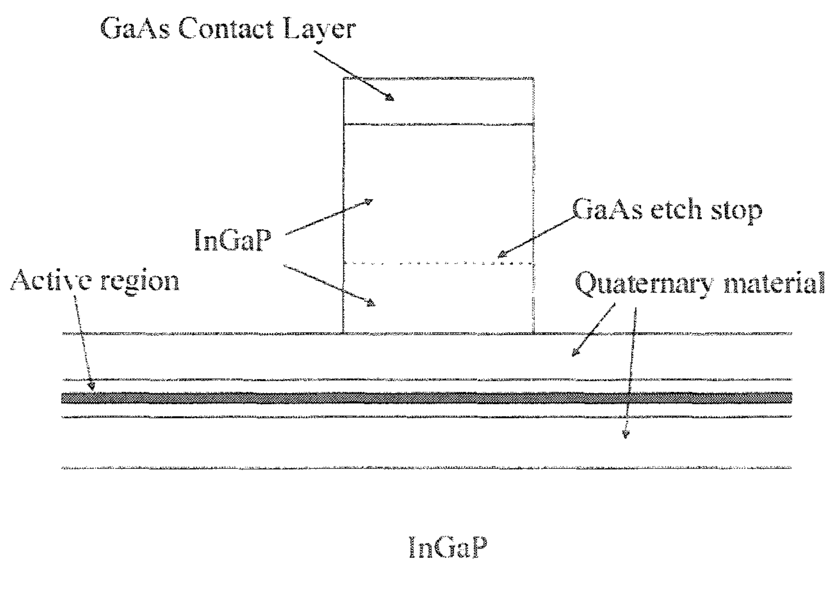

Figure 3-5: Illustration of the modified etching step (etching through the etch stop) used on the 3 AQW devices.

In an attempt to increase the optical confinement in the lateral direction, etching was continued beyond the etch stop when the next quarter of this laser material was processed. Performing this step results in a structure similar to that depicted in Figure 3-5. Unfortunately, this modification had a negligible impact on the modal properties of the device.

With the exact causes of the multimode operation unknown, a final 3-AQW structure was grown. The final structure contains a minimal amount of phosphorous in the barrier layers. This device shows a remarkable improvement over the two previous structures. Lasers fabricated from this material have a low threshold, and the onset of multi-lateral mode operation does not occur until the output power of the device exceeds 10 mW. This is deemed suitable for mode-locking experimentation since the average mode-locked output power typically achieved with the 2-AQW structure is less than 1 mW. All of the mode-locking results presented for the 3-AQW devices are obtained with this structure. Details of the structure are shown in Table 3-3. The structure consists of three wells with transition energies corresponding to wavelengths of 985 nm, 955 nm and 930 nm. In an effort to minimize the burn-in time required while maintaining the advantages offered by the quaternary material, both GaAs and InGaAsP are used in the design. The quaternary material is used on either side of the active region, while GaAs is used as the quantum-well barrier material for the quantum-wells. The conduction band for the active region of this structure is shown in Figure 3-6.

Table 3-3: Triple asymmetric quantum well laser structure

Layer	Material	Thickness
Contact	GaAs	0.15 μm
Cladding	*p* InGaP	1.3 μm
Etch stop	*p* GaAs	5 nm
Cladding	*p* InGaP	0.12 μm
Quaternary	InGaAsP	110 nm
Barrier	GaAs	15 nm
Quantum Well	InGaAs	5 nm
Barrier	GaAs	10 nm
Quantum Well	InGaAs	5 nm
Barrier	GaAs	10 nm
Quantum Well	InGaAs	5 nm
Barrier	GaAs	15 nm
Quaternary	InGaAsP	110 nm
Cladding	*n* InGaP	1.42 μm
Buffer	n^+ GaAs	0.1 μm
Substrate	n^+ GaAs	

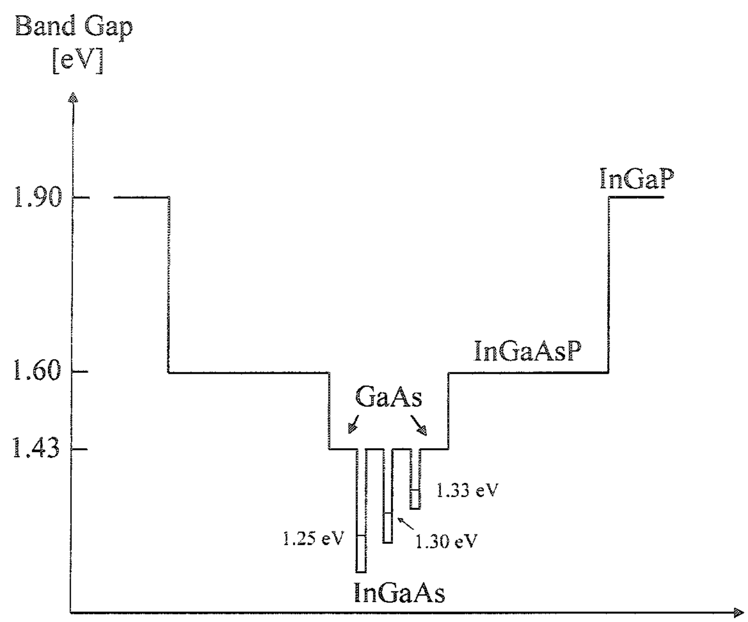

Figure 3-6: Conduction band for the triple asymmetric quantum well laser structure.

3.2.4 Long-wavelength (λ~1075 - 1085 nm) GaAs lasers

Long-wavelength GaAs lasers incorporating a single quantum-well were fabricated for preliminary study. The laser structure is shown in Table 3-4. It consists of a 6 nm quantum well with GaAs barriers. The longer operating wavelength ensures that GaAs barriers provide sufficient electron/hole confinement without the need for quaternary barriers.

Table 3-4: Long wavelength InGaAs/GaAs laser structure.

Layer	Material	Thickness
Contact	GaAs	0.15 μm
Cladding	*p* InGaP	1.25 μm
Etch stop	*p* GaAs	5 nm
Cladding	*p* InGaP	0.12 μm
Barrier	GaAs	110 nm
Quantum Well	InGaAs	6 nm
Barrier	GaAs	110 nm
Cladding	*n* InGaP	1.37 μm
Buffer	n^+ GaAs	0.1 μm
Substrate	n^+ GaAs	

3.3 Gain Calculations

Gain calculations are made for the various asymmetric quantum well structures in order to see the effect of carrier density on the gain bandwidth. The calculations follow the method outlined in reference [105]. The expression for the material gain as a function of photon energy is obtained using Fermi's Golden Rule and is given by

$$g(\hbar\omega) = \left(\frac{1}{\hbar\omega}\right)\frac{\pi e^2\hbar}{\varepsilon_0 c m_0^2}\frac{1}{n}|M_T|^2 \rho_{red}\left(E_{eh} - E_g^{'}\right)(f_c - f_v) \qquad (3.3)$$

where $\hbar\omega$ is the photon energy, m_0 is the mass of the electron, e is electron charge, c is the speed of light in vacuum, n is the refractive index of the material, M_T is the transition matrix element, ρ_{red} is the reduced density of states, E_{eh} is the electron-hole transition energy ($E_{eh}= \hbar\omega$), E'_g is the bandgap between two given sub-bands in the quantum well, and f_c and f_v are the Fermi-Dirac distributions for the electrons in the conduction band and valence bands, respectively.

In the evaluation of equation (3.3), parabolic sub-bands are assumed. While this is a reasonable approximation for the conduction band of a quantum well, the valence band of a quantum well is far from parabolic [105]. The approximation is slightly better for the case of strained quantum wells, yet it remains a source of error in the calculated gain spectra. However, since the calculations are used to explore the general trends of the gain spectra as a function of carrier density for the asymmetric quantum well structures, they remain useful from that standpoint.

The carrier density in each of the quantum wells is also taken to be equal for the calculations. However, there is evidence of a non-uniform carrier distribution in multiple-quantum well lasers [106-109]. This will introduce another source of error into the gain calculations for the asymmetric quantum well lasers.

Spectral broadening of each transition is included by convolving the expression for the gain with a Lorentzian lineshape function assuming an intra-band relaxation time of 100 fs [110]. The Lorentzian lineshape was chosen over more sophisticated lineshape functions [111, 112] for simplicity.

3.3.1 Dual asymmetric-quantum-well lasers

The results of gain calculations for the dual asymmetric quantum well laser structure, presented in section 3.2.2, are shown in Figure 3-7 and Figure 3-8. The first figure shows the gain of the individual wells and the total gain for a carrier density of 4 x 10^{18} cm^{-3}. At this carrier density, the total gain bandwidth of the system is broadened beyond what would be achievable with a symmetric quantum well system. In fact, this is the case for all carrier densities yielding positive gain.

The second figure, Figure 3-8, illustrates the total gain for different carrier densities. As the carrier density in the wells increases, the gain bandwidth broadens and the peak in the gain shifts toward the blue end of the spectrum. The shift in the gain peak is due to the red well possessing a positive gain at higher energies for larger carrier densities. This positive gain at high energies begins to overlap with the gain curve of the blue well, resulting in a shift of the gain peak.

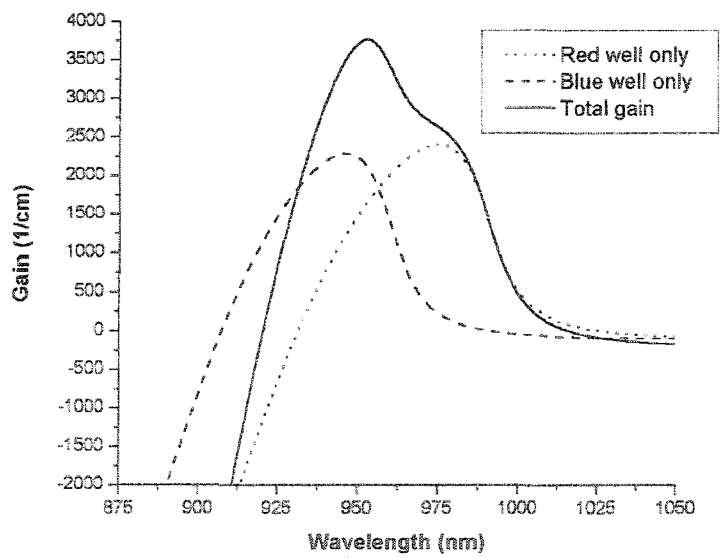

Figure 3-7: Gain of the 2-AQW laser structure for a carrier density of 4 x 10^{18} cm^{-3}. The gain of the individual wells and the total gain are shown. The traces show the TE polarization gain only.

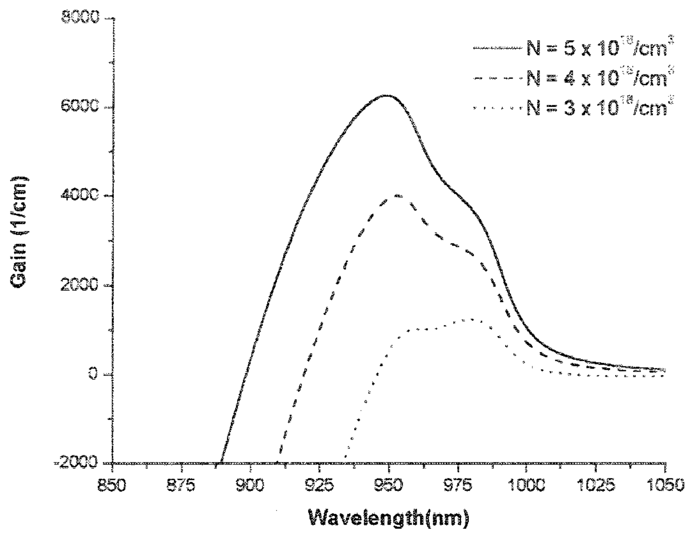

Figure 3-8: Total gain calculated for the 2-AQW laser structure at different carrier densities.

3.3.2 Triple asymmetric-quantum-well lasers

The results of the gain calculations for the triple asymmetric-quantum-well structure are shown in Figure 3-9, Figure 3-10 and Figure 3-11. In the first figure, the gain of each of the individual wells making up the active region is plotted for a carrier density of 4 x 10^{18} cm^{-3}. The feature to take note of is the large absorption value of well #1 in the vicinity of the gain peak of well #3. The absorption is sufficiently large so that the addition of a third well negligibly affects the gain bandwidth at this carrier density. This is illustrated in Figure 3-10 where the total gain for all three wells, and the total gain for well #1 and well #2 are plotted for a carrier density of 4 x 10^{18} cm^{-3}. In comparing the two traces, it is seen that the addition of a third well at the blue end of the spectrum does not dramatically increase the gain bandwidth over the 2-AQW structure for this carrier density.

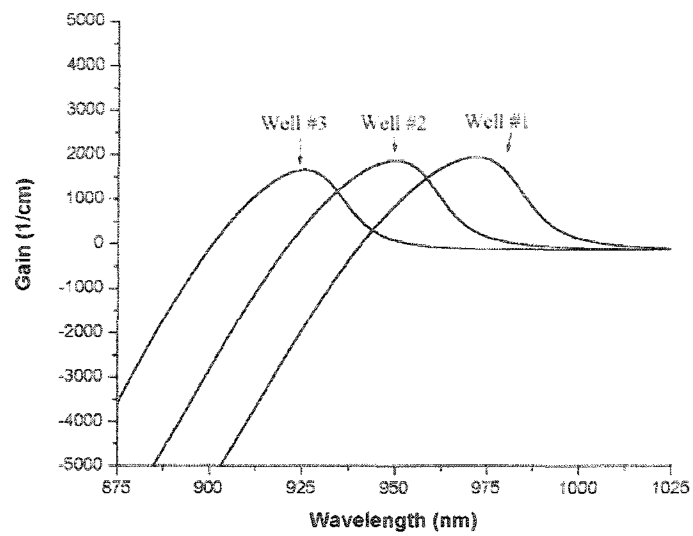

Figure 3-9: Gain of the 3-AQW laser structure for a carrier density of 4 x 10^{18} cm^{-3}. The gain of the individual wells and the total gain are shown. The traces show the TE polarization gain only.

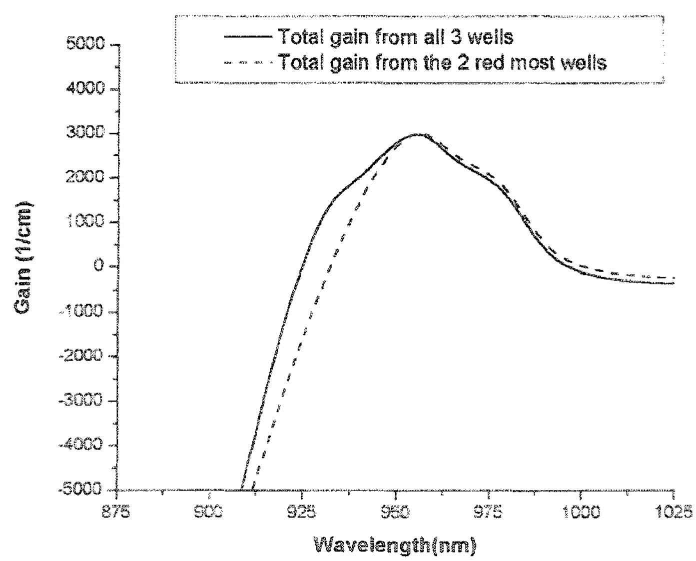

Figure 3-10: Total gain of the 3-AQW laser structure for a carrier density of 4 x 10^{18} cm^{-3}. For comparison purposes, the total gain from the two red most wells at the same carrier density is plotted as well.

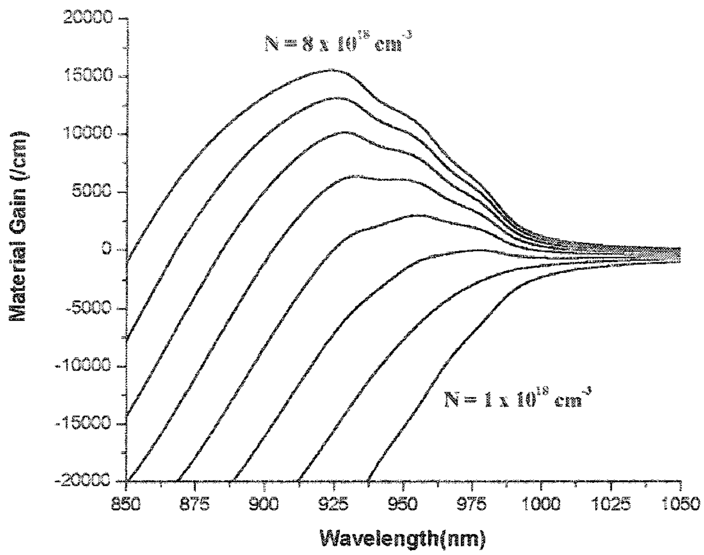

Figure 3-11: Total gain of the 3-AQW laser structure for carrier densities ranging from 1 x 10^{18} cm^{-3} to 8 x 10^{18} cm^{-3} in 1 x 10^{18} cm^{-3} increments.

Larger carrier densities are required in order to make use of the potential bandwidth increase offered by the 3-AQW system. This is shown in Figure 3-11 where the total gain is plotted for carrier densities ranging from 1 x 10^{18} cm^{-3} to 8 x 10^{18} cm^{-3}. At carrier densities of 5 x 10^{18} cm^{-3} and higher, the contributions of the third well are quite evident. Keeping in mind that the gain calculations are based upon a number of simplifications, specifying a carrier density of 5 x 10^{18} cm^{-3} is somewhat arbitrary. The important thing to note is that the contribution of the third well becomes more significant as the carrier density is increased.

3.4 Waveguide structure

All of the devices used throughout this work were fabricated as edge-emitting ridge-waveguide devices using wet chemical etching. A cross-sectional view of a ridge-waveguide is shown in Figure 3-12.

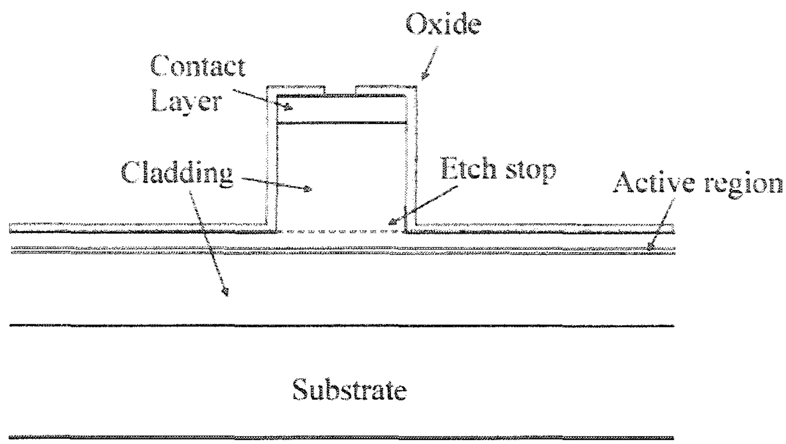

Figure 3-12: Cross sectional view of a ridge waveguide laser. Not drawn to scale.

3.5 *Multi-electrode ridge-waveguide lasers*

Fabrication of multi-electrode ridge-waveguide lasers allows for the direct incorporation of a saturable absorber. A section of the device will act as a saturable absorber by operating it below its transparency point. A schematic of a multi-electrode device is shown in Figure 3-13. The gap in the ridge is made during the same chemical etching stage used to define the ridge. An oxide layer separates the metal contacts on each of the sections. Since a reverse bias is typically applied to the absorber section, a large resistance is desirable between the two contacts. The resistance between the two contacts depends upon the thickness and doping level of the material immediately below the etch stop and on the size of the gap. Adjustment of the cladding layer thickness below the etch stop affects the waveguiding properties of the structure, and as such, care must be taken when adjusting this parameter. The introduction of a gap in the ridge structure results in additional optical losses for the device. As the gap size is increased, the optical coupling between the two sections is reduced. A large gap size also introduces a section of the device that is not pumped by current. Making the gap too small presents difficulties in the device fabrication process. The metal lift-off procedure, which removes the metal between the different sections of the laser, may not be very effective for gaps smaller than approximately 10 μm.

A gap size of 10 μm was chosen for most of the multi-electrode devices fabricated. This provides a resistance of approximately 10 kΩ between the two sections for all of the laser structures discussed in section 3.2. For gap sizes much larger than 60 μm, the optical losses of the device were too large to provide any meaningful results. In fact, most of the devices with larger gap sizes did not lase even with both sections under forward bias.

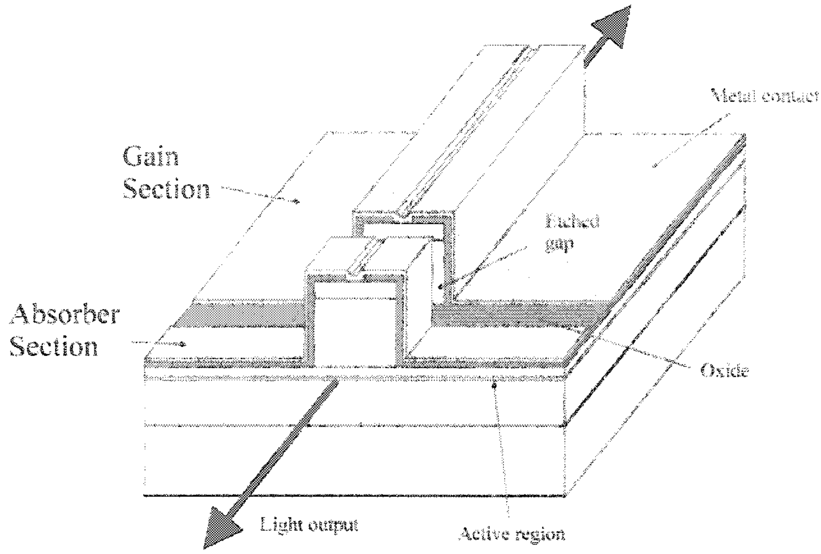

Figure 3-13: Illustration of a multi-electrode semiconductor laser.

3.6 Near-field and Far-field Analysis

One of the steps in designing a laser structure is the analysis of both the near-field and the far-field of the laser output. The typical desirable qualities are single mode output with a low divergence angle. While a ridge-waveguide laser can usually be made to operate single mode in both the lateral and transverse directions, achieving a low divergence angle is quite difficult.

The near-field for the various laser structures was calculated using the transfer-matrix method outlined by Walpita [113] in conjunction with the effective index method [114]. The far-field was computed by evaluating equation (3.4) from reference [115].

$$u(x,y,z) = -\frac{iz}{\lambda r}\frac{\exp(ikr)}{r}\int_{-\infty}^{\infty}\int_{-\infty}^{\infty} u(x',y')\exp\left[-\frac{ik}{r}(xx'+yy')\right]dx'dy' \quad (3.4)$$

where $u(x',y')$ is the near-field and $r=(x^2+y^2+z^2)^{\frac{1}{2}}$.

Since the near-field solution obtained from the Walpita method is a set of piecewise continuous exponentials, evaluation of equation (3.4) is straightforward. All of the computations were made with custom software developed in Microsoft Visual C++ 6.0.

The index profile for the symmetric quantum well laser structure is shown in Figure 3-14. The intensity of the near-field computed for this laser structure is shown in Figure 3-15 and Figure 3-16, for a wavelength of 980 nm. As seen from the figures, the waveguide was found to be multi-mode in the transverse direction (crystal growth direction). It is believed that the reason for the multi-mode behaviour is due to the GaAs cap layer in the laser structure. In Figure 3-15, the fundamental mode is seen to have most of its energy distributed within or close to the active region. The amount of energy contained within the cap layer is minimal for this mode. In contrast, most of the energy of the second mode (shown in Figure 3-16) is contained within the cap layer. The overlap of this mode with the active region is very small. As such, it was hoped that the lasers would operate single mode in the transverse direction due to the second mode having a poor overlap with the active region. Unfortunately, this was not the case. All of the lasers tested had evidence of some multi-mode structure in the transverse direction. More details on the mode profile are provided in Appendix B. Modelling indicates that shrinking the cap layer and moving the cap layer further away from the active region should alleviate the problem. Despite this issue, very good mode-locking results are achievable, as discussed in Chapter 3.

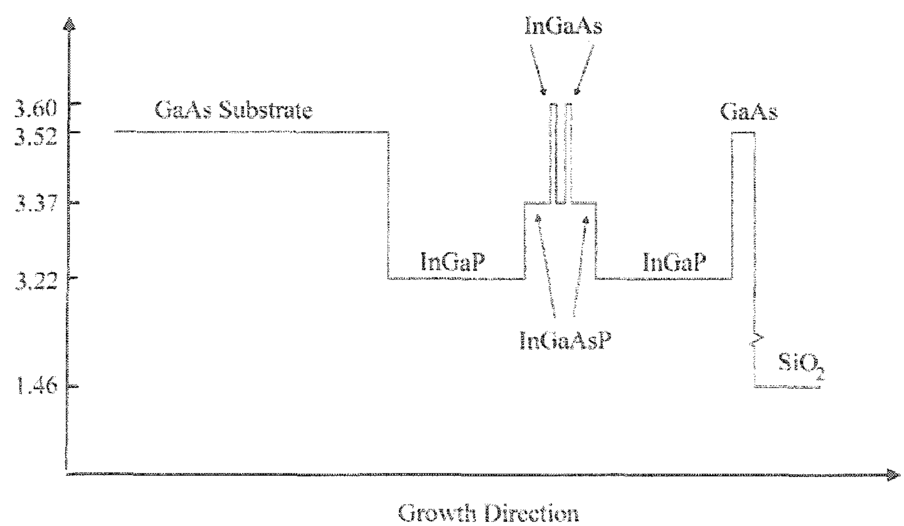

Figure 3-14: Refractive index profiles at 980 nm for the symmetric quantum well laser structure.

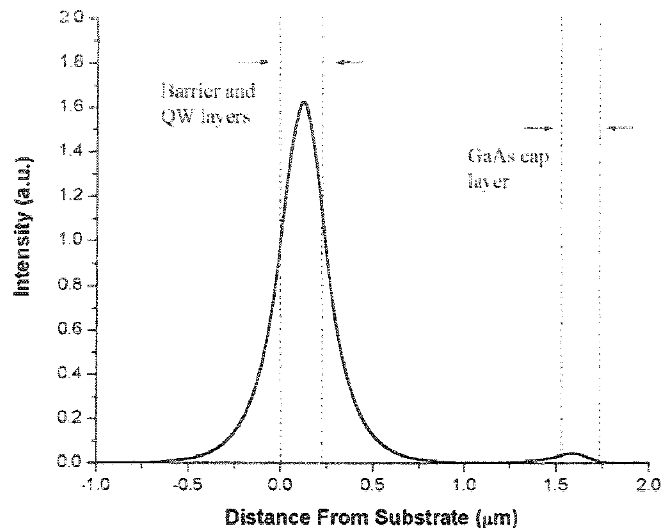

Figure 3-15: Near-field intensity in the transverse (crystal growth) direction for the fundamental mode of the symmetric quantum well waveguide structure.

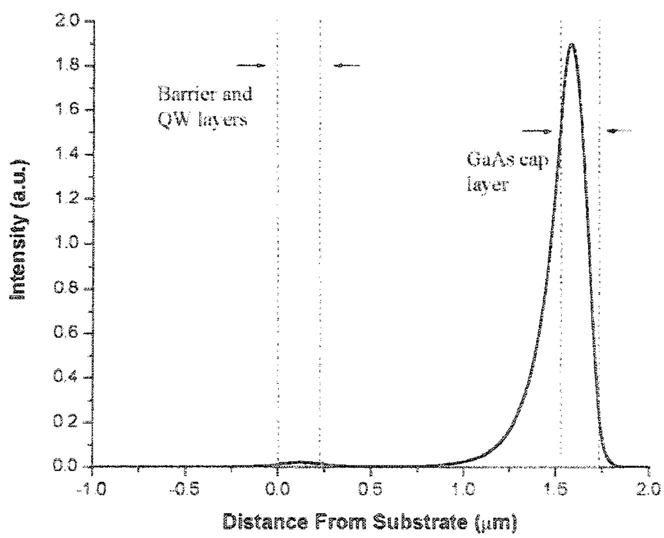

Figure 3-16: Near-field intensity in the transverse (crystal growth) direction for the second mode of the symmetric quantum well waveguide structure.

3.7 Experimental Anti-Reflection Coatings

In order to mode-lock a semiconductor laser in an external cavity, the modal reflectivity of the facet must be sufficiently suppressed. As such, anti-reflection (AR) coatings were deposited on laser facets using the McMaster Electron Cyclotron Resonance Plasma Enhanced Chemical Vapour Deposition system (ECR-PECVD) and with a *Technics* mini-PECVD. Both systems allow for the deposition of SiO_xN_y dielectric coatings. In the case of the ECR-PECVD system, the deposition rate and refractive index is monitored by an *in-situ* ellipsometer. The interested reader can find more information on this system in reference [116]. With the mini-PECVD, timing the deposition determines the thickness for a given growth rate. This requires prior growth of calibration samples in order to obtain the desired target thickness and index. The range of index of refraction covered by SiO_xN_y films varies from 1.46 for SiO_2 films to 2.0 for $SiN_{4/3}$ films. Details regarding the laser bar mounting procedure for AR depositions are outlined in Appendix C.

3.7.1 Methods of experimental anti-reflection coating analysis

The quality of the deposited anti-reflection coating can be determined by using the gain measurement technique developed by Hakki and Paoli [117] or an improved technique developed by Cassidy [118]. The gain measurement techniques are explained by considering the spectral output of a Fabry-Perot laser.

The steady-state output intensity at frequency v, $I_1(\nu)$, from facet 1 of a semiconductor Fabry-Perot laser is given by [118]

$$I_1(\nu) = \frac{B\left(1+R_2G(\nu)\right)\left(1-R_1\right)}{\left(1+\sqrt{R_1R_2}G(\nu)\right)^2 - 4\sqrt{R_1R_2}G(\nu)\sin^2(kL)} \tag{3.5}$$

where B describes the spontaneous emission at frequency v, R_1 and R_2 are the reflectivity of facet 1 and facet 2 respectively, $G(v)$ is the single pass gain, and L is the length of the device.

The Hakki-Paoli method proceeds as follows. For a given mode, taking the ratio of the mode maximum (when $\sin^2(kL) = 0$) to the mode minimum (when $\sin^2(kL) = 1$) results in

$$h = \frac{I_{\text{maximum}}}{I_{\text{minimum}}} = \frac{\left(1+\sqrt{R_1R_2}G\right)^2}{\left(1-\sqrt{R_1R_2}G\right)^2} \tag{3.6}$$

where h has been chosen to represent the ratio. Rearranging equation (3.6) yields

$$\sqrt{R_1R_2}G = \frac{\sqrt{h}-1}{\sqrt{h}+1} \tag{3.7}$$

Provided the index and thickness of the layers making up the laser structure are known, the reflectivity of the laser facets can be computed from theory. Equation (3.7) then provides a method of determining the single pass gain of the laser under study. This equation can also be used to experimentally determine the reflectivity of an AR coated laser facet. This is accomplished by measuring the amplified spontaneous emission spectra from the laser before and after applying the AR coating, under the same experimental conditions. The initial measurement provides the single pass gain of the laser for a given drive current. The second measurement, used in conjunction with the gain value determined from the first measurement, allows the reflectivity of the AR coated facet to be determined. It should be noted that this method assumes that the single pass gain of the laser remains unchanged for a given drive current before and after application of the AR coating. This assumption will not hold in the presence of gain saturation. Thus, it is best to perform the analysis for several different current values to ensure that the results are interpreted correctly.

The Cassidy method is similar, with the exception that it is the ratio of the mode sum (integral of the mode) to the mode minimum computed. This makes the method insensitive to the response function of the instrument measuring the optical spectra.

Table 3-5: Target thickness and index for an optimal anti-reflection coating for a given laser structure.

Laser structure	Target Index	Target Thickness (nm)
980 nm lasers	1.803	142
1070 nm lasers	1.880	155

3.7.2 Experimental results – straight facets

Single layer SiO_xN_y AR coatings were designed and deposited on lasers operating in the 980 nm wavelength regime and on the long wavelength (1075-1085 nm) lasers. Table 3-5 lists the optimal thickness and index for an AR coating for the two different laser structures. The ideal parameters were determined using the algorithm outlined by Vassallo [119, 120], implemented in the C programming language [121]. It should be noted that a few different 980 nm laser designs were used and that the target index and thickness varied slightly for each design. All spectra were measured with a 3/4 meter monochromator.

As an example, the optical spectra of a 980 nm regime laser before and after application of an AR coating are shown in Figure 3-17. This coating was deposited using the McMaster ECR-PECVD system. The reflectivity, which was calculated based on the spectra, is shown in Figure 3-18. For comparison purposes, results obtained with the Hakki-Paoli method and with the Cassidy method are presented. The agreement between the two techniques indicates that the resolution of the monochromator adequately resolves the Fabry-Perot modes of the laser for the purpose of this calculation. The minimum reflectivity measures approximately 2 x 10^{-4}. The index and thickness of the SiO_xN_y coating were 1.83 and 144 nm respectively. The laser is a symmetric quantum well 980 nm laser measuring 550 μm in length with a ridge width of 2 μm. The threshold current of the laser was 17 mA. The measurements shown in the figures were performed using a drive current of 15mA. Measurements were also performed at 13 mA and 14 mA. Excellent agreement was obtained between the results for all current values.

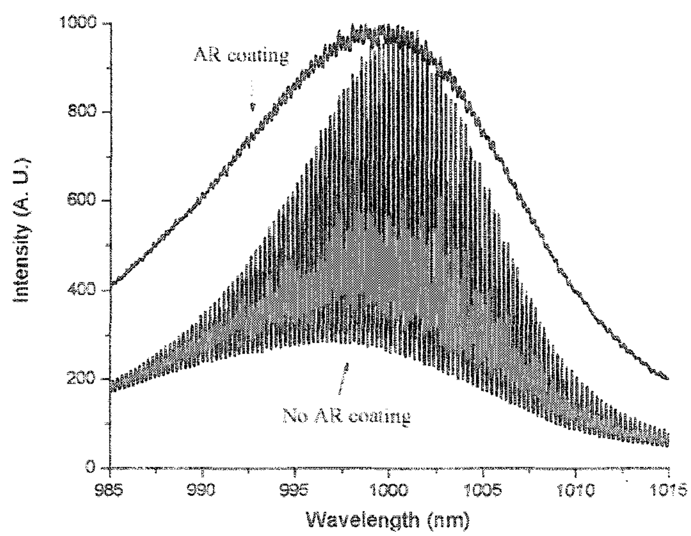

Figure 3-17: Amplified spontaneous emission spectra before and after application of an AR coating. The drive current on the device was 15 mA, which is 2 mA below threshold for this device. The AR coating had a refractive index of 1.83 and a thickness of 144 nm.

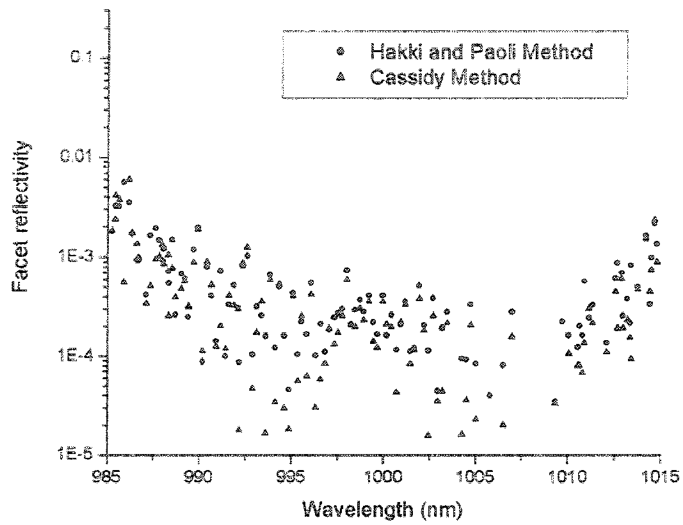

Figure 3-18: Reflectivity of the AR coated laser facet obtained from analysis of the spectra shown in Figure 3-17.

3.7.3 AR coating limitations

One of the limitations introduced by single layer anti-reflection coatings is the bandwidth over which a sufficiently low modal reflectivity is achieved that is suitable for mode-locking. As discussed in Chapter 2, theoretical models indicate that a modal reflectivity on the order of $\sim 10^{-4}$ is required for external cavity mode-locking. Figure 3-19 shows a theoretical plot of modal reflectivity as a function of wavelength for the symmetric quantum well laser design. The bandwidth where the modal reflectivity is 10^{-4} or better is approximately 20 nm. In practice, the bandwidth is typically much smaller due to difficulties in precisely achieving the target thickness and index. Also, modifications to the index of refraction of the device due to current injection and bonding strain will negatively impact the effectiveness of the coating.

The limited low-reflectivity bandwidth is a limitation that must be overcome in order to achieve a large mode-locked tuning range. One solution is to design and deposit multi-layer anti-reflection coatings. However, there are technical difficulties associated with this solution. In depositing single layer AR coatings, achieving the correct thickness and index of the dielectric layer is challenging. For multi-layer coatings, this means that this feat must be repeated consecutively for as many layers as are required.

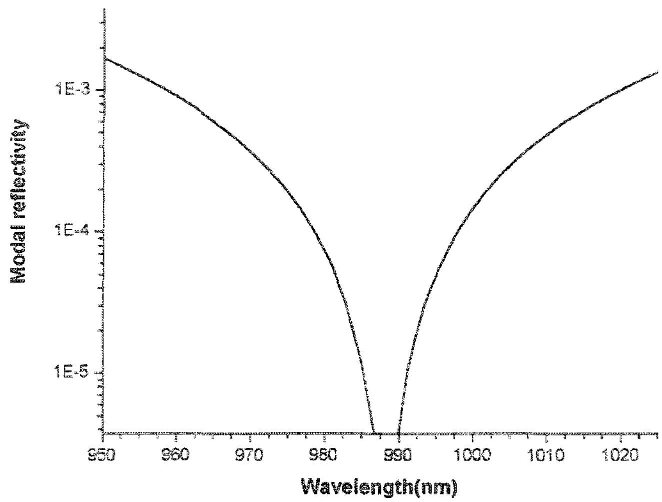

Figure 3-19: Modal reflectivity versus wavelength for an ideal AR coating deposited on the symmetric QW laser structure. The index of refraction is 1.803 and the thickness is 142 nm.

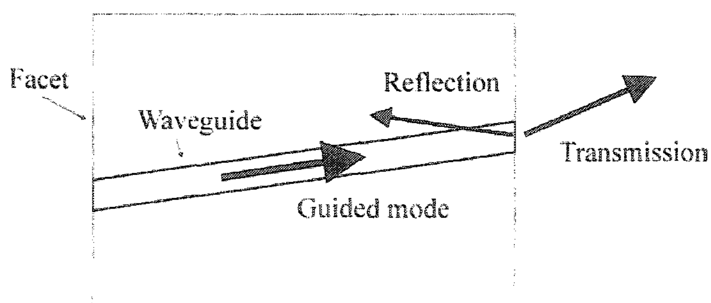

Figure 3-20: Illustration of an angled facet device.

An alternative solution is to use a device that has been designed to have a low facet modal reflectivity without an AR coating. Angled-facet devices satisfy this criterion. A schematic of an angled-facet device is shown below in Figure 3-20. The modal reflectivity of an angled facet is reduced compared with that of a straight facet due to the poor coupling of the reflected field into the waveguide. The modal reflectivity can easily be decreased to 10^{-2} by angling the facets [122].

Application of an AR coating will further reduce the modal reflectivity to the desired level. Since the modal reflectivity is already low, less precision is required during the AR coating deposition to achieve the desired performance of the coating.

3.7.4 AR coatings on angled facets

The accurate analysis of AR coatings deposited on angled facets is difficult for a number of reasons. Aside from the increased complexity in modeling the system as compared with straight facets, the change in modulation depth (mode maximum to mode minimum) before and after coating is difficult to measure accurately. The reason for this is the very small modulation depth measured prior to depositing the AR coating. This is shown below in Figure 3-21.

The device used to produce the data for Figure 3-21 is 500 μm long, and has facet angles of 7°. The pump current into the device is 30 mA. At this current, the modulation on the spectra is essentially buried in the noise. High currents are required in order to see any indications of modulation on the signal. The situation is exacerbated with the deposition of AR coating. That is, any modulation on the signal will forever be buried in the noise, resulting in an enormous uncertainty in an experimental evaluation of the AR coating quality. As such, a quantitative analysis of AR coatings on angled facets was not performed.

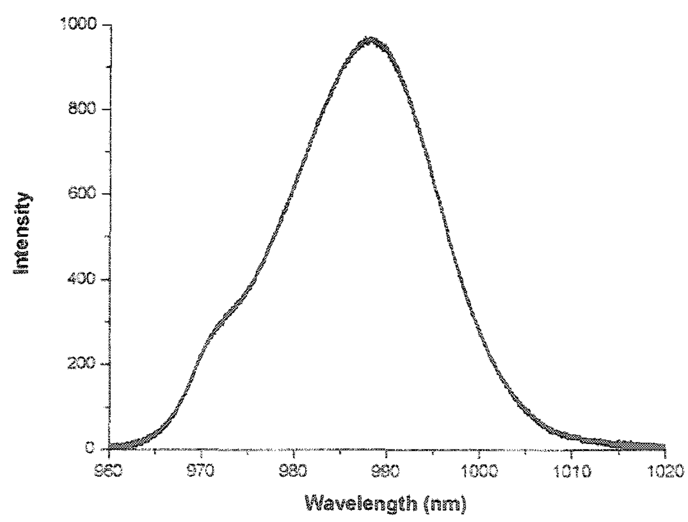

Figure 3-21: Spectrum from a dual angled facet, 500 μm long device. The pump current into the device was 30 mA.

3.8 Device design for low modal reflectivity

As discussed in the previous section, a simple method to achieve low modal reflectivity over a broad bandwidth is to tilt the waveguide of the device relative to the cleaved facet. Refer back to Figure 3-20 for a schematic representation of such a device. However, this simple solution presents difficulties from a technical standpoint. Firstly, tilting the ridge waveguide results in both facets having a low modal reflectivity, requiring external feedback on both ends of the device. The external cavities for such devices are inherently more complex in that they require a larger number of optical elements in the cavity. As a consequence, the cavities are typically larger in size as compared with devices having only one facet requiring external feedback. The second difficulty lies in the fact that the output from both facets is coupled to the external cavity. This means that AR coatings must be deposited on both ends of the device in order to ensure good coupling. While this in and of itself is not a problem, it does introduce an extra time-consuming step in the device fabrication process. Despite these difficulties, angled facet devices have been mode-locked with good success, and the results are presented in Chapter 4.

In order to overcome some of the difficulties associated with angled facet devices, a modification to the waveguide design was made. A mask was designed such that devices could be fabricated with a bend incorporated in the waveguide. A schematic of the waveguide for such a device is shown in Figure 3-22.

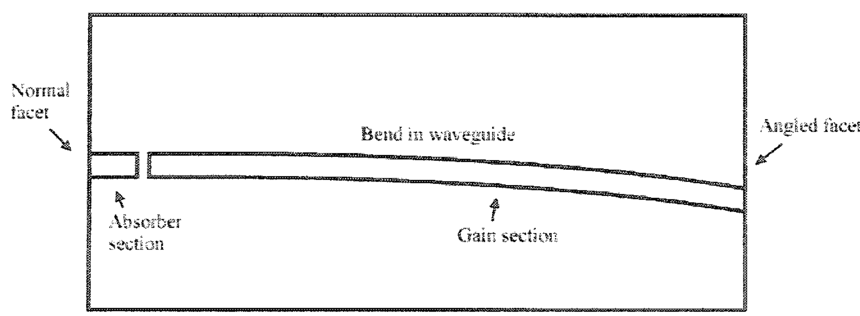

Figure 3-22: Top view of a bent-waveguide device.

With the bent-waveguide design, the waveguide terminates at a right angle with respect to one facet and at a specified angle relative to the other facet. Additional suppression of the chip's Fabry-Perot modes, and a reduction in the output coupling loss, is achieved by depositing a single layer AR coating on the angled facet. This design also permits a high-reflective (HR) coating to be deposited on the output facet if desired. Bent-waveguide devices have been used for the fabrication of super-luminescent diodes [86, 123, 124] as well as in distributed feedback lasers to produce arbitrarily chirped gratings [125]. While this design seems promising for external cavity mode-locking, the only report prior to the author's work of using such a design for this purpose was made in a brief abstract-style article [126]. More recently, Williamson *et al.* used a bent waveguide design for external cavity mode-locking [127]. As is shown in Chapter 4, the novel combination of a split-contact, bent-waveguide device incorporating an asymmetric quantum well active region has allowed for the generation of ultrashort optical pulses, tunable over a very broad wavelength range.

Chapter 4 Experimental Mode-locking results

This chapter presents the experimental mode-locking results obtained with the various laser structures and waveguide geometries. The first section describes in detail all of the components included in the experimental setup. Preliminary mode-locking results obtained with both linear and ring cavities are presented in sections 4.2.1 and 4.2.2. The key mode-locking results are found in the remaining sections of the chapter.

4.1 Experimental setup

A general layout of the experimental setup used for the generation and characterization of short optical pulses is shown in Figure 4-1. It consists of an external cavity coupled semiconductor laser with driving electronics, a grating pair pulse compressor, a monochromator and an autocorrelator. The details and design considerations involved in setting up each of these elements is discussed in the following subsections.

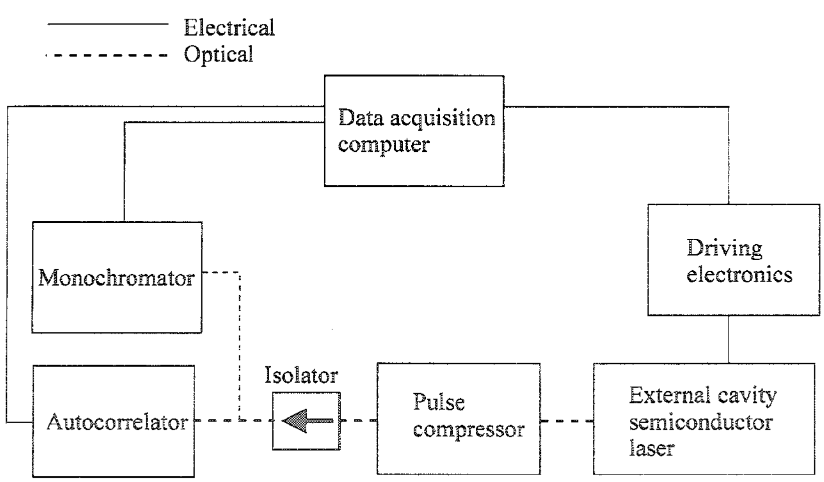

Figure 4-1: Generalized experimental setup used for short pulse generation.

4.1.1 External cavity coupled semiconductor laser

There are a number of technical details that must be addressed in order to effectively couple a semiconductor laser to an external cavity. The most important of these are thermal stability, mechanical stability, and providing access to both laser facets. These issues are addressed by the manner in which the devices are mounted for testing.

4.1.1.1 Device mounting

The requirement that both facets be accessible led to a custom design for the mounting of the devices. Illustrations of the mounting setup are shown in Figure 4-2 and in Figure 4-3. All of the devices are bonded with Epotek H20E silver epoxy to a thin copper block. The copper blocks are chosen (or sanded down) to have a thickness not much larger than the width of the laser bar, and are designed to be removable so that simply replacing the copper block allows new devices to be tested. The copper blocks are attached to a fixed piece of copper via mounting slots and a set of mounting screws. Thermally conductive paste can be applied at the interface of the two pieces of copper to ensure good thermal contact. A thermoelectric cooler regulates the temperature of the fixed piece of copper. The temperature is monitored by an attached 10K thermistor. While the placement of the thermistor is not ideal, it is a necessary trade-off to ensure flexibility in the mounting setup.

Two Thorlabs flexure stages (MDT616 and MDT631) are used to mount lenses to collect the light emitted from both facets of the device. In the case of a linear external cavity, the flexure stage with piezo control (MDT631) is used in the external cavity. The lenses are Thorlabs C230TM aspheric lenses (f = 4.51 mm, NA = 0.55) with an applied antireflection coating.

Contact with the device is made via two probes. A Keithley LV-2400 Source Meter is used to bias the absorber section of the device while an ILX Lightwave Laser Diode Controller (LDC-3724) is used to drive the gain section of the device. In the case of hybrid mode-locking, the RF signal is generated via an HP Signal Generator (model #8648B), amplified by a MiniCircuits ZHL-2-S RF amplifier and coupled into the device via a bias-T. An illustration of the drive electronics is shown below in Figure 4-4.

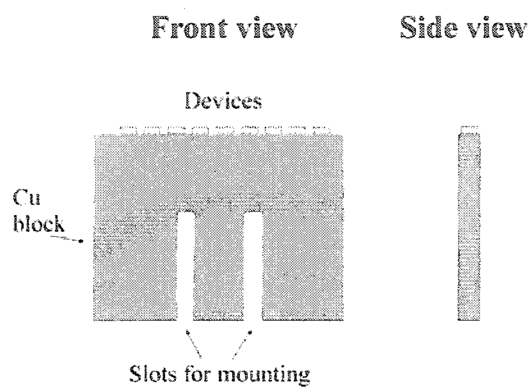

Figure 4-2: Illustration of the copper blocks upon which the devices are bonded.

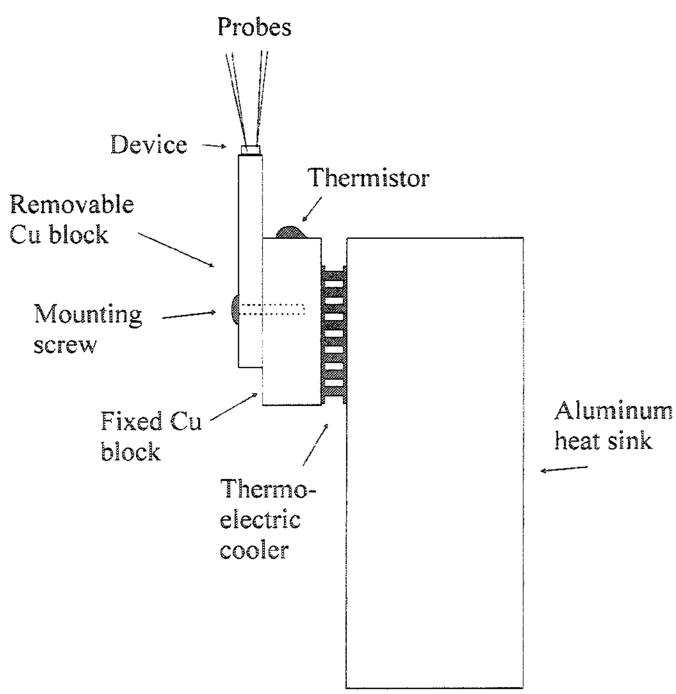

Figure 4-3: Schematic diagram of the mounting setup for the devices.

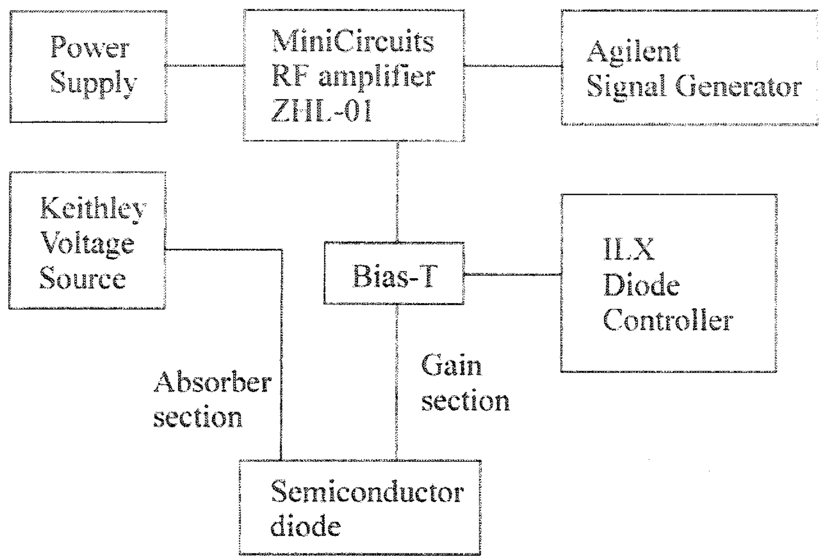

Figure 4-4: Layout of the electronics used to drive the semiconductor diode laser.

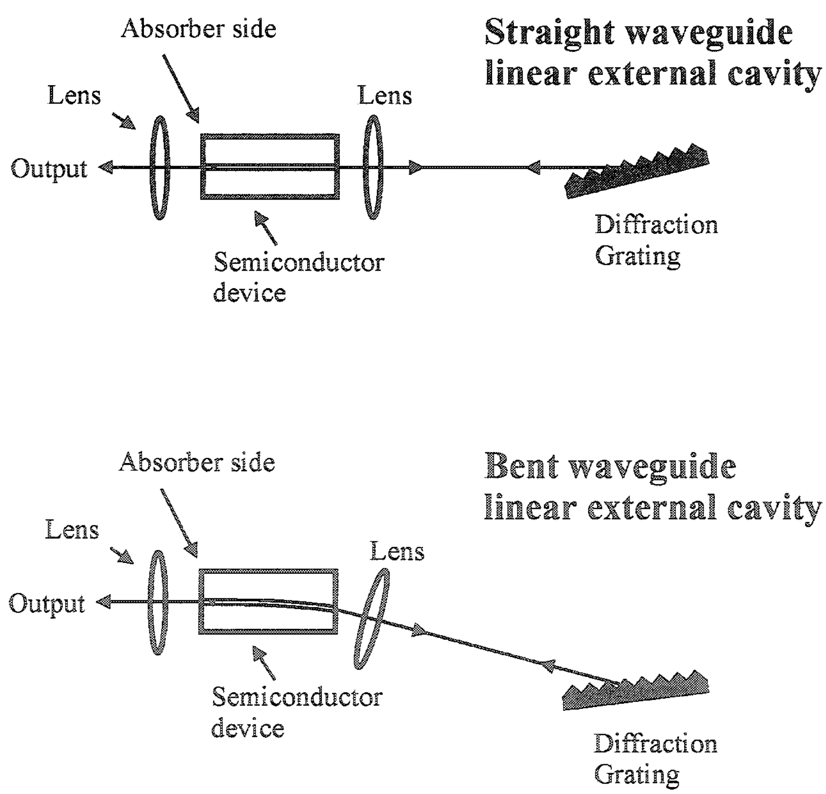

Figure 4-5: Linear external cavity arrangement used for mode-locking.

4.1.1.2 External Cavity Configurations

Two different external cavity arrangements are used for mode-locking the devices, a linear cavity and a ring cavity. The linear external cavity arrangement is shown in Figure 4-5. The figure illustrates the cavity for standard (straight) waveguide and bent-waveguide devices. With this arrangement, the repetition rate of the mode-locked laser is easily adjusted by translating the feedback element away from, or towards, the device. Wavelength selection is achieved by using a diffraction grating as the feedback element.

Figure 4-6 depicts the ring cavity arrangement used to mode-lock angled-facet devices. A beam-splitter with a transmission of ~ 10% at 980 nm was used as the output coupler for the cavity. Similar to the linear cavity case, the repetition rate of the laser is varied by changing the dimensions of the external cavity. However, due to the size of the mounts and the optical components making up the ring cavity, the repetition rate is limited to a frequency less than 400 MHz. Also, with the particular arrangement shown in Figure 4-6, changing the repetition rate is difficult and requires realignment of all of the cavity elements. In some experiments (i.e., laser synchronization), the ability to modify the repetition rate is paramount. The incorporation of a retro-reflector in the external cavity solves this problem, as is shown in Figure 4-7. Wavelength selection with the ring cavity is achieved by positioning a diffraction grating inside the cavity.

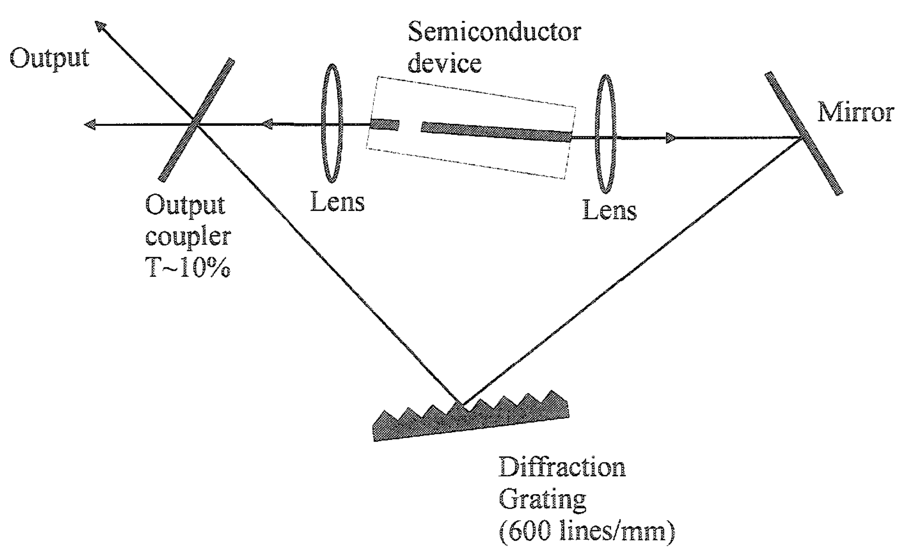

Figure 4-6: Ring cavity arrangement used for mode-locking.

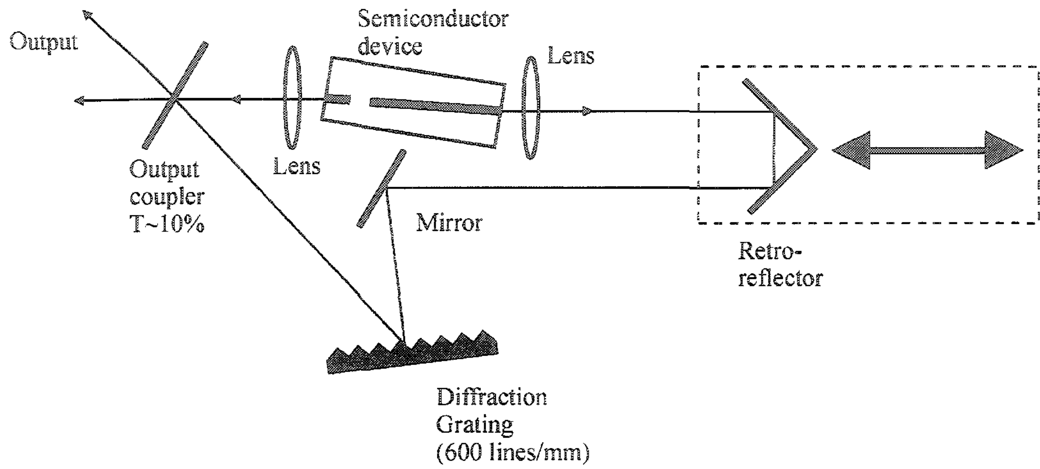

Figure 4-7: Ring cavity arrangement incorporating a retro-reflector to allow the repetition rate to be easily modified.

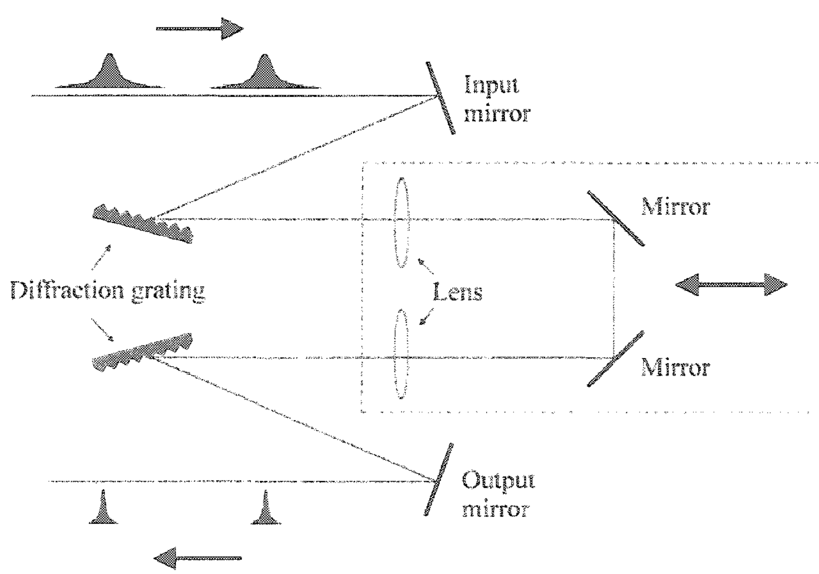

Figure 4-8: Schematic of the modified grating pair compressor used for pulse compression.

4.1.2 Pulse Compressor

A single pass modified grating pair compressor [128] is used to compress the mode-locked output from the oscillator. An illustration of the layout of the pulse compressor is shown in Figure 4-8. The compressor consists of two 1800 line/mm diffraction gratings, two 20 cm focal length biconvex lenses and several mirrors. The two lenses and two mirrors are arranged in a telescope geometry and are mounted on a moveable stage. Translating the stage adjusts the dispersion of the system. The input mirror can be positioned to maximize the compression of the optical pulses. The transmission efficiency of the compressor is approximately 50% due to the losses at the diffraction gratings.

4.1.3 Autocorrelator

An autocorrelator is used to measure the duration of the pulses generated by the mode-locked semiconductor laser. The interested reader should refer to reference [129] for more information on the use of autocorrelation for the measurement of short optical pulses. A schematic of the autocorrelator used to measure the duration of the pulses is shown below in Figure 4-9.

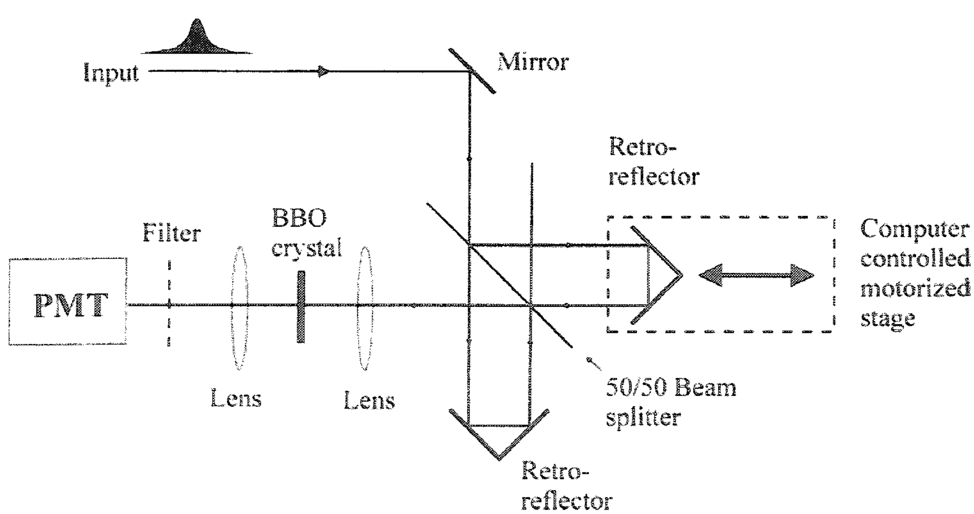

Figure 4-9: Schematic of the autocorrelator used to measure the pulse duration.

The beam-splitter is a 50/50 Newport ultrafast beam-splitter with an anti-reflection coating applied to one side. An Oriel Encoder Micrometer, model 18254, is used to change the path length on one of the arms of the interferometer.

The Oriel micrometer has a maximum travel of 25 mm, with a position resolution of 0.1 μm. The BBO crystal is 2 mm thick and has been cut for a wavelength of 1000 nm. Anti-reflection coatings at 1000 nm and at 500 nm have also been deposited on the crystal. The photomultiplier tube (PMT) is a standard 1P28 Hamamatsu PMT. Custom software was written in Microsoft Visual C++ 6.0 to drive the Oriel Encoder Micrometer while acquiring the signal from the PMT. The time resolution of the autocorrelator was assessed by measuring the second order autocorrelation trace of a ~150 fs pulse from a Ti:Sapphire laser. The full width at half maximum (FWHM) of the autocorrelation trace was measured to be 260 fs.

4.2 *Wavelength tunable pulse generation in the 980 nm wavelength regime*

This section presents the results obtained in developing a wavelength tunable mode-locked semiconductor laser in the 980 nm wavelength regime. Ultrashort pulses are generated via hybrid and passive mode-locking using a number of different laser structures and external cavity configurations. The first two subsections discuss preliminary mode-locking results obtained with both linear and ring cavities. The key results are presented in the remaining sections.

4.2.1 Preliminary mode-locking results

Preliminary work focussed on mode-locking a standard two-contact semiconductor laser operating in a linear external cavity. The reader should note that the word standard is used to imply that the waveguide of the laser does not contain any curved sections. Also, recall that the term two-contact refers to the fact that there are two separate p-contacts on top of the laser, in addition to the n-contact on the bottom of the laser.

First results were obtained with a device fabricated from the symmetric quantum well laser structure described in section 3.2.1. The two-contact device consists of gain section and an absorber section, measuring 525 μm and 125 μm, respectively. The absorber section length includes the length of a 40 μm gap separating the two sections. An AR coating is applied to the gain section facet of the device. The device is mounted in a linear external cavity with a 1200 line/mm diffraction grating for feedback, as shown in Figure 4-5. Figure 4-10 illustrates a second order intensity autocorrelation trace obtained by hybrid mode-locking this device.

For this particular case, the current applied to the gain section of the device is 45 mA and the absorber is biased with +0.9 V. The applied RF signal is at 700 MHz with a power of 30 dBm, as measured at the output of the RF amplifier. The device is operating at a wavelength of 1000 nm with a spectral width (FWHM) of approximately 0.65 nm, as shown in Figure 4-11. The secondary pulses in Figure 4-10 are a result of an imperfect AR coating having been deposited on the laser facet. Pulse durations typically achievable with this device under hybrid mode-locking measure between 2 and 5 ps, assuming a Gaussian pulse shape. The average output power ranges from as low as 300 μW to as high as 1.1 mW with typical powers lying in the 800 - 900 μW range.

Passive mode-locking of this device typically produces pulses with duration of approximately 5 ps. Average powers lie within a range similar to that achieved with hybrid mode-locking.

The mode-locked wavelength tuning range of this device is limited to a 20 nm window centred at 1008 nm. The most significant factor limiting the tuning range is believed to be the bandwidth of the imperfect AR coating. The secondary pulses visible in Figure 4-10 and the modulation at the laser chip Fabry-Perot mode spacing of the spectra shown in Figure 4-11 both indicate the need for an improved AR coating.

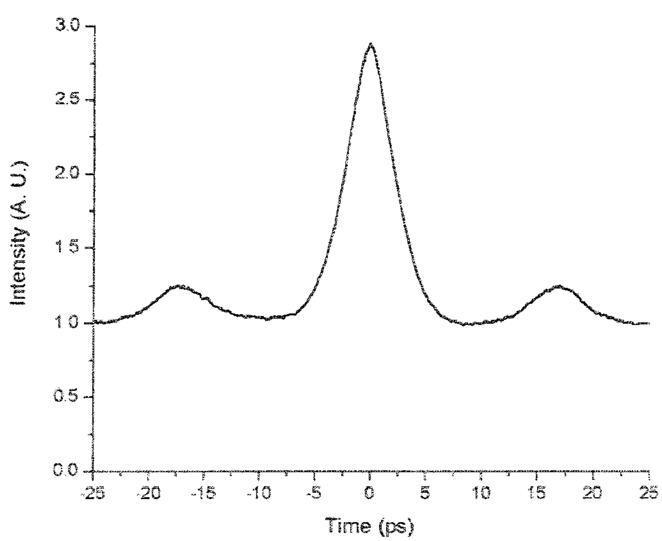

Figure 4-10: Second order intensity autocorrelation trace generated under hybrid mode-locking. The FWHM of the trace is 4.7 ps.

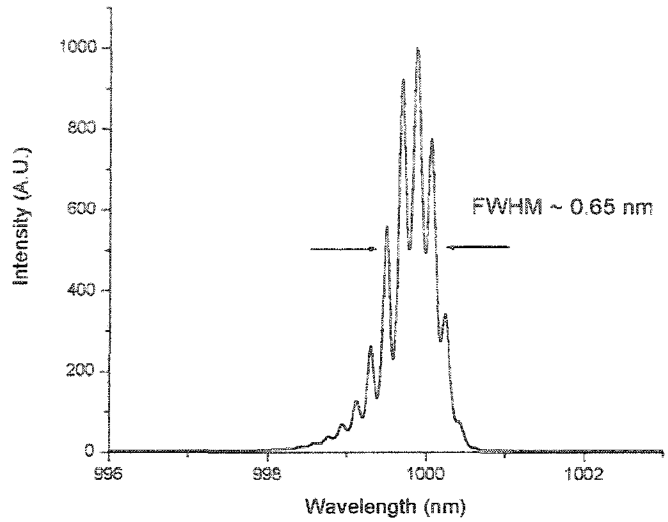

Figure 4-11: Optical spectrum measured under hybrid mode-locking for the autocorrelation trace presented in Figure 4-10.

Initial attempts at mode-locking a standard two-contact dual asymmetric quantum well device in a linear external cavity have been met with limited success. Hybrid mode-locking is achieved for a device of similar dimensions to the symmetric QW case. However, the pulses are longer in duration, typically measuring between 5 and 15 ps, and the system is not very stable while mode-locked. The underlying factor limiting the performance of this device is also deemed to be an imperfect AR coating on the facet. Spectral scans of the laser output have revealed significant modulation at the Fabry-Perot mode spacing of the device.

4.2.2 Ring Cavity Results

Due to the difficulties in routinely obtaining ideal AR coatings on the laser facets, dual angled facet devices were fabricated and tested. As discussed in section 3.7, the use of angled facets decreases the modal reflectivity of the facet, which in turn decreases the demands on the deposition process. Wavelength tunable short pulse generation with angled facet dual AQW lasers is achieved under hybrid mode-locking and passive mode-locking. Refer to Figure 4-6 for a schematic representation of the ring cavity layout.

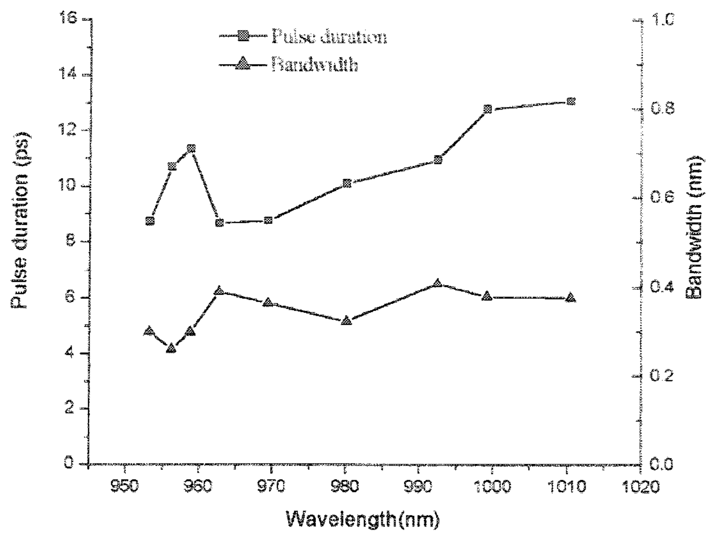

Figure 4-12: Pulse duration and bandwidth versus wavelength for an angled facet dual AQW device mounted in a ring cavity – hybrid mode-locking.

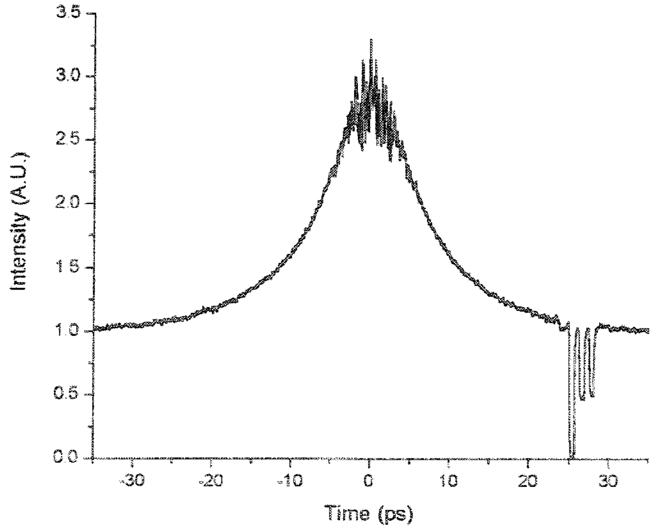

Figure 4-13: Second order autocorrelation trace of pulse train generated by hybrid mode-locking in a ring cavity. The FWHM is 12.4 ps. The first dip on the right side of the figure (from left to right) is a check of the background signal level (input to the autocorrelator was blocked). The last two dips are checks of the relative signal levels coming from each arm of the autocorrelator (ideally they should be equal).

The device used for hybrid mode-locking has a gain section measuring 400 μm in length, a 120 μm long absorber section and a gap separating the two sections that is 10 μm wide. The waveguide of the device terminates at an angle of 10° relative to the facet normal. The results for hybrid mode-locking are shown in Figure 4-12.

A mode-locked tuning range from 953 nm to 1010 nm is achieved with pulse durations ranging from 8 to 13 ps, assuming a Gaussian profile. The peak in the pulse duration data between 950 nm and 960 nm is likely due cavity alignment and the difficulty in achieving mode-locking for these wavelengths. The second order intensity autocorrelation for the data point at 969 nm is shown in Figure 4-13. The dips in the data on the right-hand side of the trace correspond to each arm of the interferometer being momentarily blocked in order to assess alignment.

The repetition rate of the mode-locked ring laser is 283 MHz. The relatively low frequency is due to the size of the external cavity required to include all the optical elements making up the ring cavity. The pump current on the gain section varies between 58 mA and 82 mA and the RF power measured at the output of the RF amplifier is 30 dBm. The average output power of the laser ranges from 200 μW to 350 μW. The spectral bandwidth of the pulses (FWHM) varies from 3 to 4 Å, resulting in time-bandwidth products ranging from 1.2 to 2.0. The time-bandwidth products are well beyond the Fourier limit indicating the presence of a large chirp on the pulse. While pulse compression is a viable option, the compressed pulses would still have durations on the order of a few picoseconds due to the limited bandwidth. From a technical perspective, this is not very interesting considering that picosecond pulses are routinely generated directly from mode-locked semiconductor lasers.

The device used for passive mode-locking in the ring cavity is 550 μm in length. The gain section is 510 μm long, the absorber section is 30 μm long, and the gap separating the two sections is 10 μm wide. The facet angles are identical to the previous case. Figure 4-14 illustrates the pulse duration and spectral bandwidth versus wavelength achieved by passively mode-locking this device.

As shown in the figure, a mode-locked tuning range from 960 nm to 1011 nm is achieved with pulse durations ranging from 7 to 15 ps, assuming a Gaussian profile. The external cavity size corresponds to a repetition rate of approximately 380 MHz. The applied current on the gain section of the device ranges from 44 to 77 mA. Average output powers are in the 270 μW to 1 mW range. The spectral bandwidth of the pulses varies from 3.1 to 6.6 Å, resulting in time-bandwidth products ranging from 1.0 to 3.2. For reasons stated earlier, compression of these chirped pulses is not pursued.

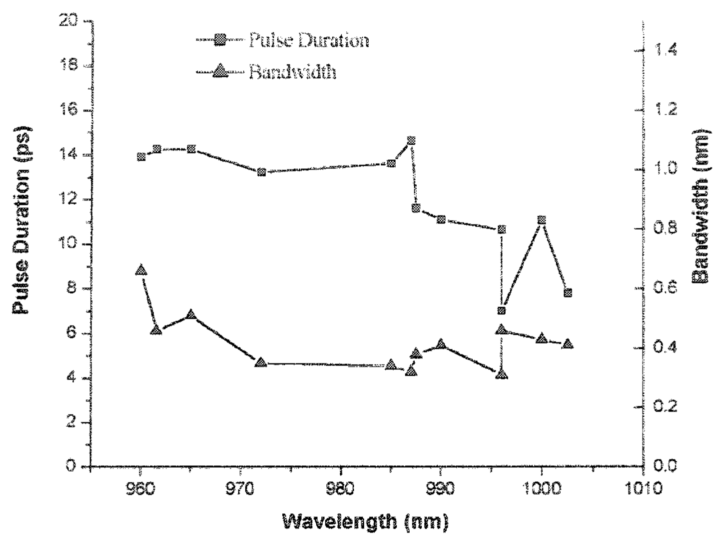

Figure 4-14: Pulse duration and bandwidth versus wavelength for an angled facet dual AQW device mounted in a ring cavity. The pulses were generated by passive mode-locking.

4.2.3 Bent Waveguide Devices – 2 AQW

This section presents the key results achieved with dual asymmetric quantum well devices incorporating a bend in the waveguide [130]. As stated in section 3.8, the bend in the waveguide allows for a simple external cavity design as compared with the ring cavity while at the same time providing easy access to a low modal reflectivity.

Passive mode-locking was first achieved with a bent waveguide device incorporating a dual asymmetric quantum well active region. Figure 4-15 depicts a schematic of the device used. The total device length is 550 μm, and is composed of two sections separated by a 10 μm gap. The saturable absorber is 40 μm in length and the gain section is 500 μm in length, with a portion of the gain section waveguide undergoing a bend over a length of 400 μm. The bend is an arc with a radius of curvature of ~ 4.6 mm, with the waveguide terminating at an angle of 5° relative to the gain section facet normal. A single layer SiO_xN_y anti-reflection (AR) coating is also applied to the angled facet end of the device.

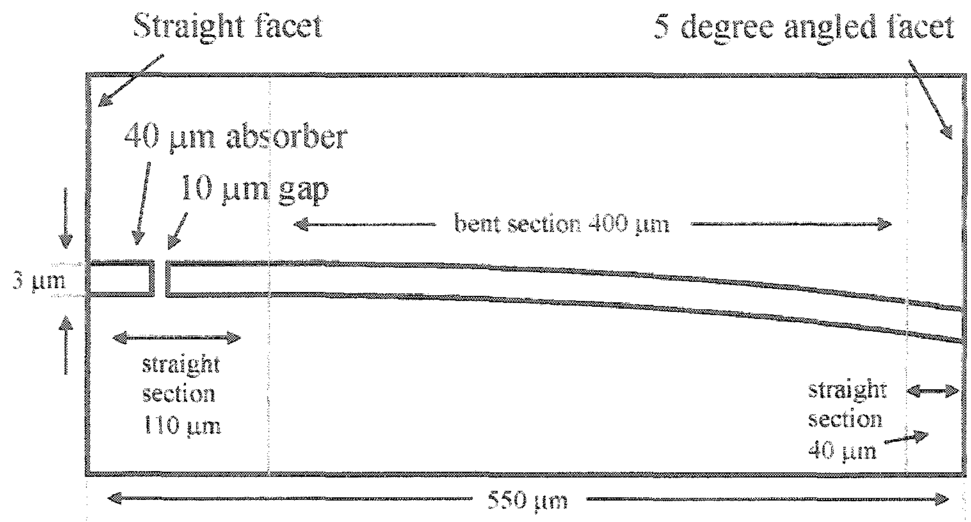

Figure 4-15: Schematic view of the two-contact, bent waveguide dual asymmetric quantum well device used for passive and hybrid mode-locking.

The external cavity configuration for this device was previously shown in Figure 4-5. Diffraction gratings of 1200 lines/mm and 600 lines/mm are used as feedback elements in the cavity. The external cavity measures approximately 21 cm in length, corresponding to a repetition rate of 700 MHz.

Passive mode-locking of the device is achieved over a tuning range of 61 nm. Figure 4-16 shows the results obtained using the 1200 lines/mm diffraction grating in the external cavity. The pulse durations are measured using the FWHM of the second order intensity autocorrelation and assuming a Gaussian pulse shape. At each wavelength, slightly different pulse durations can be obtained depending on the driving conditions of the device. The durations plotted, along with their spectral bandwidth and time-bandwidth product, correspond to the shortest pulses obtained at a given wavelength. Pulse durations between 2.5 ps and 4.3 ps are obtained over the full tuning range. The typical average powers of the pulses are approximately 500 µW, resulting in peak powers as high as 150 mW. The required current on the gain section varies from 49 mA to 89 mA, with larger values required toward the ends of the tuning range. The apparent trends in the data as a function of wavelength are not evident in all of the devices tested, making it difficult to formulate any general conclusions. At a 1005 nm wavelength and beyond, the presence of small satellite pulses delayed by the device round-trip time is evident in the autocorrelation traces. The cause of the satellite pulses is believed to be the poor performance of the AR coating at these wavelengths as well as a decreased absorption in the absorber section of the device. Tuning the wavelength below 954 nm or above 1015 nm results in longer, less stable pulses.

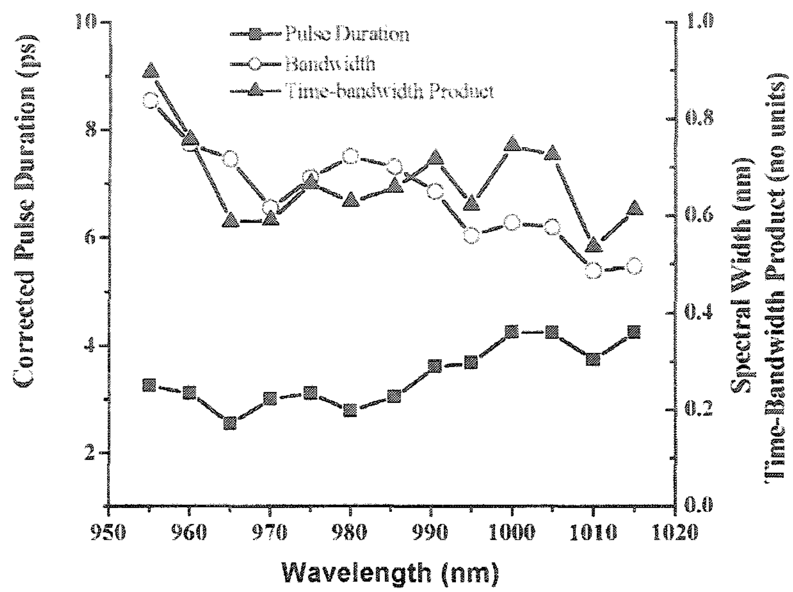

Figure 4-16: Mode-locked pulse durations, bandwidth and time-bandwidth product versus wavelength using the 1200 lines/mm diffraction grating. The pulse durations are computed assuming a Gaussian pulse shape.

In order to increase the spectral content of the pulses, a 600 lines/mm diffraction grating is used in the external cavity. The results obtained for this configuration are shown in Figure 4-17 and Figure 4-18. The average output power ranges from 450 μW to 1.3 mW. Although the pulse durations are slightly shorter with the 600 lines/mm grating as compared with the 1200 lines/mm grating, the spectral bandwidth of the pulses is 5 to 10 times larger, facilitating pulse compression. A single pass modified grating pair compressor is used to compress the output. At each wavelength, the grating pair compressor is adjusted to yield maximum pulse compression. The results for pulse compression are also shown in Figure 4-17. Pulse durations of 510 fs to 1 ps are obtained in the wavelength range of 955 nm to 1015 nm. At all wavelengths, a negative group velocity dispersion compresses the pulses, indicating a predominantly blue chirp. In addition, the time-bandwidth product of the compressed pulses remains above the transform limit by a factor of two or more, indicating the need for higher order dispersion compensation. Figure 4-19 shows a second order intensity autocorrelation trace of the shortest pulse obtained following compression, at a central wavelength of 998 nm. The compression by a factor of 7 provides a peak power of approximately 1.5 W.

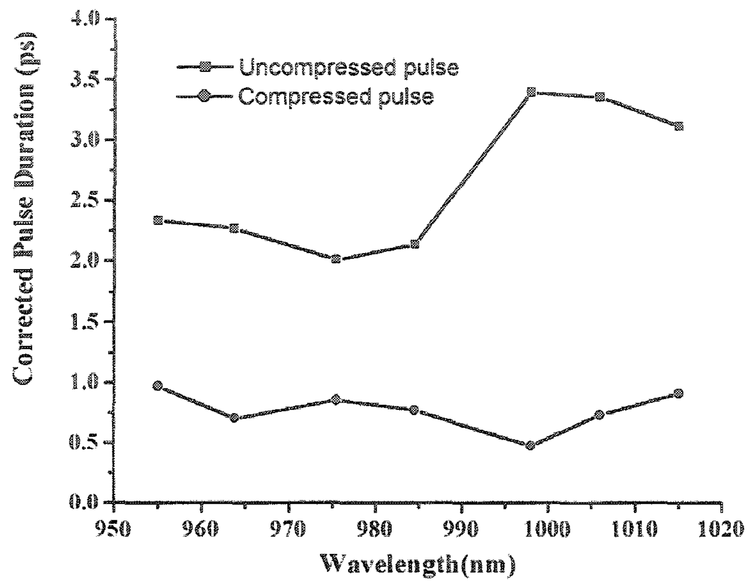

Figure 4-17: Compressed and uncompressed pulse duration versus wavelength using the 600 lines/mm diffraction grating in the external cavity

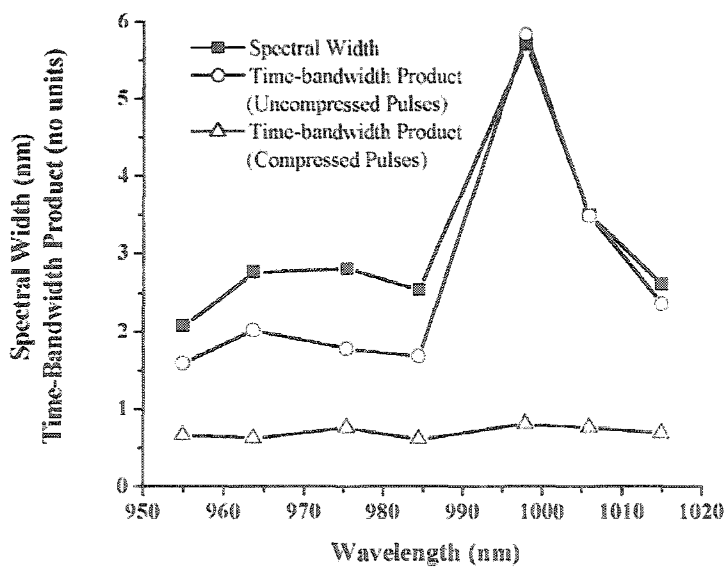

Figure 4-18: Spectral width (FWHM) and time-bandwidth product of the pulses shown in Figure 4-17.

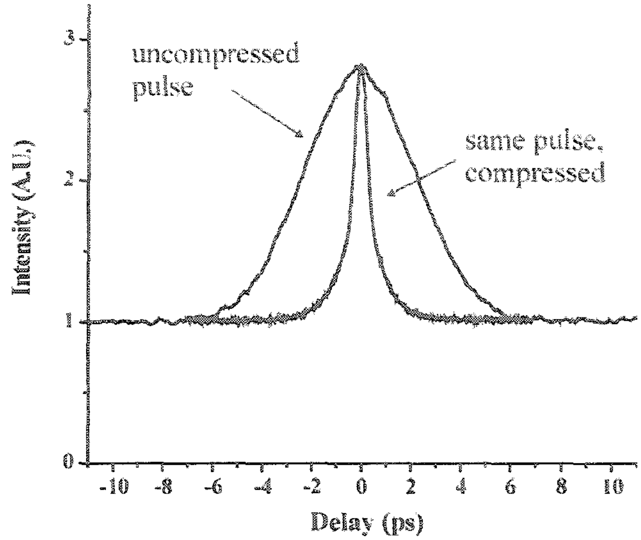

Figure 4-19: Second order intensity autocorrelation trace of a pulse before and after compression. The FWHM of the pulse before compression is 5.2 ps and 0.73 ps following compression.

To demonstrate the enhanced tuning range achieved with the use of an asymmetric quantum well active region, a similar device with a symmetric quantum well active region was mode-locked. The device is 525 μm in length, has a 40 μm long saturable absorber and a 500 μm long gain section. The gap separating the two sections is 10 μm wide. The waveguide undergoes a bend over a length of 420 μm such that it terminates at an angle of 7° relative to the facet normal. A single layer SiO_xN_y anti-reflection (AR) coating is also applied to the angled facet end of the device.

The external cavity is identical to that used for the asymmetric quantum well device. Diffraction gratings of 1200 lines/mm and 600 lines/mm are used as feedback elements in the cavity. The external cavity measures approximately 21 cm in length, corresponding to a repetition rate of 700 MHz.

Passive mode-locking is achieved over a tuning range of 35 nm. Figure 4-20 shows the results obtained using the 1200 lines/mm diffraction grating in the external cavity. The pulse durations are measured using the FWHM of the second order intensity autocorrelation and assuming a Gaussian pulse profile. Pulse durations between 5 ps and 15 ps are obtained over the explored tuning range. The typical average powers of the pulses are approximately 350 μW. The required current on the gain section varies from 59 mA to 80 mA, with larger values required toward the ends of the tuning range.

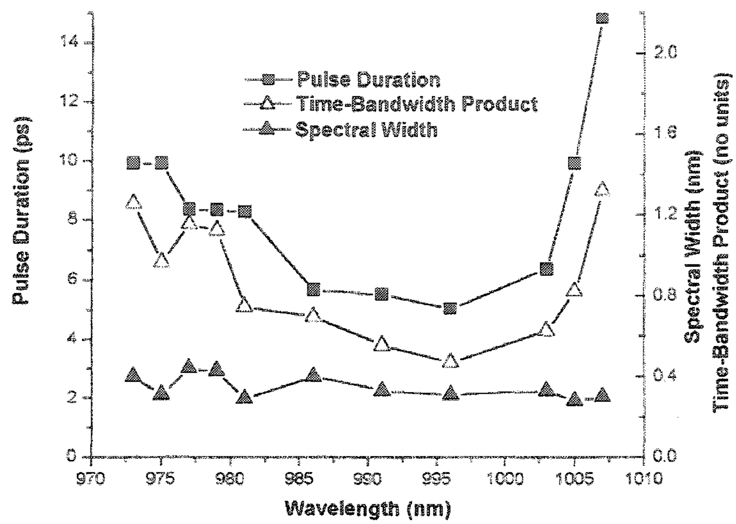

Figure 4-20: Mode-locked pulse durations, bandwidth and time-bandwidth product versus wavelength using the 1200 lines/mm diffraction grating. The active region of the device consists of two identical quantum wells.

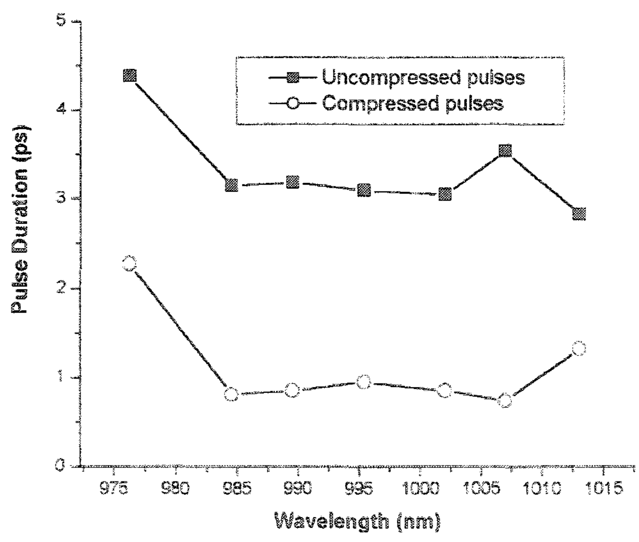

Figure 4-21: Pulse duration versus wavelength before and after compression from a passively mode-locked symmetric quantum well device. The pulse durations are determined from the autocorrelation traces by assuming a Gaussian pulse shape.

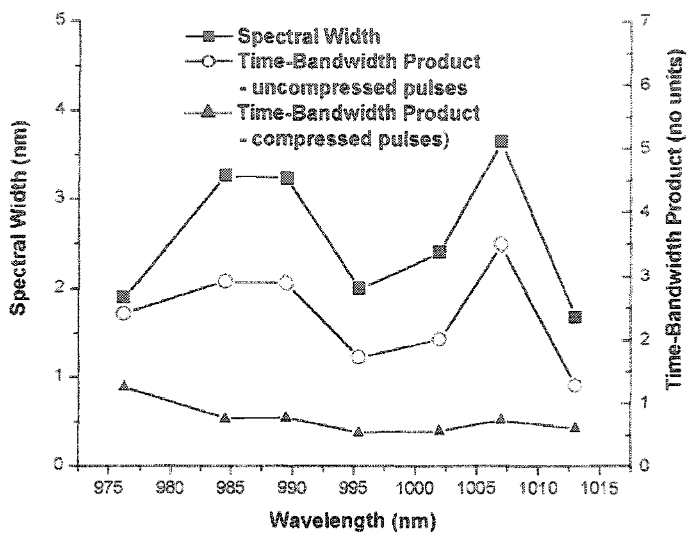

Figure 4-22: Spectral width and time-bandwidth product for the pulses shown in Figure 4-21.

As was the case with the asymmetric quantum well system, a 600 line/mm diffraction grating was introduced as the feedback element in the external cavity to broaden the spectral bandwidth of the pulses. The results obtained for passive mode-locking with the 600 line/mm grating are shown in Figure 4-21 and Figure 4-22. A tuning range of 37 nm with pulse durations ranging from 2.8 to 4.4 ps is obtained with the device. The bandwidth of the pulses varies from 1.7 nm to 3.7 nm, resulting in time-bandwidth products up to 11 times the Fourier limit. Compressed pulse durations ranging from 710 fs to 2.3 ps are achieved, with a mean duration of 1.1 ps.

In comparing the mode-locked tuning range of the asymmetric QW and symmetric QW devices, a larger tuning range is achieved for the asymmetric quantum well device. Also, it is quite difficult to achieve stable mode-locking of the symmetric quantum well device at wavelengths less than approximately 979 nm. With the asymmetric quantum well device, these difficulties are not encountered until tuning to wavelengths less than 957 nm.

4.2.4 Bent Waveguide Devices – 3 AQW

This section presents mode-locking results obtained with triple asymmetric quantum well devices incorporating a bend in the waveguide. Passive mode-locking is achieved over a broad tuning range with a number of different devices. Preliminary results indicate that the length of the device affects the overall tuning range of the mode-locked laser.

Passive mode-locking is observed using devices of three different lengths, 500 μm, 720 μm and 1260 μm. The details regarding the length of each of the sections are shown in Table 4-1.

Table 4-1: Lengths of the gain section and absorber section for each of the device lengths used. Note that the absorber section length includes the 10 μm gap, present in all devices

Device Length (μm)	Gain Section Length (μm)	Absorber Section Length (μm)
500	440	60
720	660	60
1260	1140	120

A linear external cavity with a 1200 ln/mm diffraction grating as the feedback element is used for each of the device lengths tested. The external cavity length corresponds to a repetition rate of approximately 670 MHz in all cases.

The mode-locking results obtained with the 500 μm long device are shown in Figure 4-23. Pulses ranging from 2 ps to 11 ps in duration are generated at wavelengths ranging from 942 nm to 1017 nm. Current on the gain section varies from as low as 30 mA to as high as 50 mA for the different data points. The typical average output power measures 600 μW. The spectral bandwidth typically lies within the range of 0.6 - 0.9 nm.

In comparison with the 2-AQW device, the 500 μm long 3-AQW device can achieve a 24% increase in the mode-locked tuning range. Unfortunately, the generated pulses tend to be of poor quality with this particular 3-AQW device. That is to say, a fairly broad pedestal is often evident in the autocorrelation traces. As an example, the autocorrelation trace corresponding to the data point at 944 nm is shown in Figure 4-24. The pedestal in the trace may be the result of a long secondary pulse following the main pulse.

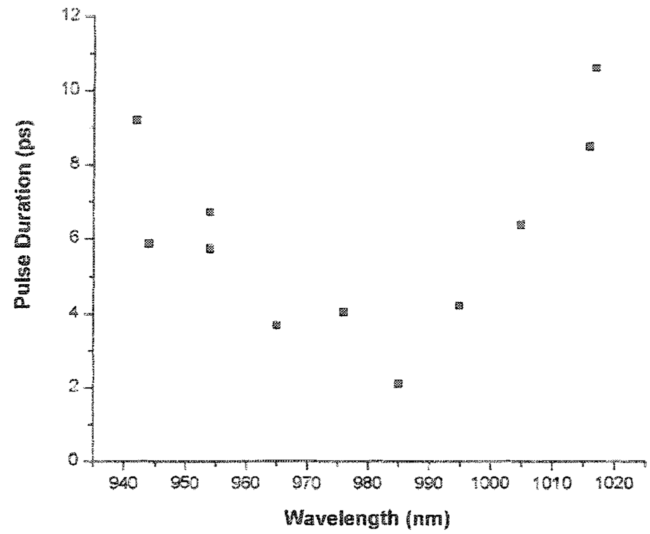

Figure 4-23: Pulse duration versus wavelength for a passively mode-locked 3 AQW laser. The total length of the device is 500 μm. A Gaussian pulse profile is assumed.

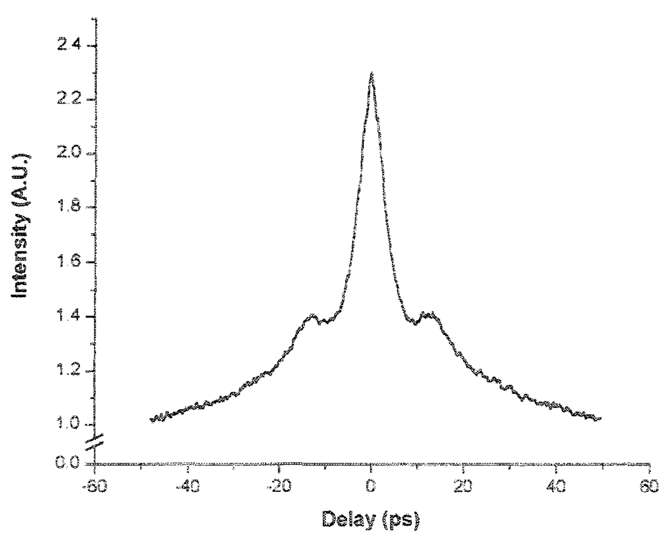

Figure 4-24: Second order intensity autocorrelation trace of a pulse train generated by the 500 μm long 3 AQW passively mode-locked laser.

The mode-locking results obtained with the 720 μm long device are shown in Figure 4-25. Pulses ranging from 2.6 ps to 6.8 ps in duration are generated at wavelengths ranging from 948 - 1013 nm, for a total tuning range of 65 nm. The current on the gain section varies from as low as 23 mA to as high as 56 mA for the different data points. The typical average output power is approximately 500 μW. The spectral bandwidth (FWHM) lies within the range of 0.6 - 1.0 nm. The scatter in the data in Figure 4-25 is due to the difficulty in passively mode-locking this particular device. This makes optimization of the pulse duration at each of the wavelengths a time-consuming process.

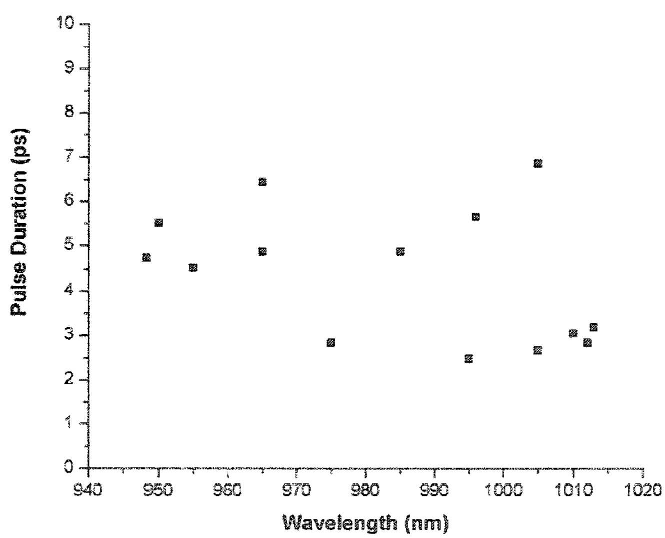

Figure 4-25: Pulse duration versus wavelength for a passively mode-locked 3 AQW laser. The total length of the device is 720 μm. A Gaussian pulse profile is assumed.

As opposed to the previous case, the pulses emitted by this device do not show any evidence of a pedestal on the autocorrelation traces. A typical second order intensity autocorrelation trace is shown in Figure 4-26. The FWHM of this particular trace is 6.4 ps, and the central wavelength is 955 nm.

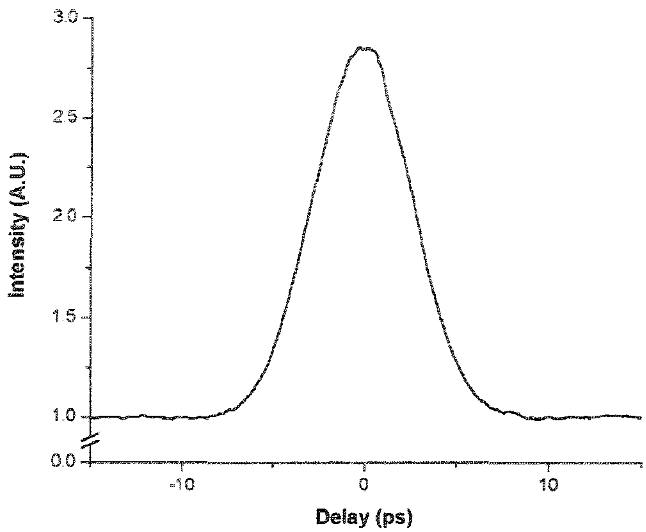

Figure 4-26: Second order intensity autocorrelation trace of a pulse train generated by the 720 μm long 3AQW passively mode-locked laser.

The mode-locking results obtained with the 1260 μm long device are shown in Figure 4-27. Pulses ranging from 2.5 ps to 9.7 ps in duration are generated at wavelengths ranging from 965 nm to 1015 nm, for a total tuning range of 50 nm. The current on the gain section varies from as low as 33 mA to as high as 64 mA for the different data points. The typical average output power is approximately 400 μW. The spectral bandwidth lies within the range of 0.6 - 1.0 nm.

The passively mode-locked tuning range obtained with each device length is summarized below in Table 4-2. For the device lengths tested, the tuning range increases as the length of the device decreases. It should also be noted that performing the tuning experiment with the laser operating in continuous-wave (cw) produced results similar to the mode-locked situation. It is believed by the author that amplified spontaneous emission is responsible for limiting the tuning range at the longer device lengths.

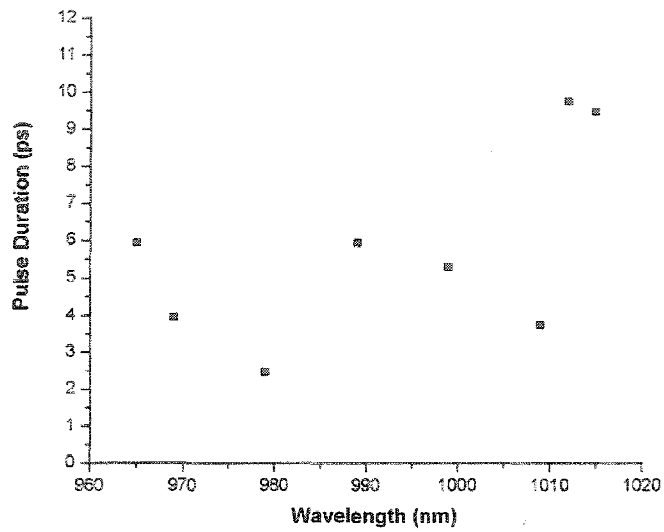

Figure 4-27: Pulse duration versus wavelength for a passively mode-locked 3 AQW laser. The total length of the device is 1260 μm. A Gaussian pulse profile has been assumed.

Table 4-2: Summary of the tuning range obtained with each device length.

Device Length (μm)	Tuning Range (nm)
500	75
720	65
1260	50

The means by which the amplified spontaneous emission is limiting the tuning range can be understood as follows. The tuning experiments are performed with an external cavity configuration incorporating a diffraction grating for feedback. The diffraction grating introduces significant losses for all wavelengths except for the band of wavelengths, λ_{FB}, being fed back into the waveguide. In order for the laser to operate at the λ_{FB} (mode-locked or cw), the gain of the system must equal the loss of the system at λ_{FB}. Now consider the situation where the short device will lase at a λ_{FB} whereas the long device will not. Assuming the losses are dominated by the external cavity, it can be assumed that the losses are approximately equal for the two systems. This means that the single pass gain (and carrier density in the quantum wells) of the short device must be larger than that of the long device at λ_{FB}. Since the long device will not operate at λ_{FB} even under high current injection, the carrier density in the quantum wells of the long device is being clamped at a much lower value as compared with the short device. The long device is not lasing at λ_{FB}, hence amplified spontaneous emission must be responsible for clamping the carrier density. The reason that the carrier density is being clamped in the long device and not in the short device is because the longer device allows for a greater build up of ASE. As discussed in section 3.3.2, the tuning range of the 3-AQW devices is expected to be very sensitive to the carrier density in the active region. At low carrier densities, the gain of the blue well (well #3 from Figure 3-9) is insufficient to overcome the losses induced by the red well (well #1 from Figure 3-9) at wavelengths within the blue well's gain bandwidth. The gain of the blue well only contributes to a positive gain at these wavelengths when the carrier density in the red well is sufficiently high such that the gain bandwidth of the red well broadens and begins to overlap with the blue well. With this in mind, it is believed that the ASE is clamping the current density in the long device to a sufficiently low value such that the gain bandwidth of the red well does not overlap with the blue well. In the short device, there is less ASE, and as such, much higher carrier densities can be achieved in the quantum wells.

Evidence supporting gain clamping due to spontaneous emission is also visible at the red end of the tuning range of for the 1260 μm long device. The device is operated cw at a wavelength of 1013 nm (tuned by a 1200 ln/mm grating), with a current of 56 mA on the gain section. With the absorber unbiased or reverse biased, the overall gain is sufficiently high such that lasing occurs with an output power of 2.3 mW. The output power is measured by looking at the power within a small spectral band (~4 nm) centred about 1013 nm. Applying a forward bias to the absorber results in a decrease in the output power of the laser, down to 760 μW at 1013 nm. This is counter intuitive since a forward bias decreases the saturation energy of the absorber section and should result in an overall increase in output power. However, the ASE, which peaks around 1003 nm, also sees a decrease in absorption. This decrease in absorption allows significant build-up of the ASE, significantly affecting lasing at 1013 nm. In fact, measuring the ASE at the output of the gain section under the different biasing conditions shows a power increase from 4.7 mW to 13.4 mW when switching from a reverse-bias (or no bias) to a forward bias on the absorber (under cw operation). Recall that the output power at 1013 nm decreases when switching from a reverse-bias (or no bias) to a forward bias.

4.3 Ultrashort pulse generation with long wavelength InGaAs/GaAs lasers

As previously discussed, growth of long wavelength InGaAs/GaAs lasers is difficult due to the large strain of the InGaAs quantum well. The first step in developing a broadly tunable mode-locked long wavelength InGaAs/GaAs laser is to generate ultrashort pulses with devices based on a single quantum well active region. This section presents the results achieved with these preliminary devices. A summary of these results can also be found in reference [131].

The devices used for short pulse generation are similar in geometry to that shown in Figure 4-15. The results presented are for a 900 μm long device containing a 90 μm long absorber section that is separated from the gain section by a 10 μm gap. The 800 μm long gain section consists of a 100 μm long straight section and a 700 μm long bend with a radius of curvature of 5700 μm that terminates at an angle of 7° relative to one of the facet normals.

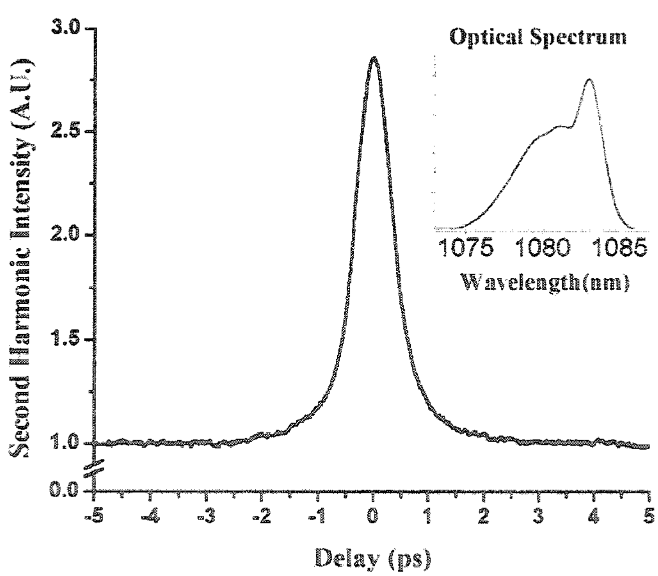

Figure 4-28: Autocorrelation trace of a pulse following compression. Assuming a Gaussian pulse shape, the pulse duration is 570 fs. The optical spectrum of the pulse train is shown in the inset.

Pulses generated by the oscillator under passive mode-locking and hybrid mode-locking typically have a duration between 2 and 5 ps. The duration is determined by measuring the full-width at half maximum of the autocorrelation trace with an assumed Gaussian pulse shape. The length of the external cavity used corresponds to a repetition rate of approximately 850 MHz. Average powers, measured at the output of the oscillator, vary from as low as 750 μW to as high as 1.8 mW. The current on the gain section varies from 45 – 60 mA, and the RF power ranges from 10 – 26 dBm, in the case of hybrid mode-locking. Under the experimental conditions tested, there was no discernable difference in pulse duration under passive mode-locking as compared with hybrid mode-locking. However, hybrid mode-locking has the advantage of increased stability and a larger parameter range over which the oscillator will remain mode-locked. This allows the operating parameters to be modified to optimize the output power, and as such, hybrid mode-locking of this oscillator tends to yield higher average output powers as compared with passive mode-locking of the oscillator.

An external modified grating pair compressor consisting of two 1800 lines/mm diffraction gratings is used to compress the pulses generated by the oscillator. Pulse durations as short as 570 fs are obtained following compression. The autocorrelation trace of a 570 fs pulse train is shown in Figure 4-28. The uncompressed pulse had a duration of 4.2 ps, and is obtained via hybrid mode-locking at a repetition rate of 873 MHz with an RF power of 11 dBm. The absorber section is biased with –1.4 V and the gain section is driven with 56 mA. A mirror is used as the feedback element in the external cavity. The average power is reduced from 1.8 mW to approximately 900 μW following compression due to the losses of the diffraction gratings.

4.4 Mode-locking and Repetition Rate

The dependence of the mode-locked output on the repetition rate was examined for a passively mode-locked symmetric quantum well device. The device is the same symmetric quantum well device used to obtain the results presented earlier in section 4.2.3. For the purposes of this study, the diffraction grating in the external cavity is replaced with a dielectric mirror (R ~ 99.9%). Modifying the repetition rate requires translation of the feedback element. If a diffraction grating were to be used in place of a mirror, the spectral bandwidth captured by the coupling lens would vary with repetition rate.

The device is passively mode-locked at repetition rates varying from 630 MHz to 2230 MHz. This corresponds to external cavity lengths ranging from 6.7 cm to 23.8 cm. In order to ensure minimal variation of the external cavity coupling at the various cavity lengths, the cavity length is changed in small increments with a translation stage. When the translation stage reaches the end of travel, the stage is repositioned. Operating the device in the cw regime and monitoring the output power allows the external cavity coupling to be maintained between coarse repositioning (moving the entire translation stage) of the end reflector.

For all of the repetition rates studied, the current on the gain section is 65 mA (bias of ~ 2.8 V) and the bias on the absorber section is –1.7 V. The wavelength of operation is 1002 nm. The output of the device into the external cavity is focussed onto the mirror by the coupling lens. The system exhibits greater stability when the beam is focussed onto the feedback element as opposed to collimating the beam.

The average output power of the mode-locked laser as a function of repetition rate is shown in Figure 4-29. The output ranges from 650 μW to 950 μW with the peak output power occurring at a repetition rate of 1400 MHz. The cw case is also plotted in the figure to ascertain whether the external cavity itself is influencing the mode-locking results. Although the cw output power is changing for the different cavity lengths, the trend is quite different than that exhibited by the mode-locked laser. One of the factors contributing to the change in cw power at different the cavity lengths is the fact that the laser output is focussed on the external cavity feedback element. As such, the position of the coupling lens needs to be changed relative to the diode facet as the cavity length is modified. This affects the amount of light captured by the lens and may affect the overall external cavity coupling efficiency. This will in turn impact the mode-locking results obtained at the different repetition rates.

Aside from the influence of the external cavity, other factors such as the gain recovery and spontaneous emission are contributing to the change in average power of the mode-locked laser at the various repetition rates.

At high repetition rates, the gain of the laser will not have a chance to fully recover between the pulses. Pulses generated at these repetition rates will experience a smaller gain than pulses generated at slower repetition rates. As such, the average output power of the mode-locked laser is expected to be larger for smaller repetition rates. Repetition rates of 630 MHz and 2200 MHz correspond to periods of 1.6 ns and 454 ps respectively. The gain recovery lifetime is typically measured in the hundreds of picoseconds [132, 133], with a full recovery of the gain not occurring for a time interval several times the lifetime. As a result, it is expected that the gain recovery lifetime will influence the output power of the laser at some of the higher repetition rates studied.

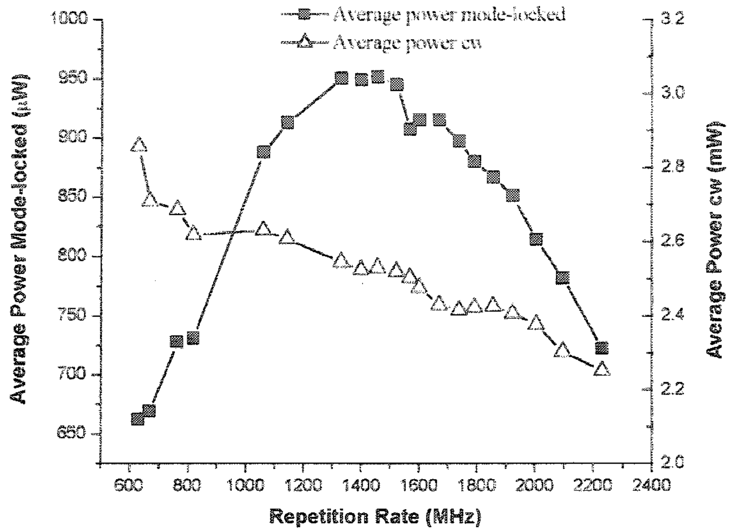

Figure 4-29: Average mode-locked power and average cw power versus repetition rate. Note: 1) In the cw case, the repetition rate label is used to indicate the length of the external cavity. 2) The relatively low cw output power is a direct result of the absorber section being biased below transparency for the cw power measurements.

Spontaneous emission will influence the output power if the period of the pulses is sufficiently large so as to allow ASE to build up between the pulses. The spontaneous emission lifetime of semiconductor laser is approximately 1 ns [29], while a repetition rate of 630 MHz corresponds to a period of 1.6 ns. At low repetition rates, the amplified spontaneous emission reduces the amount of gain available for the pulses as they pass through the gain section. The higher the repetition rate, the less time there is for the build up of amplified spontaneous emission. As such, it is expected that the average output power of the laser increase with repetition rate, assuming the period is on the order of the spontaneous emission lifetime.

The degree to which each of these effects contributes to the trend in Figure 4-29 is difficult to ascertain due to the influence of the external cavity. However, the data is still interesting from an applications perspective. For applications such as two-photon spectroscopy, the repetition rate capable of generating the largest signal is of interest. In order to determine the optimal repetition rate, other relevant parameters are examined at each of the repetition rates.

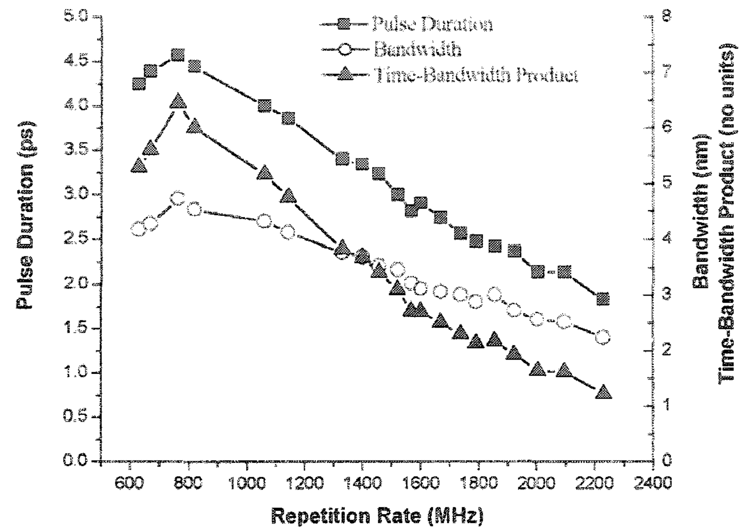

Figure 4-30: Pulse duration, bandwidth and time-bandwidth product as a function of repetition rate for the external cavity passively mode-locked symmetric quantum well laser. Note that while it may seem counterintuitive that the bandwidth is decreasing as the pulse duration is decreasing, it must be kept in mind that the time-bandwidth product of the pulses is well above the transform limit.

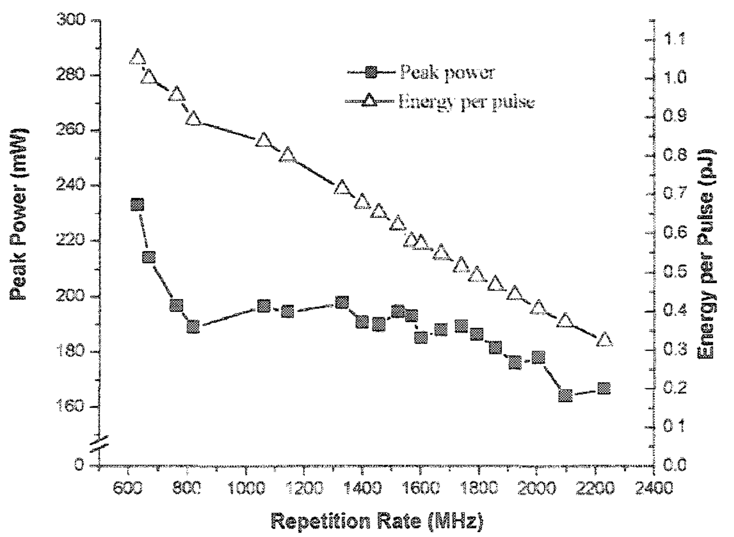

Figure 4-31: Peak power and energy per pulse versus repetition rate for the external cavity passively mode-locked symmetric quantum well laser.

The pulse duration, bandwidth and time-bandwidth product for the mode-locked laser are shown in Figure 4-30 as a function of repetition rate. In general, the values of these parameters decrease as the repetition rate increases. While it seems counter-intuitive that the pulse duration is decreasing while the bandwidth is also decreasing, recall that the pulses are not transform-limited. As such, the time-bandwidth product is tending towards the transform limit at higher frequencies.

The peak power of the pulses and the energy per pulse is shown in Figure 4-31 as a function of repetition rate. This figure is produced with the data from Figure 4-29 and Figure 4-30. The energy per pulse is monotonically decreasing as a function of the repetition rate. The peak power of the pulse is also decreasing, but at a much slower rate.

Examination of both Figure 4-30 and Figure 4-31 reveal that the pulse width is tending towards shorter values while the pulse energy is also decreasing. The pulse width versus the pulse energy is plotted in Figure 4-32. Based on the figure, the pulse width is seen to vary almost linearly with the pulse energy. This trend is in direct contrast to analytical theories based on the self-consistent profile approach developed by Haus [73]. According to Haus' theory, the pulse width is inversely proportional to the pulse energy. The model by Dubbeldam *et al.*, also based on Haus' approach, states that the pulse duration is inversely proportional to the square root of the pulse energy [134]. The disagreement between this theory and our experiment is not too surprising considering the number of approximations that are made in Haus' approach. The first approximation is that any changes to the pulse at any point in one round-trip through the laser cavity are small. This assumption is not accurate for semiconductor lasers because of the very high gain exhibited by these systems. Some of the other approximations include the neglect of self-phase modulation, treatment of the pulse as a plane wave and the neglect of spontaneous emission.

Better agreement can be achieved by using a numerical approach, such as the model outlined by Derickson *et al.* [29]. Attempting to achieve the shortest pulse possible with a passively mode-locked laser is equivalent to finding the conditions that generate the maximum pulse shaping per pass. Derickson shows that, for a given gain and absorber section configuration, there is an optimal pulse energy that results in maximum pulse shaping. Increasing or decreasing the pulse energy relative to this optimal value reduces the pulse shortening per pass. Assuming that the pulse energy is larger than the optimal value, the pulse shortening per pass will increase as the pulse energy decreases. This is predicted with a simplified version of Derickson's full model and it qualitatively agrees with what is seen in Figure 4-32.

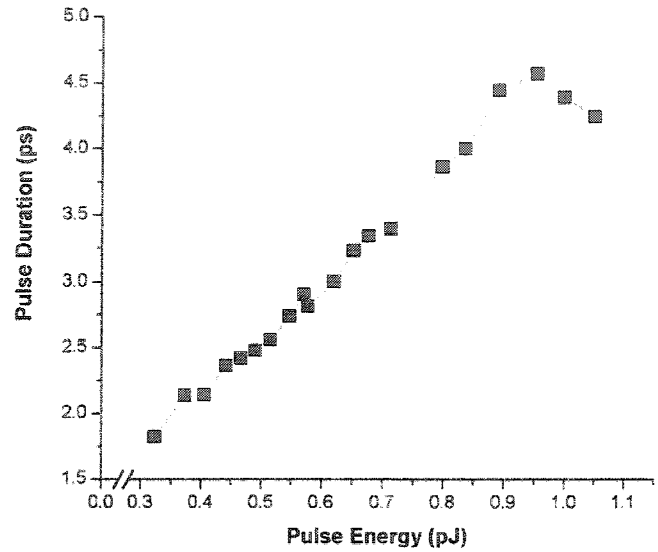

Figure 4-32: Pulse duration versus pulse energy for the data shown in Figure 4-30 and in Figure 4-31.

Referring back to Figure 4-30 and Figure 4-31, the maximum signal generation per pulse for a two-photon process will occur at 630 MHz (based on integration of Gaussian pulse shape). However, since a train of optical pulses generates the detected signal, the repetition rate needs to be taken into consideration. Although the pulse energy is lower at higher frequencies, there are more pulses in a given time interval generating signal as compared with the lower frequencies. Figure 4-33 shows an estimate of the second harmonic signal generated by the mode-locked laser relative to the peak signal value, at the different frequencies. The data points in the figure are computed assuming each pulse will generate a signal proportional to the integral of the square of its power profile, as shown in equation (4.1).

$$S \propto \int P^2(t)dt \tag{4.1}$$

where S is the second harmonic signal generated per pulse, and $P(t)$ is the power profile of the pulse. In all cases, a Gaussian profile is assumed. The results are then multiplied by the repetition rate in order to determine the amount of signal generated per second. Based on these calculations, a repetition rate between 1300 and 1500 MHz is ideal, which corresponds to external cavity lengths between 10.0 and 11.5 cm. These particular repetition rates were not used for the mode-locked tuning range data presented in the previous sections for two reasons. The first reason is that the repetition rates were kept below 1 GHz so that hybrid mode-locking could be used, if so desired. The RF amplifier operates at frequencies below 1 GHz. The second reason is that the results in this section were taken *after* (many months) the results from the previous sections had been obtained.

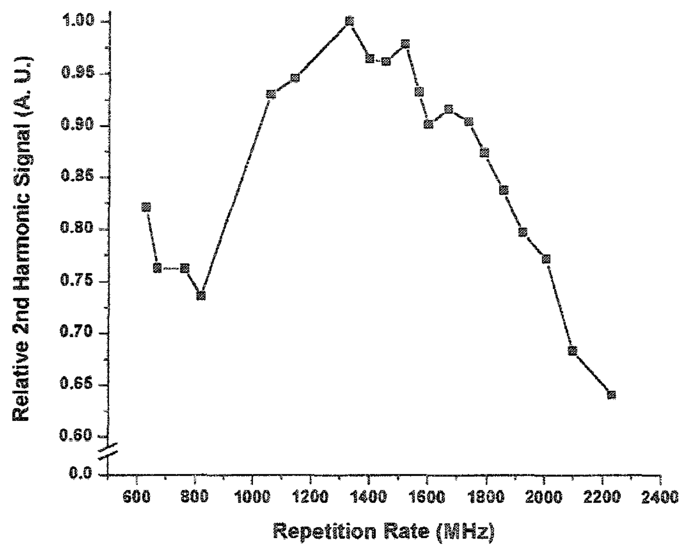

Figure 4-33: Second harmonic signal generated per second by the mode-locked laser versus repetition rate. The signal level is measured relative to the peak value of the second harmonic signal. A Gaussian profile is assumed at all repetition rates. Note that this data is derived from the data in Figure 4-30 and Figure 4-31.

4.5 Monolithic mode-locking results

While monolithic passive mode-locking of the devices does not easily permit wavelength tuning, it was briefly explored due the simplicity involved in setting up the experiment, and to provide a benchmark for the external cavity work.

Two devices of different lengths are chosen for a demonstration of monolithic passive mode-locking. The first device consists of a dual asymmetric quantum well active region and a total length of 1.2 mm. The gain section has a length of 1.1 mm, the absorber section length is 90 μm and the gap separating the two sections is 10 μm wide. The second device contains a symmetric quantum well active region and is 660 μm in length. The gain section is 600 μm long, the absorber section has a length of 50 μm and the gap separating the two sections is 10 μm wide. The facets of both devices are as-cleaved.

A second order intensity autocorrelation trace of the pulses generated with the longer of the two devices is shown in Figure 4-34. The pulses are generated with 82.6 mA of current applied to the gain section and a bias of −1.0 V applied to the absorber section. The pulse repetition rate can be determined directly from the figure and is determined to be 31 GHz. The average output power under these conditions is 1.97 mW. The pulse duration is 1.5 ps, assuming a Gaussian profile. The corresponding spectrum is shown in Figure 4-35. The time-bandwidth product is determined to be 0.53, which is a factor of 1.2 larger than the transform limit.

Changing the biasing parameters results in higher output powers. However, the pulse width and spectrum tend to be broader at the higher output powers. Also, biasing at higher currents results in a shift in the optical spectrum of the pulse towards the blue end of the spectrum. For instance, a gain section current of 156 mA and a bias of -0.96 V on the absorber section results in 2.2 ps pulses with an average output power of 7.33 mW. The central wavelength of the spectrum is 1006 nm and the time-bandwidth product is 2.47. While this does allow for pulse compression, the shortest pulse obtained by post compression is 810 fs, still a factor of two larger than the transform limit.

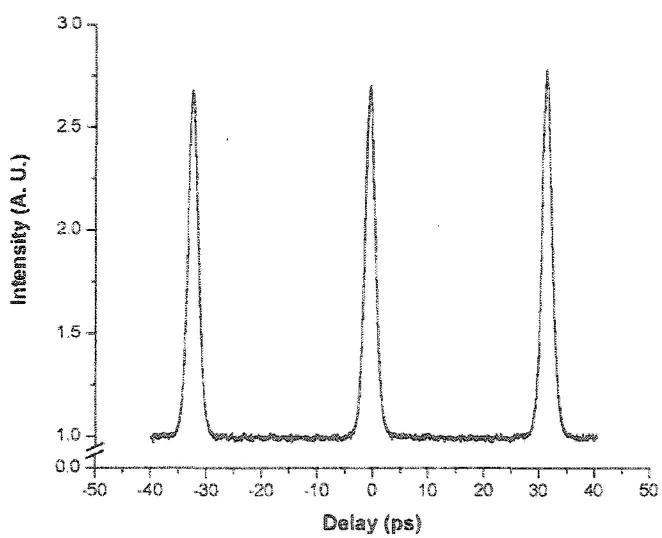

Figure 4-34: Second order intensity autocorrelation trace of a passively mode-locked monolithic semiconductor laser having a length of 1.2 mm.

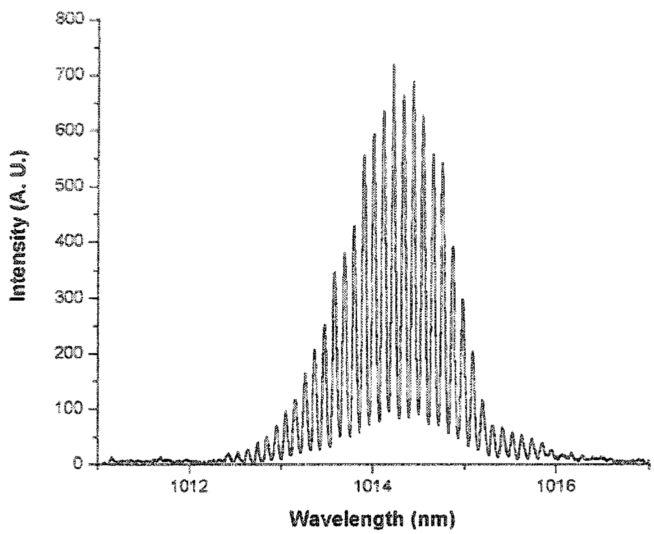

Figure 4-35: Optical spectrum for the pulse train shown in Figure 4-34.

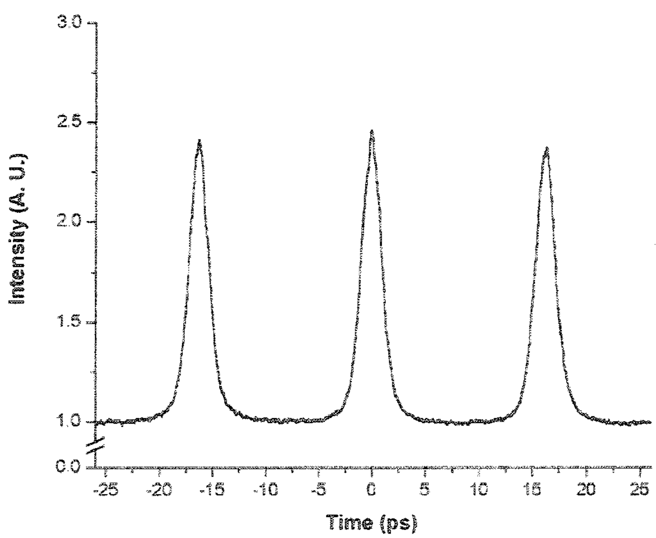

Figure 4-36: Second order intensity autocorrelation trace of a passively mode-locked monolithic semiconductor laser having a length of 660 μm.

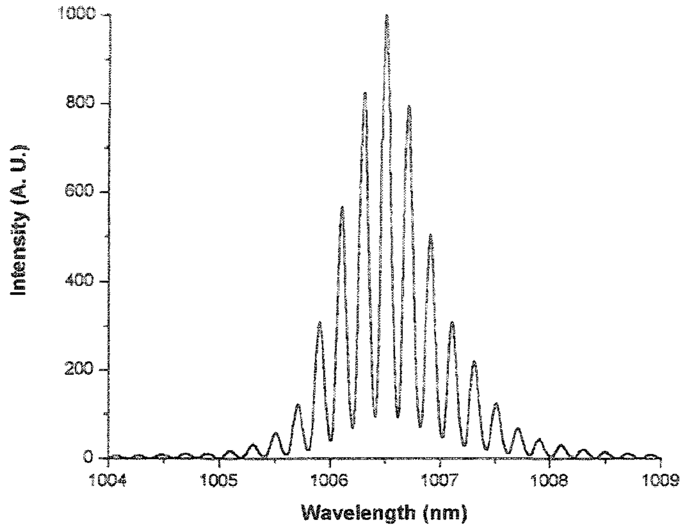

Figure 4-37: Optical spectrum for the pulse train shown in Figure 4-36.

A second order intensity autocorrelation trace of the results obtained with the 660 μm long device is shown in Figure 4-36. The pulses are generated with 33.8 mA of current applied to the gain section and a bias of –1.8 V applied to the absorber section. The pulse repetition rate is measured to be 61 GHz. The average output power under these conditions is 2.42 mW. The pulse duration is 1.5 ps, assuming a Gaussian profile. The corresponding spectrum is shown in Figure 4-37. Determination of the time-bandwidth product indicates that these pulses are transform limited.

4.6 Short pulse amplification

This section provides a brief overview of the results obtained by amplifying the pulses generated by the mode-locked external cavity lasers with semiconductor optical amplifiers (SOAs). While other members of the research group conducted the SOA experiments, a short discussion is included here due to the relevance of this work in developing a laser system suitable for two-photon applications.

J. Milgram is responsible for the early work in the development of SOAs for short pulse amplification as part of his Masters research [135]. Milgram's work focussed on the use of narrow stripe angled facet devices for short pulse amplification. Using an 870 μm long symmetric quantum well SOA, a 16 mW average power output can be achieved by amplifying a 5 ps pulse train with an average power of 550 μW operating at a repetition rate of 770 MHz [136]. The energy and peak power of the amplified pulses are 21 pJ and 5.5 W, respectively.

A. Budz has continued the SOA work started by Milgram as part of his Masters and Ph. D. research. Using a flared-waveguide geometry SOA with a symmetric quantum well active region, Budz is able to achieve average output powers as high as 115 mW by amplifying a 3 ps pulse train with an average power of 500 μW operating at 675 MHz [137]. The flared SOA is 1200 μm in length, has an applied drive current of 500 mA and the wavelength of the input pulse train is tuned to the gain peak of the SOA. Budz has also conducted research on long-wavelength single quantum well InGaAs/GaAs SOAs. Flared-waveguide long-wavelength SOAs result in average powers as high as 50 mW following amplification of a 2 ps pulse train with an average power of 1.5 mW [138, 139]. The repetition rate of the mode-locked oscillator is 840 MHz, and the wavelength of operation corresponds to the gain peak of the SOA.

4.7 Comparison with other published works

In order to put into perspective the results presented in this chapter, a comparison will be made with results presented in the relevant literature. The particular parameters that will be compared are tuning range, pulse duration and pulse energy of external cavity mode-locked semiconductor lasers.

4.7.1 Tuning range

Passively mode-locked tuning ranges of 61 nm and as large as 75 nm are achievable with 2-AQW and 3-AQW bent-waveguide semiconductor lasers, respectively. In terms of energy, the wavelength tuning spans an energy range of 78 meV for the 2-AQW device and 103 meV for the 3-AQW device. The broadest tuning range reported for a passively mode-locked semiconductor laser is 26 nm, extending from 829 to 855 nm [50]. This corresponds to an energy range of 45 meV, which is substantially less than that achievable with the 2-AQW laser and less than half the range achievable with the 3-AQW device.

Lee *et al.* have made the only report on wavelength tuning of a mode-locked asymmetric-quantum-well semiconductor laser [52]. As previously stated in section 1.4.3, Lee *et al.* generated short pulses tunable from 795 nm to 857 nm by active mode-locking an angled stripe device mounted in a ring cavity configuration. The 62 nm tuning range corresponds to an energy difference of 113 meV. While this tuning range exceeds the largest tuning range achievable by the author, the tuning range presented by Lee *et al.* is obtained by *active* mode-locking their device. A very large gain can be realized during passage of the pulse through the device due to the strong RF modulation under active mode-locking. A larger gain also implies a larger gain bandwidth, which in turn leads to a larger tuning range.

In comparing the results with actively mode-locked *symmetric* quantum well lasers, a large tuning range is reported by Hoffman *et al.* [47]. A tuning range of 115 nm, centred about 1505 nm, is achieved by active mode-locking an external cavity laser. This tuning range corresponds to an energy difference of 63 meV.

4.7.2 Pulse duration and pulse energy

The mode-locked pulses obtained in this work typically have durations ranging from 2 ps to approximately 10 ps under external cavity passive and hybrid mode-locking, prior to compression. The pulse energies vary from as low as 0.3 pJ to as high as 2.4 pJ, depending upon the device structure, wavelength and repetition rate. These pulse durations and pulse energies are quite comparable to other published works on mode-locked multi-segment semiconductor lasers. Derickson *et al.* report a pulse duration of approximately 2.5 ps and pulse energies between 0.7 pJ and 0.8 pJ for passive and hybrid mode-locking of two-segment semiconductor lasers in external cavities [140, 141]. Using an external cavity configuration identical to that used in this work, Schrans *et al.* report on the generation of pulses 2 to 5 ps in duration from a passively mode-locked two-segment AlGaAs laser [50]. It is estimated by the author that the energy per pulse is approximately 0.3 pJ in Schrans *et al.*'s work.

The results presented by Lee *et al.* provide the only data to which a comparison can be made with regard to other mode-locked asymmetric-quantum-well sources [52]. The pulses generated by Lee *et al.*'s laser have a duration ranging from 13 to 21 ps and pulse energies of approximately 2 pJ. Unfortunately, the method of mode-locking and the device geometry in Lee *et al.*'s work differ from the work presented in this thesis, making a head to head comparison of limited relevance. A comparison with the tuning range obtained by Lee *et al.* has already been made in section 4.7.1.

Post-compression of the optical pulses from the external cavity semiconductor laser has yielded pulse durations as short as 430 fs, with peak powers between 1 and 2 W. As discussed in section 1.4.1, a number of authors have reported on sub-picosecond pulse generation with semiconductor lasers. In particular, Delfyett *et al.* reported on the generation of 460 fs pulses by compressing 5 ps pulses emitted from a hybrid mode-locked AlGaAs external cavity semiconductor laser [18, 33]. The peak power of the compressed pulses is approximately 1.6 W before amplification, and 72 W after amplification. The saturable absorber consists of a multiple-quantum-well saturable absorber mirror and the compressor is a modified grating pair compressor arranged in a dual-pass configuration. In order to achieve pulses shorter than 460 fs, Delfyett *et al.* employed cubic phase compensation or intra-cavity dispersion compensation [18]. The pulse duration obtained by Delfyett *et al.* compares very well with what has been achieved in this work based on the cavity and compressor design utilized. Salvatore *et al.* generated pulses as short as 260 fs using an external cavity and compressor configuration very similar to that used in this work [51]. The main differences between Salvatore's laser and the lasers used in this work are the operating wavelength and material system (Salvatore used an AlGaAs laser operating at 850 nm) and the fact that a high-reflective (HR) coating is applied to the output facet of Salvatore's laser. The HR coating is partially to blame for the low (~50 mW) peak power of the compressed pulses.

4.8 Chapter Summary

In this chapter I presented the experimental results obtained by mode-locking external cavity (ring and linear) mounted semiconductor diode lasers, as well as results obtained by passively mode-locking monolithic devices. Using mode-locked dual asymmetric quantum well lasers, short optical pulses 2.0 to 3.9 ps in duration can be generated in the wavelength range covering 954 to 1015 nm. The average power of the pulses is typically 500 μW. Post compression with a grating pair compressor results in sub 1 ps pulses across the entire tuning range. The shortest pulse duration achievable with this laser is 510 fs (Gaussian pulse shape), corresponding to a peak power of approximately 1.5 W.

Short optical pulses covering the wavelength range extending from 942 nm to 1017 nm are generated by mode-locking a 500 μm long triple asymmetric quantum well laser. The pulses range from 2 to 11 ps in duration with typical average output powers of 600 μW. It is observed that increasing the length of the device results in a decreased tuning range.

Mode-locking long wavelength InGaAs/GaAs lasers produced pulses measuring 2 to 5 ps in duration with average powers ranging from 750 μW to 1.8 mW. Pulse compression yields pulses as short as 570 fs. The tuning range of these devices was not explored as the device only contains a single quantum well.

Mode-locking a symmetric quantum well laser at various repetition rates was studied. For this particular system, it is found that operating at a repetition rate between 1300 and 1500 MHz generates the largest signal for two-photon applications.

A select number of devices are used for monolithic passive mode-locking producing 1.5 ps pulses at repetition rates of 31 and 61 GHz.

In view of the discussion in section 1.3, the results presented in this chapter seem to indicate that the lasers are suitable for TPFS. This is assuming that the output of the mode-locked oscillator is amplified with an SOA to suitably high average powers, such as those outlined in section 4.6.

Chapter 5 Mode-locked laser synchronization

This chapter presents the results of synchronizing the mode-locked external cavity semiconductor laser to a mode-locked Ti:Sapphire laser using an all-optical synchronization method. This method of synchronization is interesting from several perspectives. Such a system permits all-optical clock extraction for digital communication [142, 143], is of general interest for frequency metrology [144], and can be used as an additional diagnostic tool by which the semiconductor laser pulses can be further characterized [145]. In relation to the work presented in previous chapters, the synchronization of a mode-locked semiconductor laser with a mode-locked Ti:Sapphire laser permits measurement of the semiconductor laser pulse shape and retrieval of the pulse phase information. This is of particular interest if future attempts at higher order chirp compensation are to be made. The synchronization work presented in this chapter also serves as preliminary work for the synchronization of two mode-locked semiconductor lasers. Such a system could be used in a multi-colour pump-probe experiment.

The basic concept of the synchronization method involves shining a small portion of light from the mode-locked Ti:Sapphire laser onto the absorber section of the mode-locked semiconductor laser. Since the method relies on bleaching of the saturable absorber to establish synchronization, it permits all-optical synchronization of mode-locked lasers operating at significantly different wavelengths.

The first section of this chapter describes the experimental setup and the tasks involved in synchronizing the two lasers. The next section summarizes and discusses the various experimental results. The last section presents a simple model that helps explain some of the trends observed in the experiments.

5.1 Experimental setup

The experimental setup used for synchronization is shown in Figure 5-1. The mode-locked Ti:Sapphire laser used in this experiment has an output power of 600 mW, a repetition rate of 80.5 MHz, a pulse duration of 80 fs and operates at a wavelength centred around 795 nm. The portion of the beam that is used for synchronization experiments has an average power of 300 mW and a pulse duration that has been broadened to approximately 120 fs. This portion of the beam is then split down two separate paths by a beam splitter. Ninety-five percent of the average power is directed down path 1 while the remaining five percent is directed down path 2.

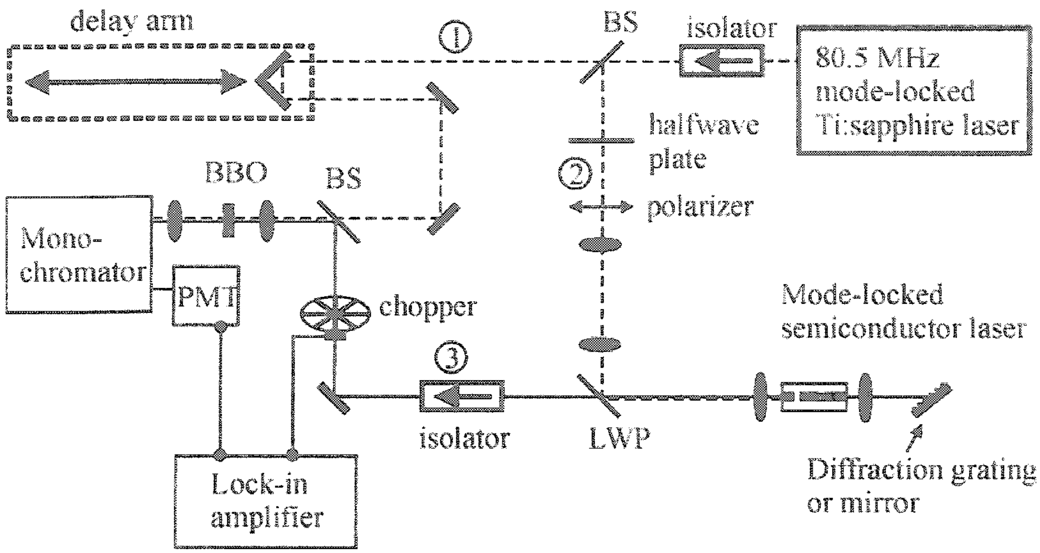

Figure 5-1: Experimental setup used for synchronizing the mode-locked semiconductor laser to the mode-locked Ti:Sapphire laser. Note that contrary to what is shown, a device with a bend in the waveguide was often used in the semiconductor diode laser (SDL) external cavity. BS – Beam splitter, LWP – Long wavelength pass beam splitter, BBO – nonlinear BBO crystal, PMT – Photo-multiplier tube.

The beam propagating down path 2 passes through a half-wave plate and polarizer combination. These two optical elements allow for variable attenuation of the Ti:Sapphire laser beam, with minimal changes to beam alignment, by rotation of the half-wave plate. A pair of lenses is then used to compensate for chromatic dispersion of the output-coupling lens of the mode-locked semiconductor laser. Since the operation wavelength of the semiconductor laser is quite different from that of the Ti:Sapphire laser, the output coupler is not optimally positioned for efficient coupling of the Ti:Sapphire laser beam. The distance between the two lenses in path 2 can be varied, allowing optimization of the coupling into the semiconductor laser. The final element in path 2 is a long-wavelength-pass beam-splitter. This element is designed to have a high reflectivity at the Ti:Sapphire laser wavelength and a high transmission at the semiconductor laser wavelength. Finally, the Ti:Sapphire laser beam is coupled into the absorber section of the semiconductor laser.

The remaining portion of the Ti:Sapphire laser beam propagating along path 1 undergoes a variable delay governed by the delay arm. The delay arm consists of a retro-reflector mounted on a computer controlled (Oriel Encoder Micrometer model 18254) translation stage. Finally, the Ti:Sapphire laser is combined with the semiconductor laser beam by a beam splitter.

The output of the semiconductor laser passes through the long-wavelength-pass beam splitter, an optical isolator, a chopper, and is combined with the Ti:Sapphire beam by a beam splitter. The combined beams are focused into a 1 mm thick BBO crystal by a 5 cm achromatic lens. The light from the BBO crystal is collected by another lens and directed through a monochromator. The monochromator is used to filter out light at the second harmonic of the Ti:Sapphire laser. The filtered output (light at the sum frequency) is detected by a PMT with the aid of a lock-in amplifier.

The cross-correlation trace is obtained by collecting signal at the PMT while the delay on the delay arm is changed. Since the semiconductor laser is set to operate at the N^{th} harmonic of the Ti:Sapphire repetition rate, a total delay arm length of approximately 1.9 m is required in order to obtain a cross correlation trace of each of the N semiconductor laser pulses. Semiconductor external cavity lengths corresponding to values of N ranging from 2 to 10 are used.

5.1.1 Cross correlation measurement bandwidth

The measurement bandwidth of the cross correlation setup is limited in part by the size of the BBO crystal used, as well as by the filtering monochromator. The bandwidth was measured by detecting the sum frequency signal generated by mixing light from the mode-locked Ti:Sapphire laser with the light from the semiconductor laser operating cw. The operating wavelength of the semiconductor laser is then tuned to larger and smaller values until the cross correlation signal drops by a factor of 2. The resultant bandwidth is 2.2 nm measured at 1000 nm. This is measured with both the input and output slits of the monochromator open to their maximum size. It is possible to increase the bandwidth to 2.8 nm by placing a lens inside the monochromator, just before the exit slit. Since the bandwidth of the mode-locked semiconductor laser is typically around 0.6 nm, this does not impose a significant constraint on the measurement. For pulses with a much larger bandwidth, a thinner BBO crystal should be used.

5.2 Synchronizing the two lasers

There are several tasks involved in synchronizing the two lasers. The first task is to roughly align the two lasers according to Figure 5-1. Once this is accomplished, the alignment of the Ti:Sapphire beam along path 2 needs to be adjusted. The goal is to optimally couple the light into the absorber section of the semiconductor device. The method used to gauge the effectiveness of the coupling is to reverse bias the absorber section, leave the gain section unbiased, and monitor the photocurrent induced in the absorber section by the Ti:Sapphire beam. The next step is to ensure that the Ti:Sapphire beam and the semiconductor laser beam are collinear at the BBO crystal. In order to perform this check, the semiconductor diode laser is made to operate in a cw regime. This way, assuming the system is roughly aligned, sum-frequency generation will occur for all positions of the retro-reflector on the delay arm. The alternative would be to adjust the alignment while the two lasers are synchronized. This approach is much more difficult because not only must the two laser beams overlap in space, the pulses must also overlap in time.

Once the basic alignment has been performed, the next step is to try and synchronize the lasers. To begin, path 2 is blocked while the semiconductor diode laser is passively mode-locked at a repetition rate that closely matches a harmonic of the Ti:Sapphire laser repetition rate. Once the semiconductor laser is mode-locking at the proper repetition rate, the beam block is removed from path 2. Removal of the beam block should typically result in synchronization. Synchronization can be monitored by detecting the optical pulses from the mode-locked semiconductor laser using a silicon photodiode and an oscilloscope triggered by the Ti:Sapphire monitor signal (Figure 5-2).

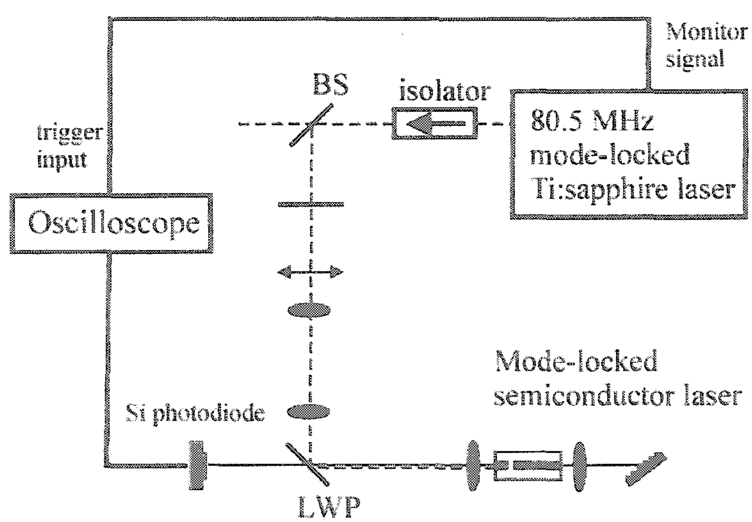

Figure 5-2: Experimental setup used to verify synchronization of the two lasers. LWP – Long wavelength pass beam splitter.

In the event that the two lasers do not readily synchronize, adjusting the cavity length of the semiconductor laser is usually sufficient to remedy the situation. If this fails, increasing the amount of power from the Ti:Sapphire laser incident upon the absorber section or adjusting the alignment of the Ti:Sapphire beam along path 2 may resolve the issue. Once the oscilloscope indicates that the two lasers are synchronized, a cross correlation measurement may be performed to verify how well the two lasers are synchronized.

5.3 Experimental results

Synchronization experiments were performed with a number of different semiconductor lasers. Synchronization experiments at low harmonics (2nd and 3rd harmonic of the Ti:Sapphire laser) were performed with ring cavity semiconductor lasers whereas experiments at higher harmonics were performed with bent-waveguide devices mounted in linear cavities. A cross correlation trace obtained with a mode-locked semiconductor laser operating that the 6th harmonic of the mode-locked Ti:Sapphire laser is shown in Figure 5-3.

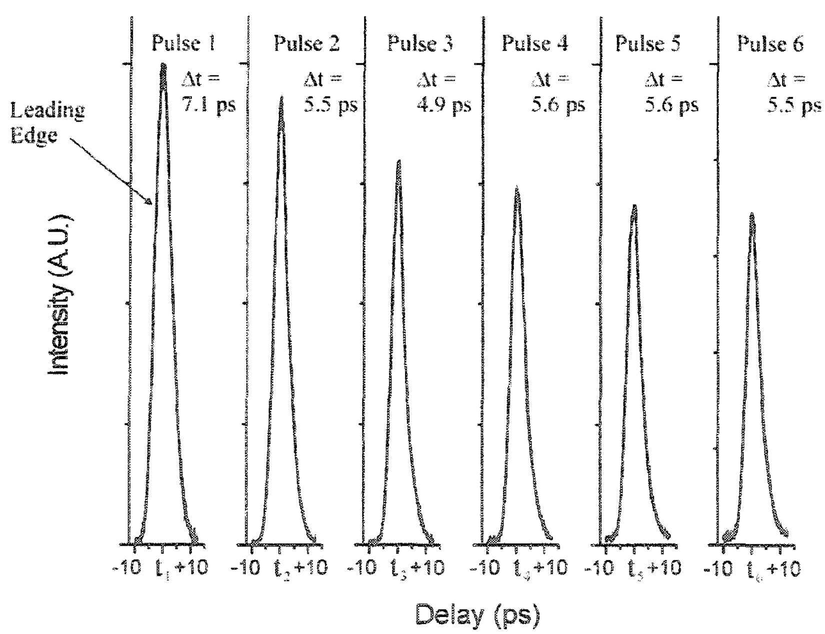

Figure 5-3: Temporal profile of semiconductor laser pulses with the laser synchronized at the 6th harmonic of the Ti:Sapphire laser. The values t_1 through t_6 are spaced by the period of the semiconductor laser pulses (t_1 = 0 ns, t_2 = 2.07 ns, t_3 = 4.14 ns, t_4 = 6.21 ns, t_5 = 8.28 ns, t_6 = 10.35 ns). Δt is the pulse duration at half maximum.

For this particular data set, the bent-waveguide semiconductor laser used in the experiment has a length of 550 μm in length and consists of a gain and an absorber section measuring 500 μm and 50 μm in length, respectively. Note that the length of the absorber section includes the 10 μm gap separating the two sections. The average output power of the laser is 650 μW at a repetition rate of approximately 483 MHz. The operating wavelength is 1000 nm. The power of the Ti:Sapphire laser beam just before the output coupler of the semiconductor diode laser is 1 mW. It can be seen from the figure that the pulse width and pulse energy varies for each of the pulses. This is a result of the Ti:Sapphire laser perturbing the operation of the semiconductor laser. The pulse durations vary from as long as 7.1 ps to as short as 4.9 ps. The largest pulse duration occurs for the semiconductor laser pulse coincident with the Ti:Sapphire laser pulse at the absorber section of the device. The energy of the semiconductor laser pulse is also largest for the first pulse since the presence of the Ti:Sapphire laser pulse aids in bleaching of the saturable absorber. The other feature to take note of is the pulse asymmetry. Information on the asymmetry of the pulse shape is, in contrast, lost in an autocorrelation measurement.

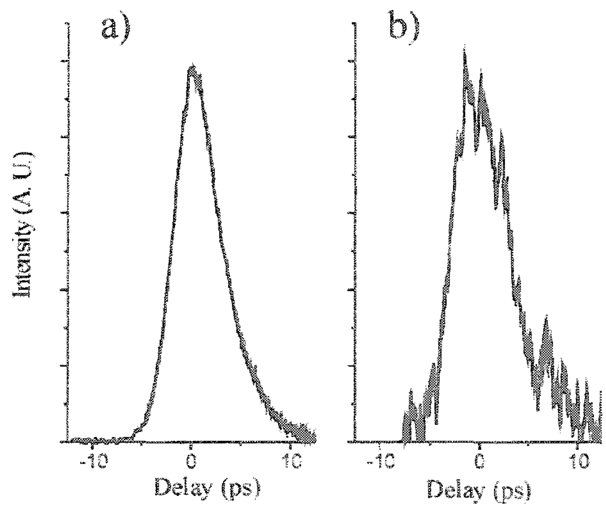

Figure 5-4: a) Temporal profile of a pulse obtained by cross correlation. The pulse energy was ~1.2 pJ energy. b) Temporal profile of a similar pulse attenuated down to an energy of 0.01 fJ.

5.3.1 Low energy pulse measurement

One of the advantages offered by cross correlation for pulse characterization is the ability to characterize extremely low energy pulses. This is made possible by the large amount of energy available from the Ti:Sapphire beam at the nonlinear crystal. To illustrate this concept, neutral density filters are used to attenuate the output of a synchronized mode-locked semiconductor laser. Figure 5-4 illustrates the case where the pulse energy is attenuated down from 1.2 pJ to 0.01 fJ. Although the trace in b) is becoming quite noisy, a fairly good representation of the pulse width and shape is still evident in the cross correlation trace. Depending upon the acceptable quality and the time taken to perform the scan, the pulse can be further attenuated and remain detectable.

5.3.2 Timing jitter analysis

One of the parameters of interest when synchronizing two lasers is the relative timing jitter between the two lasers. A simple method to measure the timing jitter makes use of the cross correlation setup. The delay arm is positioned such that sum frequency light is generated from the sharp leading edge of the mode-locked semiconductor laser pulse. In the absence of other noise sources, relative timing jitter between the pulses should result in intensity noise at the sum frequency, proportional to the pulse temporal slope [146]. The method is illustrated in Figure 5-5.

Using this technique, the RMS value of the jitter between the two lasers in the 0 to 700 Hz range was determined to be less than 50 fs. In practice, the semiconductor laser and Ti:Sapphire laser intensity noise dominate the measurement, hence the actual jitter between the two lasers should be substantially lower than 50 fs in this bandwidth.

The timing jitter of the mode-locked semiconductor laser itself is also an interesting parameter. This timing jitter refers to random fluctuations in the pulse repetition period of the mode-locked laser. It is typically measured by using the approach described by von der Linde [147]. The basic measurement technique relies on measuring the power spectrum of the mode-locked laser with a high-speed photodiode and an electronic spectrum analyzer. The spectrum consists of a series of delta-like functions at the harmonics of the mode-locked laser repetition rate. Noise on the optical pulses, both in amplitude and phase, result in noise sidebands on the signal. It has been shown by von der Linde that amplitude noise sidebands and phase noise sidebands can be distinguished from one another by noting that the power spectral density of the amplitude noise is independent of the harmonic number, whereas the power spectral density of the phase noise is proportional to the square of the harmonic number. At sufficiently high harmonic numbers, the noise sidebands are dominated by phase noise.

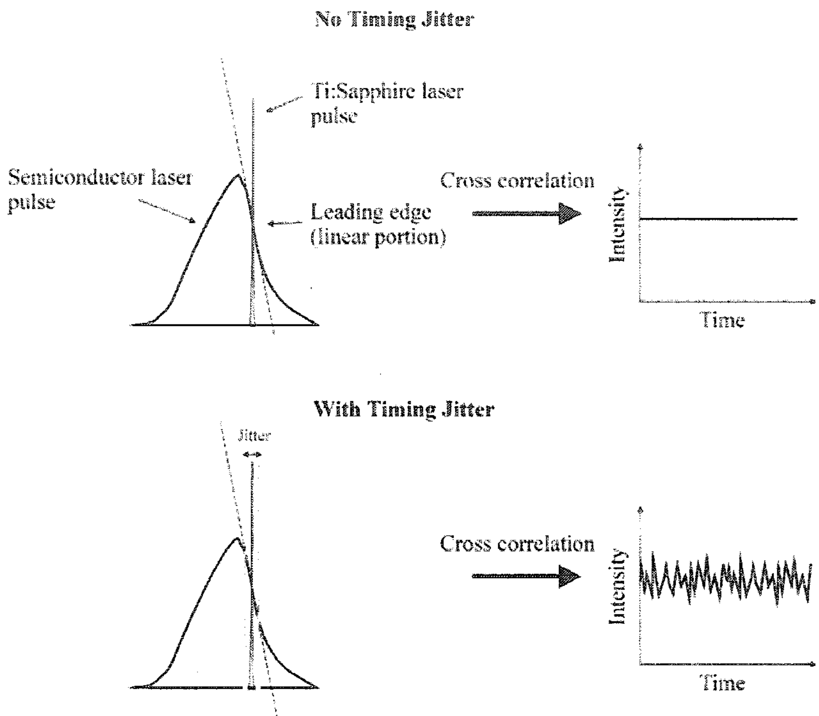

Figure 5-5: Illustration of the method used to measure the timing jitter between the two synchronized lasers [146].

There are many sources that contribute to the timing jitter on an external cavity mode-locked semiconductor laser. Included amongst these are the current source, the RF signal generator (for active or hybrid mode-locking), vibrations of optical components in the cavity, air currents in the external cavity, temperature fluctuations and spontaneous emission. Passive mode-locked external cavity semiconductor lasers have been found to have the highest timing jitter of all mode-locked semiconductor lasers [140]. This is mainly due to the absence of a high-stability driving source. The timing jitter of a mode-locked semiconductor laser can be reduced by coherent photon seeding [148], incoherent addition [149], use of a phase-locked loop [150] and by synchronization with an external, low noise, source [151, 152].

It is observed experimentally that the timing jitter of the semiconductor laser is significantly reduced by synchronization with the Ti:Sapphire laser. At the 40th harmonic of the mode-locked semiconductor repetition rate (fundamental frequency of 483 MHz), the signal on the RF spectrum analyzer is very broad, having a full-width at half maximum of 84 kHz. Synchronizing the semiconductor laser with the Ti:Sapphire laser under the same operating conditions reduces the signal width to approximately 1.5 kHz. This is the same width measured at all the lower harmonics while synchronized (recall that the phase noise goes as the square of the harmonic number). The measurement of the actual width of the signal is limited due to the low signal level not being sufficiently above the noise floor. While this permits only a qualitative analysis, it is apparent that the timing-jitter of the mode-locked semiconductor laser is significantly reduced under synchronization. In order to make a quantitative assessment, a low noise microwave amplifier and spectrum analyzer are required.

5.3.3 Phase recovery

Determining the shape of the semiconductor laser pulse via a cross correlation measurement allows the phase information to be recovered. The algorithm developed by Gerchberg and Saxton [153] and independently by Gonsalves [154] allows retrieval of the phase of a complex signal f, given that the modulus $|f|$ is known along with the Fourier transform of f. For this experiment, the modulus of f is obtained via the cross correlation measurement and the power spectrum of f is obtained by measuring the optical spectrum.

It is also assumed that the electric field of the pulse, $E(t)$, can be written as

$$E(t) = \frac{1}{2}\varepsilon(t)e^{i\phi(t)}e^{i\omega_0 t} + c.c. \tag{5.1}$$

This is known as the slowly varying envelope approximation. In equation (5.1), $\varphi(t)$ is the time dependent phase, ω_0 is the carrier frequency, and $\varepsilon(t)$ is the time dependent field envelope. The time dependent carrier frequency can then be written as

$$\omega(t) = \omega_0 + \frac{d}{dt}\phi(t) \tag{5.2}$$

The algorithm is based on an iterative technique and proceeds as follows. Given $|f(x)|$, a trial function $f_1(x)$ is defined such that

$$f_1(x) = |f(x)|e^{i\phi(x)} \tag{5.3}$$

where $\varphi(x)$ is some arbitrarily defined phase function.

Next, $f_1(x)$ is Fourier transformed and $F_2(\omega)$ is set as

$$F_2(\omega) = |F(\omega)| \left[\frac{F_1(\omega)}{|F_1(\omega)|} \right] \tag{5.4}$$

where $F(\omega)$ is measured, and F_1 is the Fourier transform of $f_1(x)$. This step basically replaces the magnitude of $F_1(\omega)$ while leaving the phase intact.

The third step is to take the inverse Fourier transform of $F_2(\omega)$ and set $f_3(x)$ as

$$f_3(x) = |f(x)| \left[\frac{f_2(x)}{|f_2(x)|} \right] \tag{5.5}$$

The last step is to repeat the process until convergence is achieved.

As a demonstration, the algorithm was applied to the pulse profile and spectrum shown in Figure 5-6. Following assignment of an arbitrary phase, the spectrum computed from the pulse shape is plotted along with the measured optical spectrum in Figure 5-7. The fitted spectrum, following 500 iterations of the algorithm, is plotted in Figure 5-8.

The recovered phase information is plotted as the time dependent carrier frequency (see equation (5.2)) in Figure 5-9. The phase information where the intensity of the pulse is falling off towards zero should be neglected. In retrieving the phase, a number of assumptions were made with respect to the pulse profile and pulse spectra. First, it is assumed that the pulse shape measured is the actual shape of an individual pulse from the semiconductor laser. Timing jitter or changes in the pulse shape from one pass to the next will affect the shape measured via cross correlation. Secondly, it is also assumed that the measured spectrum is the actual spectrum of the pulse, and not an *average* spectrum from *different* spectra from many pulses. Given that the assumptions are valid, it is seen from Figure 5-9 that the leading edge of the pulse is blue-chirped (angular frequency is increasing), with the sign of the chirp changing for the remainder of the pulse (angular frequency is decreasing).

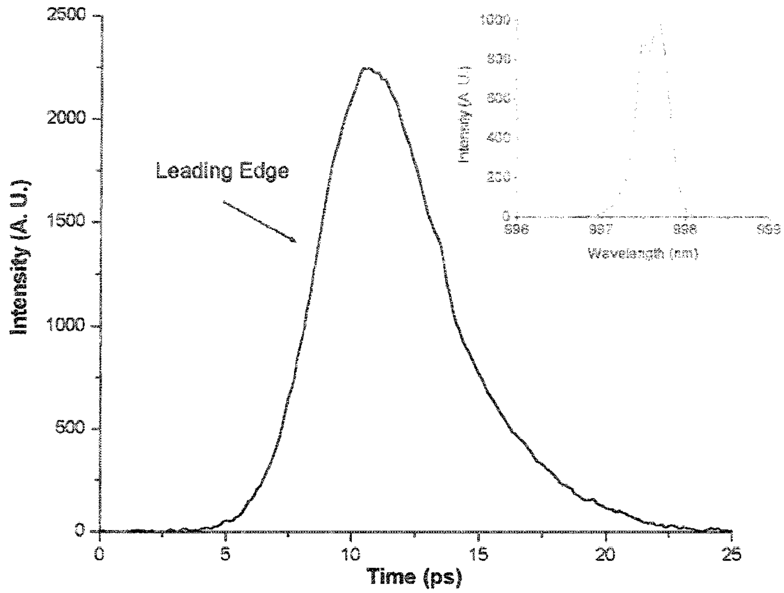

Figure 5-6: Pulse profile and pulse spectrum to be used in the iterative fitting algorithm for phase retrieval. The spectra is shown in the inset.

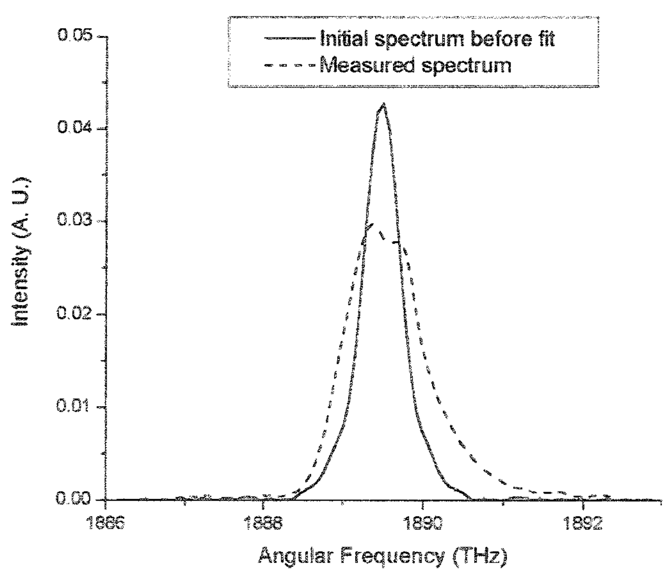

Figure 5-7: Computed and measured optical spectrum before applying the fitting algorithm.

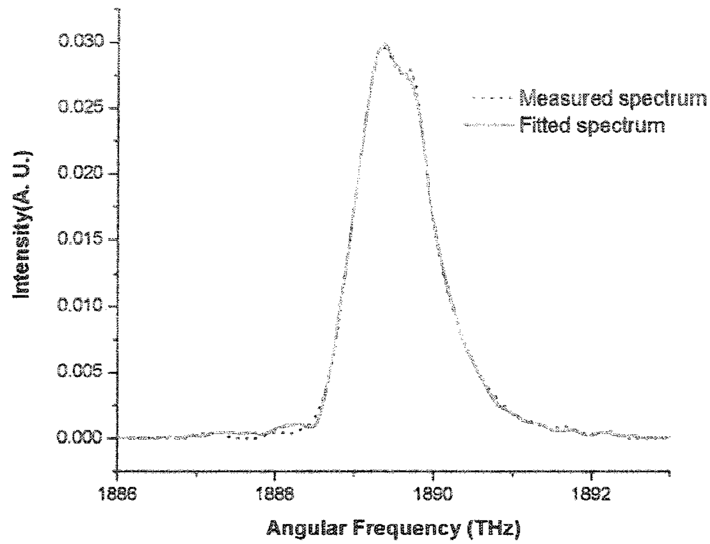

Figure 5-8: Computed and measured optical spectrum following 500 iterations of the fitting algorithm.

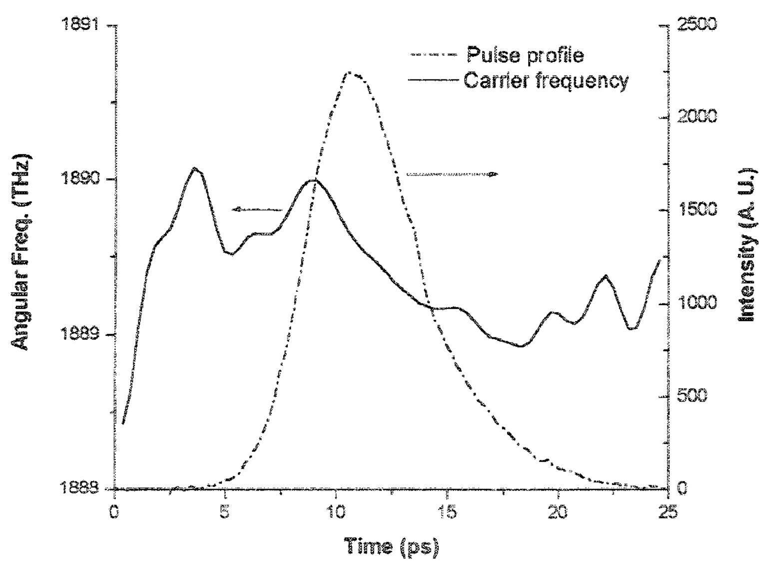

Figure 5-9: Time dependent carrier frequency of the pulse determined by application of the fitting algorithm. The pulse profile is also plotted.

5.4 Synchronization model and experimental verification

In order to help explain the mechanism responsible for synchronization of the two lasers, a simple model was developed. The model also aids in determining which parameters to modify to optimize the synchronization process.

5.4.1 The model

The synchronization process is modelled by considering two counter-propagating pulses incident upon a saturable absorber. It is a much simplified version of the model presented by Khalfin *et al.* [155]. The model allows examination of the effect of the Ti:Sapphire pulse upon the timing of the semiconductor laser pulse when both pulses pass through the saturable absorber at different times. The process modelled is shown in Figure 5-10.

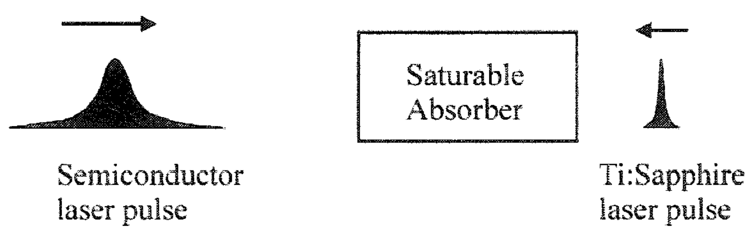

Figure 5-10: Schematic representation of the process that is modeled.

Similar to reference [155], the process is analyzed using the rate equation set outlined by Agrawal and Olsson [156, 157]. The time evolution of the gain (or absorption), is governed by the equation

$$\frac{\partial g}{\partial t} = \frac{g_0 - g}{\tau_c} - \frac{g P_{tot}}{E_{sat}} \tag{5.6}$$

where g is the gain per unit length, g_0 is the unsaturated gain per unit length, τ_c is the recovery time of the absorber, P_{tot} is the power of both of the optical pulses and E_{sat} is the saturation energy of the absorber.

The electric field representing a pulse is written as

$$E(z,t) = \sqrt{P}\exp(i\phi) \tag{5.7}$$

where $P(z, t)$ and $\varphi(z, t)$ are the power and phase respectively. The time evolution of the pulse power and phase is then governed by the following two rate equations

$$\frac{\partial P}{\partial z} = \left(g - \alpha_{\text{int}}\right) P \tag{5.8}$$

$$\frac{\partial \varphi}{\partial z} = -\frac{1}{2}\alpha g \tag{5.9}$$

where α_{int} is the internal scattering loss per unit length and α is the linewidth enhancement factor[85].

The model is then analyzed by dividing the saturable absorber into small segments, and applying equations (5.6), (5.8) and (5.9) to each section of the absorber and to each of the counter propagating pulses. It should be noted that in the case of the Ti:Sapphire pulse, it is assumed that the absorber does not saturate at this wavelength. Also, the phase information generated by the model is not used at this point in time.

5.4.2 Analysis of the synchronization process

Analysis is performed by examining the change in the semiconductor laser pulse at the output of the saturable absorber as a function of various parameters. Parameters that can be adjusted are:

- The relative arrival time of the semiconductor laser pulse and Ti:Sapphire laser pulse at the saturable absorber
- Parameters defining the pulses (duration, energy)
- Parameters defining the saturable absorber (length, saturation energy, scattering loss)

To begin, consider the case of a semiconductor laser pulse incident upon the saturable absorber delayed by 17 ps relative to the arrival time of the Ti:Sapphire laser pulse. Note that the position in time of the peak power of the pulse is used in determining the relative delay between the two pulses. Also note that the arrival time of the semiconductor laser pulse is measured relative to the left hand side of the absorber (see Figure 5-10) and that the arrival time of the Ti:Sapphire pulse is measured relative to the right-hand-side of the absorber. The values of the parameters used for the simulation are found in Table 5-1.

Propagation of the semiconductor laser pulse through the saturable absorber in the absence of the Ti:Sapphire laser pulse is shown in Figure 5-11. The leading edge of the pulse is absorbed by the saturable absorber and shifts the pulse to a later position in time relative to the input pulse. Depending upon the conditions, the saturable absorber can also produce a large asymmetry in the output pulse shape.

Table 5-1: List of parameters used for the simulation results shown in Figure 5-11 and in Figure 5-12.

Parameter	Value
Diode pulse duration	14 ps
Diode pulse energy	$5\cdot E_{sat}$
Diode pulse shape	Gaussian
Ti:Sapphire pulse duration	200 fs
Ti:Sapphire pulse energy	$1\cdot E_{sat}$
Ti:Sapphire pulse shape	Gaussian
Absorber size	50 μm
Absorber saturation energy	0.5 pJ
Unsaturated absorption	20000 cm^{-1}
Absorber recovery time	30 ps
Optical confinement factor	0.02
Segment size for simulation	1 μm

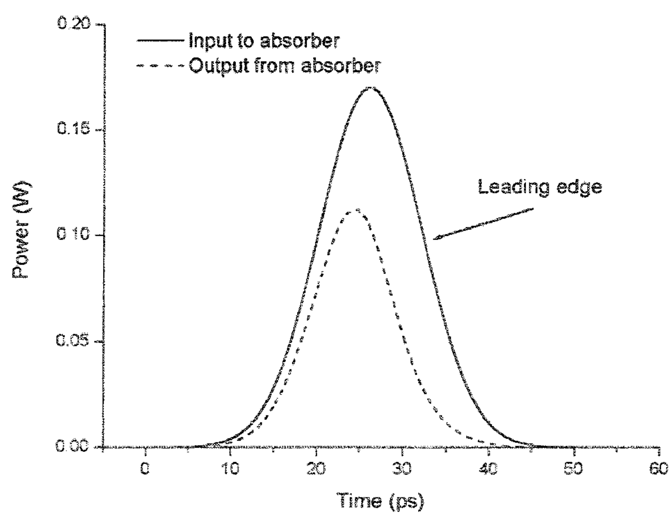

Figure 5-11: Results of propagation of the semiconductor laser pulse through the saturable absorber in the absence of the Ti:Sapphire pulse.

Repeating the simulation with the Ti:Sapphire laser pulse incident upon the absorber results in the pulse profiles shown in Figure 5-12. The Ti:Sapphire laser pulse begins to saturate the absorber prior to the arrival of the semiconductor laser pulse. This means that less of the energy contained within the leading edge of the semiconductor laser pulse will be absorbed. The end result is that the semiconductor laser pulse has more energy and is pulled forward in time as compared with the semiconductor laser pulse propagated in the absence of the Ti:Sapphire laser pulse.

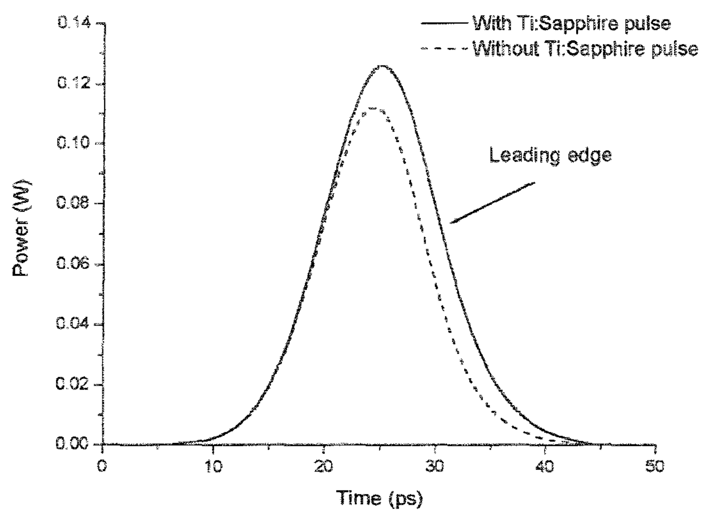

Figure 5-12: Results of propagation of the semiconductor laser pulse through the saturable absorber with a counter-propagating Ti:Sapphire laser pulse.

The curves generated by repeating the above simulation for different arrival times of the Ti:Sapphire pulse are shown in Figure 5-13. Plotted in the figure is the change in mean position of the pulse (time) versus the arrival time of the Ti:Sapphire pulse. A negative arrival time for the Ti:Sapphire laser pulse indicates that it arrives at the saturable absorber prior to semiconductor laser pulse. The dominant effect of the Ti:Sapphire laser pulse occurs for arrival times less than zero. Under these circumstances, the Ti:Sapphire laser beam contributes to bleaching the saturable absorber prior to the arrival of the semiconductor laser pulse. An earlier arrival time for the Ti:Sapphire laser pulse means less of the semiconductor laser pulse will be absorbed in the saturable absorber. This results in a greater and greater forward shift in position of the semiconductor laser pulse as the Ti:Sapphire laser pulse arrives earlier and earlier in time. A maximum forward shift is ultimately achieved around the time when the leading edge of the semiconductor laser pulse enters the absorber just as the Ti:Sapphire pulse has finished propagating through the absorber. Beyond this point, the finite recovery time of the absorber begins to influence the extent to which the semiconductor laser pulse is affected. For arrival times larger than zero, the semiconductor laser pulse has already entered the saturable absorber, and as such, the presence of the Ti:Sapphire pulse has a small effect on the mean position of the semiconductor laser pulse. The Ti:Sapphire pulse is capable of slightly pulling the semiconductor laser pulse back in time due to the small absorption that occurs towards the trailing end of the semiconductor laser pulse (refer back to Figure 5-11).

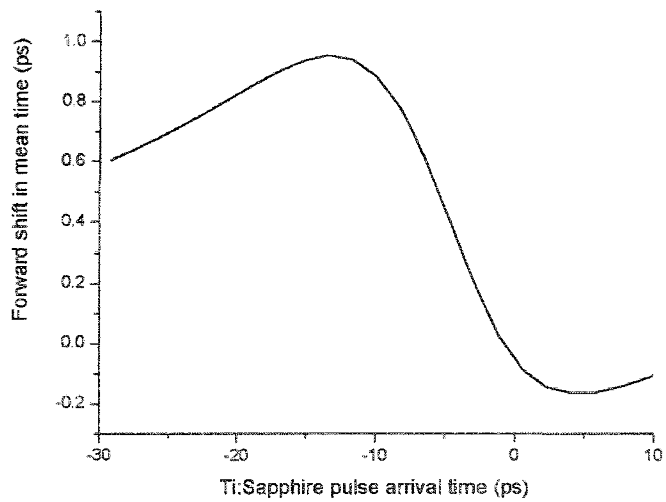

Figure 5-13: Shift in position (mean time) of the semiconductor laser pulse as a function of the Ti:Sapphire pulse arrival time. A negative arrival time implies that the peak of the Ti:Sapphire pulse arrives at the saturable absorber *before* the peak of the semiconductor laser pulse.

The influence of the other parameters on the synchronization process can be studied by generating series of curves similar to that shown in Figure 5-13. The results of these simulations are discussed in the subsections that follow.

5.4.2.1 Variation of Ti:Sapphire laser power

One of the parameters of interest is the influence of the Ti:Sapphire power upon the synchronization process. All of the parameters used in the simulation are identical to those shown in Table 5-1 with the exception that the diode pulse duration is 4 ps and the diode pulse energy is $10 \cdot E_{sat}$. The results of the simulation are shown in Figure 5-14. The maximum shift in semiconductor pulse position increases as a function of Ti:Sapphire pulse energy for low Ti:Sapphire pulse energies. As the absorber becomes heavily saturated, the resultant shift in semiconductor laser pulse position approaches a maximum value. This maximum value corresponds to the case of a semiconductor laser pulse propagating through a fully bleached absorber. This effect is more clearly illustrated in Figure 5-15 where the maximum shift in semiconductor laser pulse position is plotted as a function of Ti:Sapphire pulse energy.

The slope of the linear portion of the curves shown in Figure 5-14 is also of interest from a synchronization standpoint, and is plotted in Figure 5-16. A steeper slope implies that the overall system will be able to compensate for noise (timing jitter between the two lasers) better than operating under conditions giving rise to a less steep slope. The slope is very shallow for low Ti:Sapphire pulse energies and approaches a maximum value as the absorber becomes more saturated with increasing pulse energy.

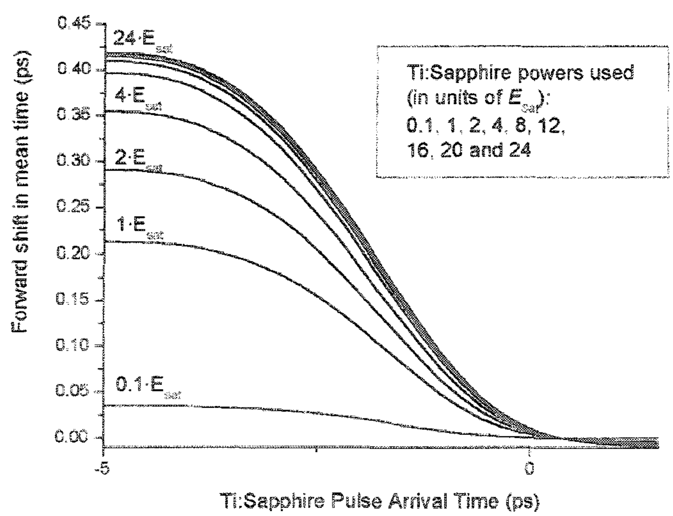

Figure 5-14: Shift in position of the semiconductor laser pulse as a function of Ti:Sapphire laser pulse arrival time for different Ti:Sapphire pulse energies.

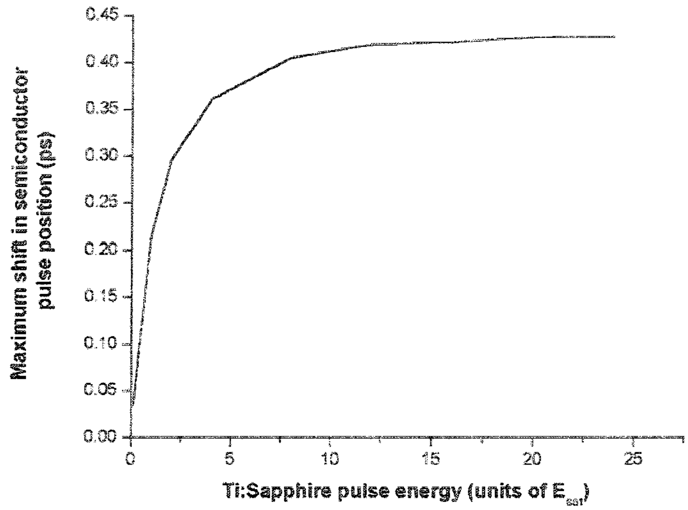

Figure 5-15: Maximum shift in the position of the semiconductor laser pulse versus the Ti:Sapphire laser pulse energy.

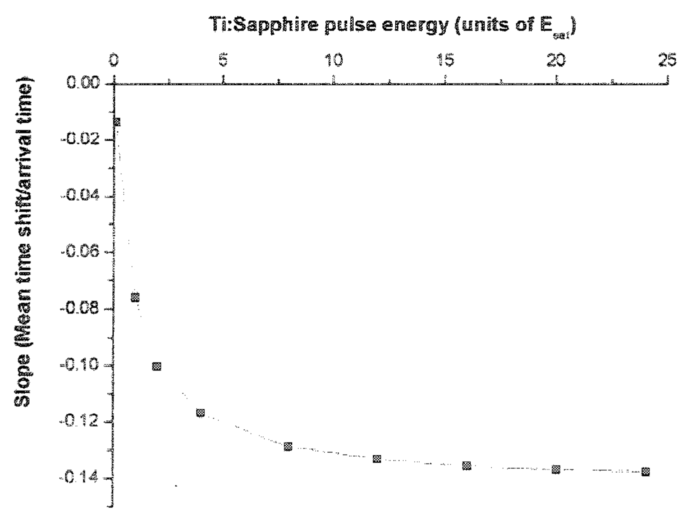

Figure 5-16: Slopes of the linear portion of the curves shown in Figure 5-14 versus the Ti:Sapphire pulse energy.

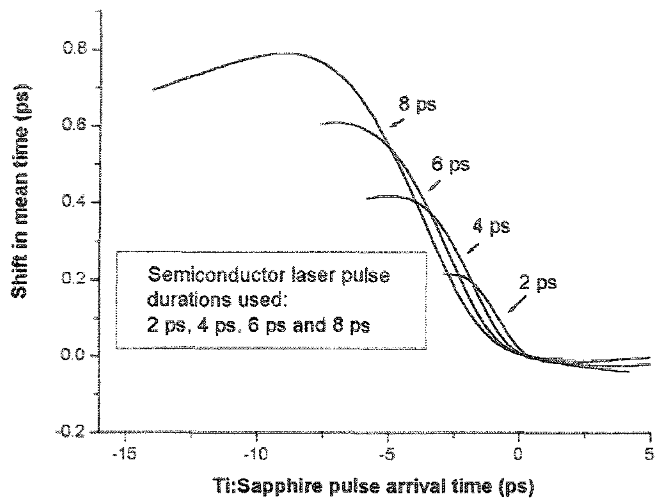

Figure 5-17: Shift in position of the semiconductor laser pulse as a function of Ti:Sapphire laser pulse arrival time for different semiconductor laser pulse durations.

5.4.2.2 Variation of semiconductor laser pulse duration

Another parameter of interest is the effect of the duration of the semiconductor laser pulse on the synchronization process. The parameters used for the simulation are identical to those shown in Table 5-1 with the exception that the diode pulse energy is $10{\cdot}E_{sat}$ and the Ti:Sapphire pulse energy is $20{\cdot}E_{sat}$. The results of the simulation are shown in Figure 5-17. The longer pulses from the semiconductor laser are more easily influenced by the presence of the Ti:Sapphire laser pulse as compared with the shorter pulses. This is an expected result since the longer pulses have their energy spread out over a longer time window, and the presence of the Ti:Sapphire pulses reduces the absorption of the leading edge of the semiconductor laser pulse.

5.4.2.3 Variation of Ti:Sapphire pulse duration

Variation of the Ti:Sapphire pulse duration is an interesting case study which aids in determining the necessary properties required of the external pulse train to achieve good synchronization. For this simulation, all of the parameters used are identical to those shown in Table 5-1 with the exception that the diode pulse energy is $10{\cdot}E_{sat}$ and the Ti:Sapphire pulse energy is $20{\cdot}E_{sat}$. The results of the simulation are shown in Figure 5-18.

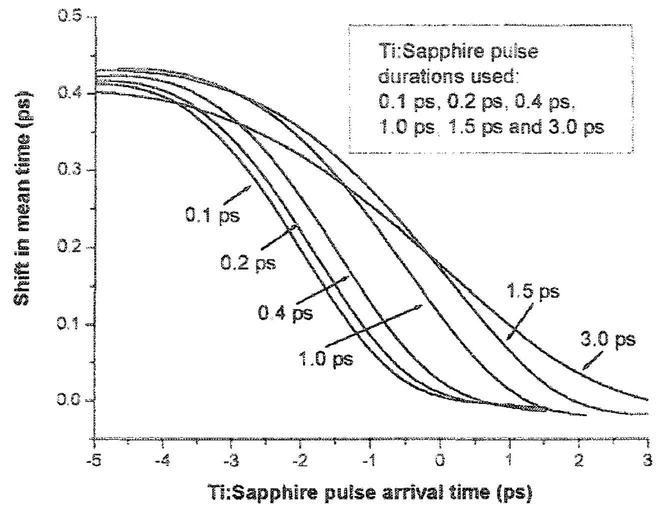

Figure 5-18: Shift in position of the semiconductor laser pulse as a function of Ti:Sapphire laser pulse arrival time for different Ti:Sapphire laser pulse durations.

The change in the Ti:Sapphire pulse duration has little impact on the overall shift in the mean time of the semiconductor laser pulse for durations shorter than the semiconductor laser pulse duration. For these Ti:Sapphire laser pulse durations, the only change is a translation of the curves in the horizontal direction. The main reason behind this horizontal shift is that the arrival time is measured with respect to the peak of the pulse. The leading edge of a longer pulse will interact with the absorber before the leading edge of a shorter pulse given the same position of the peaks of the pulses. For Ti:Sapphire pulse durations that approach the duration of the semiconductor laser pulse, the largest change comes in the form of a decrease in slope of the curves in Figure 5-18. As discussed previously, a steeper slope is preferable for synchronization.

5.4.3 Optimal synchronization conditions

Based upon the results discussed in section 5.4.2, the conditions which should yield optimal synchronization between the semiconductor laser and the Ti:Sapphire laser can be assessed. The simulation data indicates that a maximum *pulling range* is achieved for larger Ti:Sapphire pulse energies as well as for longer pulses from the semiconductor laser. The pulling range required to successfully synchronize the two lasers will depend upon other factors, such as the repetition rate of the mode-locked semiconductor laser as well as the stability of the two lasers. The data also indicates that it is much easier to *pull the pulse forward* in time with the Ti:Sapphire laser pulse as opposed to *pulling it back* in time. Thus it is best to operate the semiconductor laser at a repetition rate such that the arrival time of the Ti:Sapphire laser pulse at the saturable absorber corresponds to a position on the linear portion of the curves shown in Figure 5-14. This allows the system to compensate for noise causing a change (positive or negative) in arrival time of the pulse relative to this operating point. The data also indicates that the Ti:Sapphire pulse duration negligibly affects the synchronization process provided that it is sufficiently short.

5.4.4 Limitations of the model

This section describes the limitations of the model presented and discussed in sections 5.4.1 through 5.4.3. The model is quite simple in that the only element modelled of a complex mode-locked semiconductor laser system is the saturable absorber. Since the presence of the Ti:Sapphire laser pulse can significantly perturb the system under some conditions, a more rigorous model needs to take into account the dynamics of the mode-locked laser. The model also ignores gain dispersion (or absorption dispersion) in the saturable absorber. For semiconductor laser pulses with a significant bandwidth, this assumption may result in a change in the pulling range computed. The model also ignores the reflection at the absorber facet. For facets with high reflectivity, it has been shown that interactions of the forward travelling pulse with the reflected pulse reduce the energy required to bleach the absorber [29]. This will have an impact on the simulated results.

Despite the simplicity of the model and the number of approximations made, it will be shown in section 5.4.5 that there is very good qualitative agreement between the trends predicted by the model and those measured experimentally.

5.4.5 Experimental verification

Due to the number of approximations made in constructing the model, no attempt is made to fit the experimental results to the model. Instead, the experimental results are used to verify trends predicted by the model.

5.4.5.1 Frequency pulling range

The first experiment consisted of modifying the repetition rate of the semiconductor laser while synchronized and observing the frequency range over which the two lasers remain synchronized. This observation was then repeated as a function of Ti:Sapphire power, and is equivalent to the simulation discussed in section 5.4.2.1. That is, the frequency pulling range is directly dependent upon the maximum shift in time that the Ti:Sapphire laser pulse can induce on the semiconductor laser pulse.

The frequency pulling range was measured with the aid of an Agilent frequency counter (model# 53131A) and the following method. While the two lasers are synchronized, the external cavity length of the mode-locked semiconductor laser is adjusted until the two lasers are no longer synchronized. At each extreme, the Ti:Sapphire laser beam incident upon the semiconductor laser absorber facet is blocked and the free running frequency of the mode-locked semiconductor laser is measured.

Since the model predicts that the frequency pulling range is larger for longer pulse durations, passively mode-locked semiconductor lasers generating pulses > 10 ps are utilized. It was found that for short pulses (2 to 4 ps), the pulling range is too short to accurately measure by hand-adjusting the length of the external cavity.

The first case is demonstrated with a semiconductor laser operating at 985 nm with pulse duration of 14 ps. The spectral bandwidth of the pulse is 0.3 nm. The laser is synchronized at the 6^{th} harmonic of the Ti:Sapphire laser, with the Ti:Sapphire laser operating at 772 nm. The results of the experiment are shown in Figure 5-19.

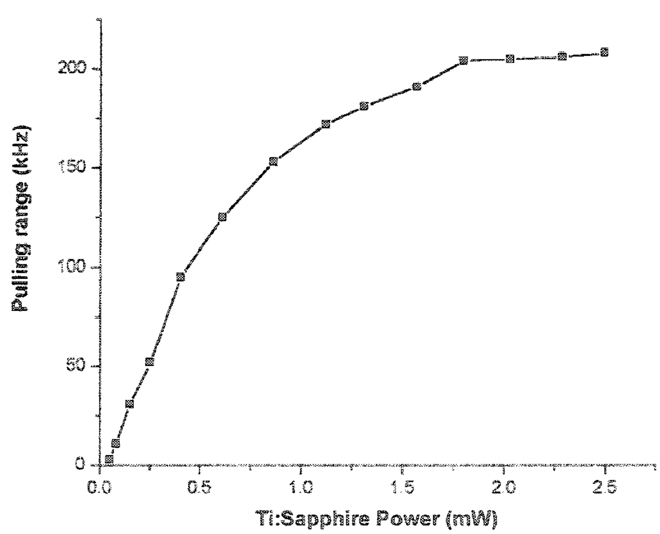

Figure 5-19: Frequency pulling range versus Ti:Sapphire power for the two synchronized lasers.

For this case, the frequency pulling range is measured for Ti:Sapphire powers ranging from as low as 0.05 mW to as high as 2.50 mW. The general trend in the data is very similar to that seen for the theoretical case presented in Figure 5-15. At low Ti:Sapphire powers, the frequency pulling range increases rapidly with increasing Ti:Sapphire power. At higher powers, the frequency pulling range is approaching a "saturation" value of approximately 210 kHz. Ti:Sapphire powers higher than 2.50 mW are not used to minimize the chance of inducing damage at the facet of the device.

5.4.5.2 Shift in leading edge position

The second experiment consists of observing the shift in position (time) of the output semiconductor laser pulse as a function of the external cavity free-running frequency. Only frequencies within the pulling range of the Ti:Sapphire laser for a given Ti:Sapphire pulse energy are used. In terms of the model, modifying the repetition rate is analogous to changing the arrival time of the Ti:Sapphire laser pulse relative to the semiconductor laser pulse arrival time. Repeating this measurement at different Ti:Sapphire pulse energies and determining the slopes is equivalent to the analysis presented in Figure 5-16.

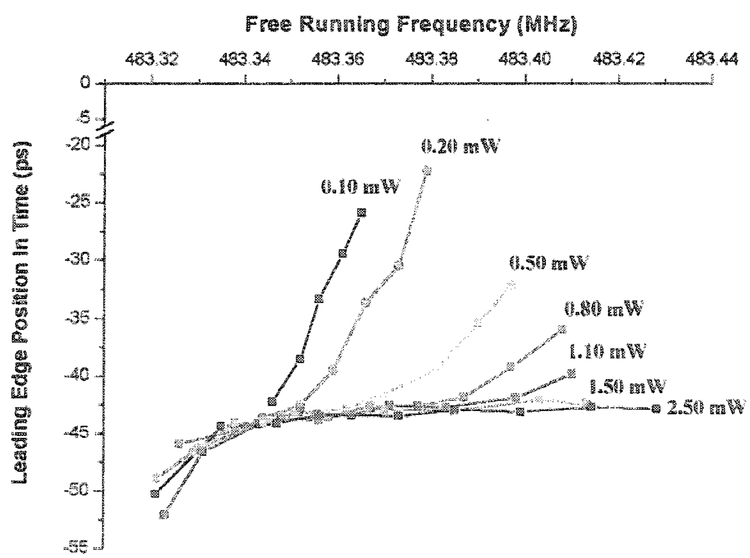

Figure 5-20: Position of the semiconductor laser pulse versus the free running frequency of the laser for different Ti:Sapphire powers. The Ti:Sapphire powers are labeled beside each trace.

Performing a cross-correlation measurement and tracking the position of the delay arm (refer back to Figure 5-1) for all of the measurements determines the shift in position. The position resolution of the delay arm is approximately 0.1 μm. The results from the experiment are summarized Figure 5-20.

Prior to examining the slopes of each of the curves, there is additional information worth discussing. Based on the experimental data, there is an optimal free running frequency for this external cavity semiconductor laser. At approximately 483.35 MHz, the traces in Figure 5-20 intersect, with the exception of the trace at 0.10 mW. At 0.1 mW, the pulling range is too small for synchronization to occur at 483.35 MHz. Operating at a free running frequency corresponding to 483.35 MHz is deemed optimal since any change in Ti:Sapphire power will result in a very small change in the position of the semiconductor laser pulse. In other words, intensity noise on the Ti:Sapphire laser will not induce additional timing jitter between the two lasers. This is of particular relevance when operating at low Ti:Sapphire pulse energies. Away from the optimum position, intensity noise on the Ti:Sapphire laser will influence the position of the semiconductor laser pulse. For large Ti:Sapphire pulse powers, the traces begin to overlap and level off, indicating that operating at the optimum repetition rate is no longer crucial.

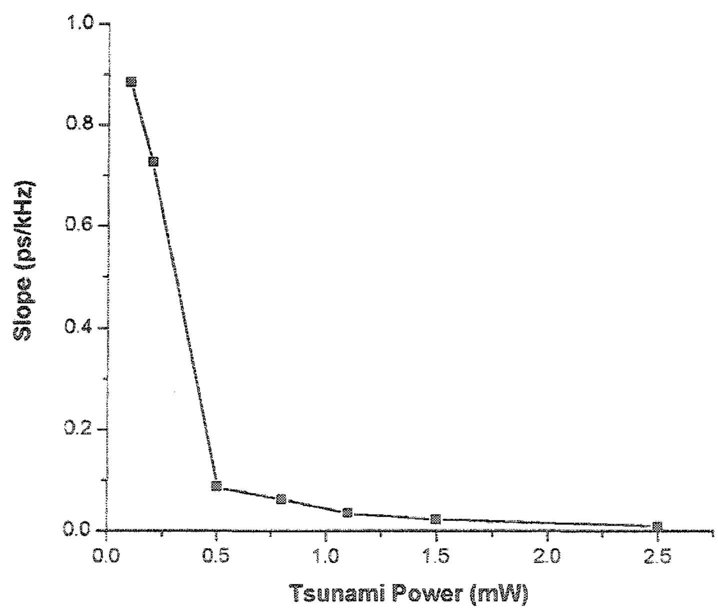

Figure 5-21: Slope from the traces in Figure 5-20 versus Ti:Sapphire power.

The slopes of the linear portion of the curves shown in Figure 5-20 are plotted in Figure 5-21. Comparing this with Figure 5-16, there is good qualitative agreement between the trend predicted by the model, and the trend measured experimentally. At low Ti:Sapphire pulse energies, a small change in repetition rate produces a large shift in the position of the semiconductor laser pulse. Increasing the Ti:Sapphire pulse energy causes the shift in position to become less pronounced, while approaching a constant value for large Ti:Sapphire pulse energies.

5.5 Comparison with other published works

There have been several reports on the synchronization of mode-locked semiconductor lasers to other mode-locked sources. Hoffman *et al.* report on the synchronization of an actively mode-locked semiconductor laser to a mode-locked Ti:Sapphire laser [158]. The Ti:Sapphire laser is used to trigger an electrical pulse generator which in turn is used to drive the semiconductor laser. The length of the external cavity for the semiconductor laser was set such that it closely matched the repetition rate of the Ti:Sapphire oscillator. Under these conditions, Hoffman was able to synchronize the two lasers, but was only able to achieve a temporal resolution of 10 ps in pump-probe experiments due to the large temporal jitter between the two lasers. As shown earlier, the method presented in this chapter was used to successfully synchronize a mode-locked semiconductor laser to a Ti:Sapphire laser with low time jitter between the two lasers.

Wang *et al.* [159] and Kurita *et al.* [160] use a technique similar to that presented in this chapter to synchronize two mode-locked semiconductor lasers. The pulses generated by a 1 GHz external cavity hybrid mode-locked semiconductor laser were used to synchronize the pulsed output of a passively mode-locked, two-section monolithic device operating at 40 GHz. The main difference between the work presented by Wang and the work presented in this chapter is the fact that both of Wang's lasers operate at the same wavelength. This means that there are two available mechanisms by which synchronization can occur, the first being absorber bleaching, and the second being pulse injection into the gain medium.

In order to synchronize a mode-locked semiconductor laser to another mode-locked source with ultra-low jitter, steps must be taken similar to Jones *et al.* [144]. Jones *et al.* synchronized a hybrid mode-locked external cavity semiconductor laser to a mode-locked Ti:Sapphire laser by modulating the absorber section with an external clock signal. The external clock signal is generated by the mode-locked Ti:Sapphire laser phase-locked to a highly stable optical frequency standard. To further reduce the timing-jitter, the mirror in the semiconductor laser external cavity is mounted on a piezo actuator that is connected to an electronic feedback loop. This enables the length of the external cavity to be adjusted to compensate for jitter due to spontaneous emission. This experimental setup has allowed the authors to obtain an ultra-low timing jitter of 22 fs (1 Hz to 100 MHz). The implementation by Jones *et al.* is far more complex than the relatively simple synchronization method presented in this chapter. However, it does provide indications of where improvements can be made in the current experimental setup if better performance is warranted for a given application.

5.6 Chapter summary

In this chapter I presented the results of synchronizing the mode-locked semiconductor laser ($\lambda \sim 980$ nm) to a mode-locked Ti:Sapphire laser ($\lambda \sim 800$ nm) via an all-optical synchronization method. Synchronization of the two systems was demonstrated for the semiconductor laser operating at repetition rates as high as the tenth harmonic of the Ti:Sapphire repetition rate. The RMS value of the timing jitter between the two lasers was measured to be as low as 50 fs in the 0 to 700 Hz range. A simple model based on counter-propagating pulses in a saturable absorber was used to simulate the synchronization process. Good qualitative agreement was obtained between the model and the experimental results.

Chapter 6 Summary and Future Work

6.1 Summary

In this thesis the development of broadly tunable mode-locked semiconductor lasers suitable for operation in a compact external cavity was presented. A novel laser design was used in order to achieve the largest passive (and hybrid) mode-locked tuning range ever reported. The ridge waveguide device has two electrical contacts for easy integration of a saturable absorber into the laser cavity. The active region consists of asymmetric quantum wells in order to obtain a large gain-bandwidth. The waveguide contains a bend such that a low facet modal reflectivity can be achieved for efficient external cavity operation.

Preliminary work on the development of mode-locked long-wavelength InGaAs/GaAs lasers was performed. Two-contact, bent-waveguide devices were used for external cavity mode-locking.

Results were also presented on the synchronization of the mode-locked external cavity semiconductor lasers with a mode-locked Ti:Sapphire laser. A simple model was developed to explain and to aid in optimizing the synchronization process.

A summary of the specific results related to each of the areas discussed follows.

6.1.1 Mode-locked external cavity semiconductor lasers

The experimental results obtained by mode-locking external cavity mounted semiconductor diode lasers were presented. The novel two section bent-waveguide device incorporating an asymmetric quantum well active region has produced, to the best of the author's knowledge, the largest tuning range ever achieved with a passively mode-locked semiconductor laser. In particular, tuning ranges of 61 nm and 75 nm have been achieved with dual and triple asymmetric quantum well lasers, respectively. Typical pulses have durations of a few picoseconds, with pulse durations as short as 510 fs achievable after post-compression.

The experimental results obtained by passive and hybrid mode-locking of long wavelength ($\lambda \sim 1070$ nm) InGaAs/GaAs lasers were also presented. This represents, to the best of the author's knowledge, the first experimental demonstration of mode-locking with an electrically pumped, edge-emitting, long wavelength InGaAs/GaAs laser. Pulses measuring 2 to 5 ps in duration are common, with pulses measuring as short as 570 fs achievable following compression.

Mode-locking as a function of the repetition rate was studied using a symmetric quantum well laser. For this particular system, it was found that operating at a repetition rate between 1300 and 1500 MHz would generate the largest signal for two-photon applications.

A select number of devices were used for monolithic passive mode-locking producing 1.5 ps pulses at repetition rates of 31 and 61 GHz.

As a separate benchmark, the shortest pulse obtained measured 430 fs in duration and was achieved using an external cavity mode-locked symmetric quantum well laser.

6.1.2 Laser synchronization

The mode-locked external cavity semiconductor laser was synchronized to a mode-locked Ti:Sapphire laser using an *all-optical* synchronization method. Synchronization was obtained for the semiconductor laser operating at repetition rates as high as the tenth harmonic of the Ti:Sapphire repetition rate. Good qualitative agreement was obtained between the simple model developed and experiment results. In particular, it was found that for a sufficiently high Ti:Sapphire pulse energy, a further increase in the pulse energy does not readily improve the synchronization conditions. At low pulse energies, it was experimentally shown that there is an optimal repetition rate at which to operate the semiconductor laser in order to minimize timing jitter produced by intensity fluctuations on the Ti:Sapphire pulse train.

This synchronization method is simple to set up and can be used as an additional diagnostic tool in studying passively mode-locked semiconductor lasers.

6.2 Future Work

Based on the results presented in this thesis, there are a number of avenues along which future work can proceed. Some of the areas suggested are a simple extension of the work already done, whereas other areas represent a significant new undertaking.

6.2.1 Improved mode profile

As discussed in section 3.6, the far-field pattern of the lasers tested exhibit some substructure in the vertical (growth) direction. This substructure is undesirable from a number of perspectives. The first is that it may be limiting the performance (pulse duration, pulse energy) of the mode-locked external cavity laser. Secondly, a beam with this far-field pattern cannot be focused as well as a beam with clearly defined single mode far-field. This is of particular importance when trying to optimize the system for two-photon applications. Spatial filtering can be used to improve the mode-profile, however, this comes at the expense of power. Improvements need to be made to the overall laser structure design to eliminate the substructure.

6.2.2 Improved laser mounting setup

Further improvements can be made to the mounting setup for better stability and reliability. In particular, the semiconductor laser should be properly packaged. This includes bonding the laser to a *thermally-matched* sub-mount, wire-bonding the contacts, enclosing the laser so that it is not open to air, and the use of a better bonding agent should be explored. There are two reasons why a better bonding agent is suggested. The first is that the Epotek epoxy may be introducing unnecessary additional stress on the laser chip, as compared with a gold/tin alloy. Secondly, it is unknown as to whether or not the chemicals making up the epoxy will interact with the laser facet in a negative manner, either during the curing stage or during the long-term operation of the laser.

6.2.3 Improved 3 AQW laser design

A number of difficulties were encountered while growing and testing the three asymmetric quantum well laser samples. While each design modification resulted in improvements over the previous iteration, the most recent triple AQW laser design is far from optimized. Beyond a certain current value (typically ~ 50 mA for 350 μm long devices), the devices begin to operate multimode in the lateral direction. This is of particular concern if the laser material is to be used to fabricate semiconductor optical amplifiers, which will be typically operated at high current values.

The only significant difference between the 2-AQW and 3-AQW laser structures is the addition of a single quantum well, which significantly increases the strain of the active region. Studying the strain of the 2-AQW and 3-AQW laser structures with a degree of polarization measurement [161] would be beneficial.

Extending the tuning range beyond that which is currently achievable could take a number of different approaches. The first approach is to use an improved 3-AQW structure (as discussed above). An improvement to the overall operating characteristics of the device at high currents may yield a small extension to the tuning range. The second approach is to modify the energy spacing between the quantum wells to further broaden the gain bandwidth. Moving the middle quantum well closer in energy to the highest energy quantum well may help extend the tuning range at the blue end of the spectrum. The final approach is to incorporate additional quantum wells of energy greater than or equal to the bluest quantum well in the 3-AQW design. While this approach is the most promising for significantly extending the tuning range, growing the structure with strain-compensating GaAsP layers would be required. As previously discussed, initial attempts to incorporate GaAsP barriers into the laser design were not very successful. As such, this issue needs to be studied in greater detail.

6.2.4 Long wavelength InGaAs/GaAs lasers

The results presented with the long wavelength InGaAs/GaAs lasers were based on laser structures containing a single quantum well. The success of these preliminary results suggests that the development of these lasers continue. One area to explore is the design and growth of a two quantum-well long wavelength InGaAs/GaAs lasers. As suggested in section 3.1.1, this may be accomplished by incorporating strain-balancing GaAsP layers into the laser design. This also requires further study of GaAsP grown on GaAs, including the index of refraction of the material in order to design optimized waveguides.

Another area of interest, which was mentioned in the introduction, is the use of mode-locked long wavelength InGaAs/GaAs lasers as a seed source for ytterbium-doped fibre amplifiers. Studies should continue in order to ascertain the effectiveness of such a configuration.

6.2.5 Higher order chirp compensation

The need for higher order chirp compensation is apparent when examining the results presented in Chapter 4. The time-bandwidth product of the optical pulses emitted directly from the semiconductor laser is typically a factor of 4 to 6 larger than the transform limit. Compression results in optical pulses with a time-bandwidth product larger than the theoretical limit by a factor of 2 to 3. Higher order chirp compensation is required in order to further compress the pulses. One possible avenue is to include additional optical elements in the laser cavity. Intra-cavity chirp compensation allowed Gee *et al.* to generate 250 fs pulses from a mode-locked external cavity laser [162]. Resan *et al.* report on 274 fs pulse generation from a dispersion-managed semiconductor mode-locked ring laser [163]. Since the phase information can be retrieved by synchronizing the laser with the Ti:Sapphire laser, this may prove to be an invaluable tool in attempting to compensate for the higher order chirp. As an alternative, the phase information can be retrieved through the use of a frequency resolved optical gating (FROG) technique [164]. However, the output of the oscillator would require amplification with an SOA so that there is a sufficient amount of power for the FROG measurement, similar to the work by Delfyett *et al.* [165].

6.2.6 Synchronization

Since good qualitative agreement was achieved between the simulated and experimental results, it is suggested that a more rigorous model, such as that presented by Khalfin *et al.* [155], be implemented. This would allow for further study of the dynamics of the mode-locked semiconductor laser in the presence of an external perturbation.

On the experimental side, it would also be interesting to perform the synchronization experiments with a wide range of control wavelengths. Also, given the fact that mode-locked semiconductor lasers operating at 980 nm and 1070 nm have been developed, the all-optical synchronization method can be used to synchronize two mode-locked semiconductor lasers. Such a system would be a useful tool for performing pump-probe experiments, which would allow the pump and the probe wavelengths to be independently tuned. Synchronizing the lasers using the all-optical synchronization method requires the 980 nm laser to be used as the master-oscillator. The 980 nm laser could be hybrid mode-locked, as opposed to passive mode-locked, to take advantage of the increased stability introduced by hybrid mode-locking. In order to have sufficient optical power for synchronization and measurement, the output of the master-oscillator will require amplification with an SOA. Furthermore, following the discussion in section 5.4.2, the pulses from the master-oscillator should be compressed.

6.2.7 Two-photon spectroscopy

The development of mode-locked, broadly tunable, semiconductor lasers has progressed sufficiently far that initial experiments with two-photon spectroscopy should be conducted. This avenue of research requires the continued development of semiconductor optical amplifiers in order to achieve sufficiently high pulse energies. Average powers in the 60-90 mW range are currently achievable with flared waveguide geometry SOAs developed within our research group [166].

Initial experiments with two-photon spectroscopy could include the study of two-photon absorption of various dyes of different concentrations. Results from these preliminary experiments would indicate which direction further efforts should take.

6.3 Concluding remarks

The development of a broadly tunable, ultra-short pulse semiconductor laser has been presented. The broad tuning range was achievable through the use of a novel laser design. Work was also presented on the development of mode-locked long wavelength InGaAs/GaAs lasers and on the synchronization of a mode-locked semiconductor laser with a mode-locked Ti:Sapphire laser. Both of these research areas have presented promising and interesting results. A number of suggestions have been made for future research, and it is hoped that some of these areas will be pursued in order to build on the work presented in this thesis.

Appendix A List of publications and conference contributions

M. J. Brennan, A. J. Budz, B. J. Robinson, P. Mascher and H. K. Haugen, "Ultrashort optical pulse generation with a mode-locked long wavelength (1075 nm – 1085 nm) InGaAs/GaAs semiconductor laser", *accepted for publication IEEE Photon. Tech. Lett.*, August 2004.

A. J. Budz, **M. J. Brennan** and H. K. Haugen, "Generation and amplification of ultra-short optical pulses from a mode-locked long-wavelength (1075 nm – 1085 nm) InGaAs/GaAs quantum well laser", *Conference for Lasers and Electro-Optics, accepted for presentation May 2004.*

M. J. Brennan, J. N. Milgram, A. J. Budz, P. Mascher, and H. K. Haugen, "Generation and amplification of wavelength tunable short optical pulses from asymmetric quantum well semiconductor devices", *Conference for Lasers and Electro-Optics*, June 2003, paper #CThM10

M. J. Brennan, J. N. Milgram, P. Mascher and H. K. Haugen, "Wavelength Tunable ultrashort pulse generation from a passively mode-locked asymmetric-quantum-well semiconductor laser", *Appl. Phys. Lett.* **81**, 2502 (2002).

M. J. Brennan, P. Mascher and H. K. Haugen, "Broadly Tunable Ultra-Short Pulse Generation Using Mode-Locked Asymmetric Quantum Well Semiconductor Lasers", *Photonics North and CAP Congress,* June 2002.

M. J. Brennan, H. F. Tiedje and H. K. Haugen, "Passively mode-locked semiconductor laser synchronization and pulse cross-correlation with a Ti:sapphire laser", *Electron. Lett.*, **38**, 14 (2002).

J. N. Milgram, **M. J. Brennan**, H. F. Tiedje, H. K. Haugen, "Picosecond pulses from mode-locked quantum well semiconductor lasers", *OPTO Canada: SPIE Regional Meeting on Optoelectronics, Photonics and Imaging*, SPIE vol. TD01, 21 (2002).

M. J. Brennan, J. N. Milgram, S. G. Wallace, P. Mascher and H. K. Haugen, "Broadly tunable short pulse generation using mode-locked asymmetric QW InGaAs/InGaAsP/InGaP diode lasers", *CAP Congress*, June 2001

S. G. Wallace, **M. J. Brennan**, H. K. Haugen and P. Mascher, "Short pulse asymmetric quantum well InGaAs/InGaAsP/InGaP Lasers", *Conference on Lasers and Electro-Optics (CLEO)*, May 2000, paper #CTuA61

Appendix B Beam profiles

The typical beam profiles of the semiconductor lasers are shown below in Figure B-1 and in Figure B-2. Since multimode behaviour was only seen in the vertical (growth) direction, only the profiles for this direction are shown. The profiles are obtained using a Ophir BeamStar CCD camera and are measured after collimating the laser output with a Thorlabs C230TM aspheric lens. The beam profile measured at a distance of approximately 7 cm from the collimating lens is shown in Figure B-1. At this distance from the laser, the laser output seems to consist of a single mode in the vertical direction.

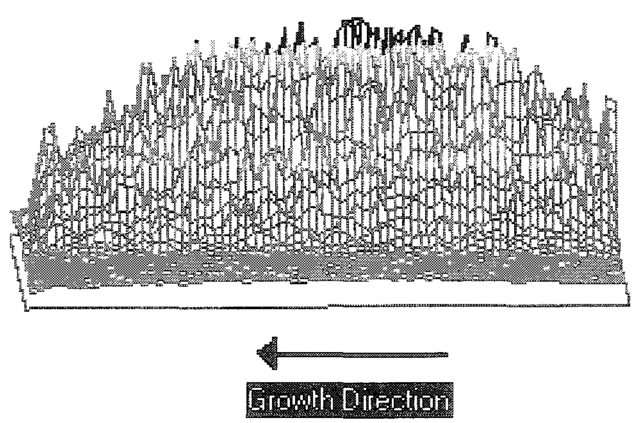

Figure B-1: Beam profile of the semiconductor lasers measured at a distance of approximately 7 cm from the collimating lens.

The beam profile at a distance of several meters from the collimating lens is shown in Figure B-2. In this case, the multimode structure in the vertical direction is clearly visible. The fact that the laser output looks to be single mode at a closer distance to the laser facet led the author to draw the wrong conclusion regarding the mode profile during the first measurements. When the full extent of the issue became known, a large number of laser structures (2-AQW, 3-AQW) had already been grown and many devices had already been fabricated and tested. The large turnaround time between laser design, growth, processing and testing limits the amount of trouble shooting that can be accomplished in a given time period. Devices from a new laser structure in which the contact layer has been moved further away from the active region are currently being fabricated. It is hoped that the modified design will eliminate the multi-mode behaviour.

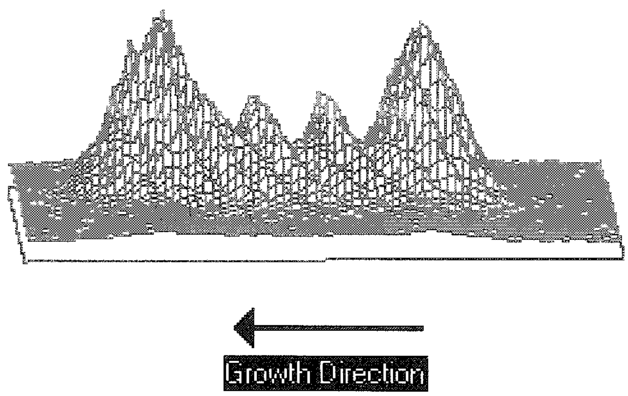

Figure B-2: Beam profile of the semiconductor lasers measured at a distance of several meters from the collimating lens.

Appendix C Sample Mounting for AR coating

This appendix outlines the procedures for mounting laser bars in the ECR-PECVD system and the mini PECVD system for AR coatings. The method used for mounting the samples in both systems is designed for use with lasers in bar format. The laser bar is mounted on end and is held in place by two pieces of silicon, as shown in Figure C-1.

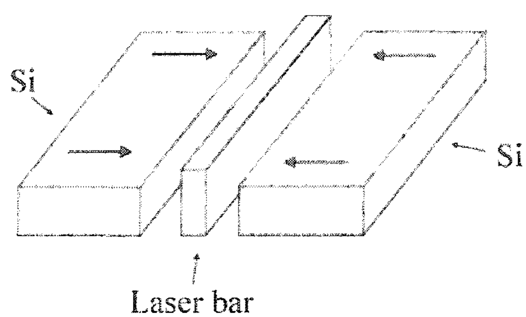

Figure C-1: Laser bar positioning and mounting for anti-reflection coating deposition.

Care must be taken when positioning the laser bar so as not to incur damage to the laser facet. Aside from holding the laser bar in place, the silicon also plays the role of witness sample for determining the index and thickness of the film deposited. There are a couple of considerations involved in correctly choosing the silicon pieces. The first is the thickness of the silicon wafer. The best results are obtained with pieces of Si that are 50 to 100 μm thinner than the width of the laser bar. For pieces of Si thicker than the width of the laser bar, shadowing effects limit deposition on the laser facet. For Si pieces much thinner, oxide is deposited on both the p-side and n-side metals layers, making electrical contact difficult. The second issue to consider is the quality of the cleaved edge of the Si piece. The desired case is for both pieces of Si to have nice straight cleaved edges. Poorly cleaved edges make it difficult to securely mount the laser bar and increase the risk of damaging the sample during the mounting process. Obtaining proper cleaves becomes difficult as the thickness of the Si wafers increase. For laser bars requiring thick pieces of Si (~750 μm or larger), an alternative mounting procedure is used. In this case, two sacrificial laser bars are cleaved (typically from older, unused material) with slightly shorter lengths than the original laser bar. The laser bar is then mounted as shown in Figure C-2. This method allows the use of thinner pieces of Si and also allows for deposition on large width laser bars where it may be difficult to obtain suitable pieces of Si.

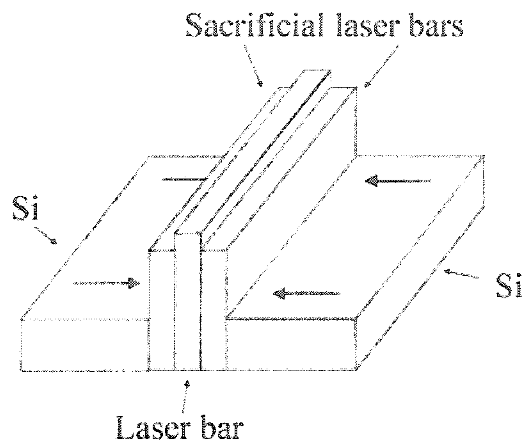

Figure C-2: Anti-reflection coating deposition mounting for large laser bars.

Appendix D AR coating with mini-PECVD

This appendix demonstrates that quality AR coatings can also be obtained with the mini-PECVD system. While the system does not provide as much control over the growth parameters as does the ECR-PECVD system, reproducible results are attainable. The amplified spontaneous emission spectrum of a laser before and after application of an AR coating are shown in Figure D-1. The analysis of the spectrum is shown in Figure D-2. The data is for a 350 μm long 3-AQW ridge waveguide laser. A minimum reflectivity of approximately 1.8×10^{-4} was achieved at a wavelength of 985 nm.

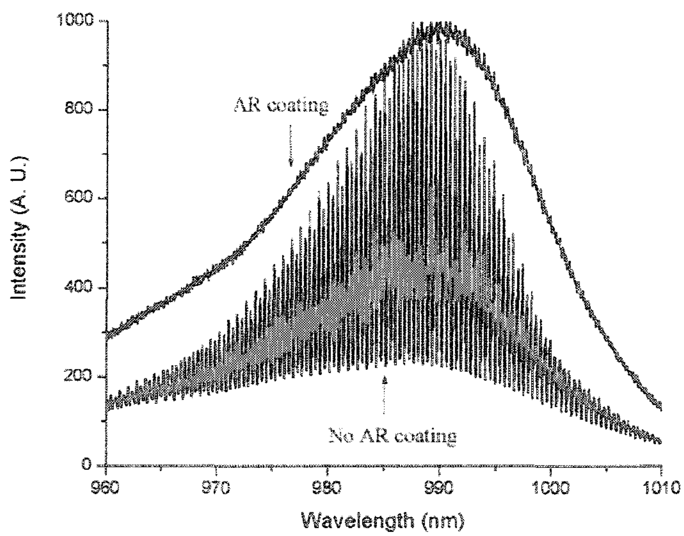

Figure D-1: Amplified spontaneous emission spectrum before and after application of an AR coating using the mini-PECVD. The drive current on the device was 6 mA, with the threshold current of the device measuring 9 mA. The AR coating had a refractive index of 1.81 and a thickness of 144 nm.

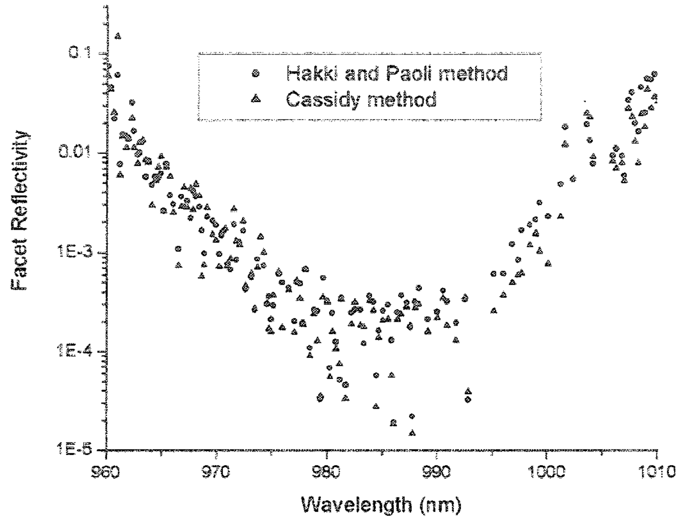

Figure D-2: Reflectivity of the AR coated laser facet obtained from analysis of the spectra shown in Figure D-1.

References

1 A. Lago, A. T. Obeidat, A. E. Kaplan, J. B. Khurgin and P. L. Shkolnikov, "Two-photon-induced fluorescence of biological markers based on optical fibers", *Opt. Lett.*, vol. 20, pp. 2054-2056, 1995.

2 J. Sytsma, J. M. Vroom, C. J. De Grauw, G. C. Gerristsen, "Time-gated fluorescence lifetime imaging and microvolume spectroscopy using two-photon excitation", *J. Microscopy*, vol. 191, pp. 39-51, 1998.

3 X. Michalet, A. N. Kapanidis, T. Laurence, F. Pinaud, S. Doose, M. Pflughoefft, S. Weiss, "The power and prospects of fluorescence microscopies and spectroscopies", *Annual Review of Biophysics and Biomolecular Structure*, vol. 32, pp. 161-182, 2003.

4 P. T. C. So, C. Y. Dong, B. R. Masters, and K. M. Berland, "Two Photon Excitation Fluorescence Microscopy", *Annu. Rev. Biomed. Eng.*, vol. 2, pp. 399-429, 2000.

5 C. Xu, W. W. Webb, "Measurement of two-photon excitation cross sections of molecular flourophores with data from 690 to 1050 nm", *J. Opt. Soc. Am. B.*, vol. 13, pp. 481-491, 1996.

6 R. P. Haugland, *Handbook of Fluorescent Probes and Research Products, 9th Ed.* (Molecular Probes, Eugene OR., 2002).

7 V. Cautaerts, D. J. Richardson, R. Paschotta, D. C. Hanna, "Stretched pulse Yb 3+ silica fiber laser", *Opt. Lett.*, vol. 22, pp. 316-318, 1997.

8 H. Lim, F. O. Ilday and F. W. Wise, "Generation of 2-nJ pulses from a femtosecond ytterbium fiber laser", *Opt. Lett.*, vol. 28, pp. 660-662, 2003.

9 Blend Orta, Ammar Hideur, Thierry Chartier, Marc Brunel, Cafer Zkul and Franois Sanchez, "90-fs stretched-pulse ytterbium-doped double-clad fiber laser ", Opt. Lett., 28, 1305 (2003).

10 O. G. Okhotnikov, L. Gomes, N. Xiang, T. Jouhti and A. B. Grudinin, "Mode-locked ytterbium fiber laser tunable in the 980 1070-nm spectral range ", Opt. Lett., 28, 1522 (2003).

11 P. T. Ho, L. A. Glasser, E. P. Ippen and H. A. Haus, "Picosecond Pulse Generation with a CW GaAlAs Laser Diode", *Appl. Phys.* Lett, vol. 33, pp. 241-242, 1978.

12 L. A. Glasser, "C.W. Modelocking of a GaInAsP Diode Laser," *Electronics Letters*, vol. 14, pp. 725-726, 1978.

13 M. B. Holbrook, W. E. Sleat and D. J. Bradley, "Bandwidth-limited picosecond pulse generation in an actively mode-locked GaAlAs diode laser", *Appl. Phys. Lett*, vol. 37, pp. 59-61, 1980.

14 J. P. van der Ziel, "Active mode locking of double heterostructure lasers in an external cavity", *J. Appl. Phys.*, vol. 52, pp. 4435-4446, 1981.

15 A. Olsson and C. L. Tang, "Active Mode Locking of Linear and Ring External-Cavity Semiconductor Lasers", *IEEE J. Quantum. Electron.*, vol. 17, pp. 1977-1978, 1981.

16 S. W. Corzine, J. E. Bowers, G. Przybylek, U. Koren, B. I. Miller and C. E. Soccolich, "Actively mode-locked GaInAsP laser with subpicosecond output", *Appl. Phys. Lett.*, vol. 52, pp. 348-350, 1988.

17 A. Takada, K. Sato, M. Saruwatari and M. Yamamoto, "Pulse width tunable subpicosecond pulse generation from an actively modelocked monolithic MQW laser/MQW electroabsorption modulator", *Electron. Lett.*, vol. 30, pp. 898-900, 1994.

18 P. J. Delfyett, L. T. Florez, N. Stoffel, T. Gmitter, N. C. Andreadakis, Y. Silberberg, J. P. Heritage, G. A. Alphonse, "High-Power Ultrafast Laser Diodes", *IEEE J. Quantum. Electron.*, vol. 28, pp. 2203-2219, 1992.

19 J. E. Bowers, P. A. Morton, A. Mar and S. W. Corzine, "Actively Mode-Locked Semiconductor Lasers", *IEEE J. Quantum. Electron.*, vol. 25, pp. 1426-1439, 1989.

20 P. P. Vasil'ev, *Ultrafast Diode Lasers, Fundamentals and Applications* (Artech House, Boston, 1995), section 4.1.3, pp. 108-112.

21 E. P. Ippen, D. J. Eilenberger and R. W. Dixon, "Picosecond pulse generation by passive mode locking of diode lasers", *Appl. Phys. Lett.*, vol. 37, pp. 267-269, 1980.

22 H. Yokoyama, H. Ito and H. Inaba, "Generation of subpicosecond coherent optical pulses by passive mode locking of an AlGaAs diode laser", *Appl. Phys. Lett.*, vol. 40, pp. 105-107, 1981.

23 J. P. van der Ziel, W. T. Tsang, R. A. Logan and W. M. Augustyniak, "Pulsating output of separate confinement buried optical guide lasers due to the deliberate introduction of saturable loss", *Appl. Phys. Lett.*, vol. 39, pp. 376-378, 1981.

24 J. P. van der Ziel, W. T. Tsang, R. A. Logan, R. M. Mikulyak and W. M. Augustyniak, "Subpicosecond pulses from passively mode-locked GaAs buried optical guide semiconductor lasers", *Appl. Phys. Lett.*, vol. 39, pp. 525-527, 1981.

25 J. P. van der Ziel, R. A. Logan, R. M. Mikulyak, "Generation of subpicosencond pulses from an actively mode locked GaAs laser in an external ring cavity", *Appl. Phys. Lett*, vol. 39, pp. 867-869, 1981.

26 C. Harder, J. S. Smith, K. Y. Lau, A. Yariv, "Passive mode locking of buried heterostructure lasers with nonuniform current injection", *Appl. Phys. Lett.*, vol. 42, pp. 772-774, 1983.

27 P. A. Morton, J. E. Bowers, L. A. Koszi, M. Soler, J. Lopata and D. P. Wilt, "Monolithic hybrid mode-locked 1.3 μm semiconductor lasers", *Appl. Phys. Lett.*, vol. 56, pp. 111-113, 1990.

28 J. F. Martins-Filho, E. A. Avrutin, C. N. Ironside and J. S. Roberts, "Monolithic Multiple Colliding Pulse Mode-Locked Quantum-Well Lasers: Experiment and Theory", *IEEE J. Sel. Topics Quantum Electron.*, vol. 1, pp. 539-551, 1995.

29 D. J. Derickson, R. J. Helkey, A. Mar, J. R. Karin, J. G. Wasserbauer, J. E. Bowers, "Short Pulse Generation Using Multisegment Mode-Locked Semiconductor Lasers", *IEEE J. Quantum. Electron.*, vol. 28, pp. 2186-2201, 1992.

30 Y. Silberberg, P. W. Smith, D. J. Eilenberger, D. A. B. Miller, A. C. Gossard and W. Wiegmann, "Passive mode locking of a semiconductor diode laser", *Optics Letters*, vol. 9, pp. 507-509, 1984.

31 W. A. Stallard and D. J. Bradley, "Bandwidth-limited picosecond pulse generation in a synchronously pumped GaAs laser containing a variable absorber diode", *Appl. Phys. Lett.*, vol. 43, pp. 626-628, 1983.

32 J. McInerney, L. Reekie, and D. J. Bradley, "Bandwidth-limited picosecond pulse generation by hybrid mode-locking in a ring cavity GaAlAs Laser", *Electron. Lett.*, vol. 21, pp. 117-118, 1985.

33 P. J. Delfyett, C.-H. Lee, L. T. Florez, N. G. Stoffel, T. J. Gmitter, N. C. Andreadakis, G. A. Alphonse, J. C. Connolly, "Generation of subpicosecond high-power optical pulses from a hybrid mode-locked semiconductor laser", *Opt. Lett.*, vol. 15, pp. 1371-1373, 1990.

34 P. J. Delfyett, L. Florez, N. Stoffel, T. Gmitter, N. Andreadakis, G. Alphonse and W. Ceiclik, "200-fs optical pulse generation and intracavity pulse evolution in a hybrid mode-locked semiconductor diode-laser/amplifier system", *Opt. Lett.*, vol. 17, pp. 670-672, 1992.

35 H. Inaba, "Generation and control of transform-limited optical pulses in subpico- and picosecond regions from semiconductor diode lasers", *Int. J. Electronics*, vol. 60, pp. 5-21, 1986.

36 T. Schrans, R. A. Salvatore, S. Sanders and A. Yariv, "Subpicosecond (320 fs) pulses from cw passively mode-locked external cavity two-section multiquantum well lasers", *Electron. Lett.*, vol. 28, pp.1480-1482, 1992.

37 A. G. Weber, M. Schell, G. Fischbeck and D. Bimberg, "Generation of Single Femtosecond Pulses by Hybrid Mode Locking of a Semiconductor Laser", *IEEE J. Quantum Electron.*, vol. 28, pp. 2220-2229, 1992.

38 N. Stelmakh and J.-M. Lourtioz, "230 fs, 25 W pulses from conventional mode-locked laser diodes with saturable absorber created by ion implantation", *Electron. Lett.* Vol. 29, pp. 160-162, 1993.

39 J. Yu, M. Schell, M. Schulze, and D. Bimberg, "Generation of 290 fs pulses at 1.3 mm by hybrid mode-locking of a semiconductor laser and optimization of the time-bandwidth product", *Appl. Phys. Lett.*, vol. 65, pp. 2395-2397, 1994.

40 P. P. Vasil'ev, *Ultrafast Diode Lasers, Fundamentals and Applications* (Artech House, Boston, 1995), section 4.2.3, pp. 121-123.

41 J. Chen, W. Sibbett and J. I. Vukusic, "Tunable mode-locked semiconductor lasers incorporating Brewster-angled diodes", *Optics Communications*, vol. 48, pp. 427-431, 1984.
42 J. E. Epler, G. S. Jackson, N. Holonyak Jr., M. Weinstein, R. D. Burnham and T. L. Paoli, "Mode-locked coupled-stripe quantum well laser operation (λ~7350Å) in a tunable external grating cavity", *Appl. Phys. Lett.*, vol. 47, pp. 1022-1023, 1985.
43 M. Serenyi, J. Kuhl, and E. O. Göbel, "Pulse shortening of actively-mode-locked diode lasers by wavelength tuning", *Appl. Phys. Lett.*, vol. 50, pp. 1213-1215, 1987.
44 A. S. Hou, R. S. Tucker and G. Eisenstein, "Pulse Compression of an Actively Modelocked Diode Laser Using Linear Dispersion in Fiber", *IEEE Photon. Tech. Lett.*, vol. 2, pp. 322-324, 1990.
45 J. M. Wiesenfeld, M. Kuznetsov and A. S. Hou, "Tunable, Picosecond Pulse Generation using a Compressed, Modelocked Laser Diode Source", *IEEE Photon. Tech. Lett.*, vol. 5, pp. 319-321, 1990.
46 D. M. Bird, R. M. Fatah, M. K. Cox, P. D. Constantine, J. C. Regnault and K. H. Cameron, "Miniature packaged actively mode-locked semiconductor laser with tunable 20 ps transform limited pulses", *Electron. Lett.*, vol. 26, pp. 2086-2087, 1990.
47 M. Hofmann, W. Weise, W. Elsäßer and E. O. Göbel, "High spectral tuning range of a modelocked InGaAs/InGaAsP MQW laser diode due to light hole gain contribution", *IEEE Photon. Tech. Lett.*, vol. 6, pp. 1306-1308, 1994.
48 K. Akimoto, Y. Katagiri, K-I. Suzuki and S. Nagaoka, "Widely tunable mode-locked laser diodes using optical disk filter", *IEEE Photon. Tech. Lett.*, vol. 12, pp. 615-617, 2000.
49 W. C. Wu, Y. K. Chen, T. Tanbun-Ek, R. A. Logan and M. A. Chin, "Tunable monolithic colliding pulse mode-locked quantum-well lasers", *IEEE Photon. Tech. Lett.*, vol. 3, pp. 874-876, 1991.
50 T. Schrans, S. Sanders and A. Yariv, "Broad-band wavelength tunable picosecond pulses from CW passively mode-locked two-section multiple quantum-well lasers", *IEEE Photon. Tech. Lett.*, vol. 4, pp. 323-326, 1992.
51 R. A. Salvatore, T. Schrans and A. Yariv, "Wavelength Tunable Source of Subpicosecond Pulses from CW Passively Mode-Locked Two-Section Multiple-Quantum-Well Laser", *IEEE Photon. Tech. Lett.*, vol. 5, pp. 756-758, 1993.
52 B-L. Lee, C-F. Lin, "Short-pulse generation with broad-band tunability from semiconductor lasers in an external ring cavity", *IEEE Photon. Tech. Lett.*, vol. 12, pp. 618-620, 2000.
53 H.-F. Liu, Y. Ogawa and S. Oshiba, "Generation of an extremely short single mode pulse (~2 ps) by fiber compression of a gain-switched pulse from a 1.3 μm distributed-feedback laser diode", *Appl. Phys. Lett.*, vol. 59, pp. 1284-1286, 1991.
54 H. Ohta and T. Oki, "310-Femtosecond optical pulse generation from a gain-switched laser diode using soliton compression", *Jpn. J. Appl. Phys.*, vol. 33, pp. L1604-L1606, 1994.
55 E. Yamada, K. Suzuki and M. Nakazawa, "Subpicosecond optical demultiplexing at 10 GHz with zero-dispersion, dispersion-flattened, nonlinear fibre loop mirror controlled by 500 fs gain-switched laser diode", *Electron. Lett.*, vol. 30, pp. 1966-1967, 1994.
56 H. Ohta, S. Nogiwa, Y. Kawaguchi and Y. Endo, "Generation of 650-femtosecond optical pulses from a gain-switched laser diode using second-harmonic generation", *Jpn. J. Appl. Phys.*, vol. 38, pp. 5905-5909, 1999.
57 C. Lin, P. L. Liu, T. C. Damen, D. J. Eilenberger and R. L. Hartman, "Simple Picosecond Pulse Generation Scheme for Injection Lasers", *Electron. Lett.*, vol. 16, pp. 600-602, 1980.
58 E. O. Gobel, G. Veith, J. Kuhl, H. U. Habermeier, K. Lubke and A. Perger, "Direct Gain Modulation of a Semiconductor Laser by a GaAs Picosecond Optoelectronic Switch", *Appl. Phys. Lett.*, vol. 42, pp. 25-27, 1983.
59 H. Ito, H. Yokoyama, S. Murata and H. Inaba, "Picosecond Optical Pulse Generation from an RF Modulated AlGaAs DH Diode Laser", *Electron. Lett.*, vol. 15, pp. 738-740, 1979.
60 P. L. Liu, C. Lin, I. P. Kaminow and J. J. Hsieh, "Picosecond Pulse Generation from InGaAsP Lasers at 1.25 and 1.3 μm by Electrical Pulse Pumping", *IEEE J. Quantum Electron.*, vol. 17, pp. 671-674, 1981.

61 D. Bimberg, K. Ketterer, E. H. Bottcher and E. Scholl, "Gain modulation of unbiased semiconductor lasers: ultrashort light-pulse generation in the 0.8 μm – 1.3 μm wavelength range", *Int. J. Electronics*, vol. 60, pp. 23-45, 1986.

62 C. Lin and J. E. Bowers, "Measurement of 1.3 and 1.55 μm Gain-Switched Semiconductor Laser Pulses with a Picosecond IR Streak Camera and a High-Speed InGaAs PIN Photodiode", *Electron. Lett.*, vol. 21, pp. 1200-1202, 1985.

63 C. T. Chang, C. K. Sun, D. J. Albares and E. W. Jacobs, "High-energy (59 pJ) and Low-Jitter (250 fs) picosecond pulses from gain-switching of a tapered-stripe laser diode via resonant driving", *IEEE Photon. Tech. Lett.*, vol. 8, pp. 1157-1159, 1996.

64 K. A. Williams, I. H. White, R. V. Penty and F. R. Laughton, "Gain-switched dynamics of tapered waveguide bow-tie lasers: Experiment and theory", *IEEE Photon. Tech. Lett.*, vol. 9, pp 167-169, 1997.

65 A. E. Siegman, *Lasers*, (University Science Books, Mill Valley CA, 1986)

66 J. T. Verdeyen, *Laser Electronics*, (Prentice Hall, Englewood Cliffs NJ, 1995)

67 D. Z. Tsang, J. N. Walpole, Z. L. Liau, S. H. Groves and V. Diadiuk, "Q-Switching of a Low Threshold Buried Heterostructure Diode Lasers at 10 GHz", *Appl. Phys. Lett.*, vol. 45, pp. 204-206, 1984.

68 Y. Arakawa, A. Larsson, J. Paslaski and A. Yariv, "Active Q-Switching in a GaAs/GaAlAs Multiquantum Well Laser with an Intracavity Loss Modulator", *Appl. Phys. Lett.*, vol. 48, pp. 561-563, 1986.

69 D. R. Dykaar, K. Berthold, A. F. J. Levi, T. Tanbun-Ek and R. A. Logan, "Large-Signal Picosecond Response of InGaAs/InP Quantum Well Lasers with an Intracavity Loss Modulator", *Appl. Phys. Lett.*, vol. 56, pp. 1629-1631, 1990.

70 T. L. Koch, P. Wilt and A. yariv, "Q-Switching of Semiconductor Lasers with Picosecond Light Pulses", *Picosecond Phenomena II*, R. M. Hochstrasser, W. Kaiser and C. V. Shank, Eds., Berlin: Springer-Verlag, 1980, pp. 34-37.

71 B. J. Thedrez, S. E. Saddow, Y. Q. Liu, C. Wood, R. Wilson and C. H. Lee, "Experimental and Theoretical Investigation of Large Output Power Q-Switched AlGaAs Semiconductor Lasers", *IEEE Photon. Tech. Lett.*, vol. 5, pp. 19-22, 1993.

72 P. P. Vasil'ev, "Ultrashort pulse generation in diode-lasers" ,*Opt. Quant. Electron.*, vol. 24, pp. 801-824, 1992.

73 H. A. Haus, "Theory of mode-locking with a slow saturable absorber", *IEEE J. Quantum. Electron.*, vol. 11, pp. 736-746, 1975.

74 M. Schell, A. G. Weber, E. Scholl, and D. Bimberg, "Fundamental limits of sub-ps pulse generation by active mode locking of semiconductor lasers: the spectral gain width and the facet reflectivities", *IEEE J. Quantum. Electron.*, vol. 27, pp. 1661-1668, 1991.

75 M. Dülk, M. Döbeli and H. Melchior, "Fabrication of Saturable Absorbers in InGaAsP-InP Bulk Semiconductor Laser Diodes by Heavy Ion Implantation", *IEEE J. Sel. Topics Quantum. Electron.*, vol. 7, pp. 124-134, 2001.

76 P. W. Smith, Y. Silberberg, and D. A. B. Miller, "Mode locking of semiconductor diode lasers using saturable excitonic nonlinearities", *J. Opt. Soc. Am. B*, vol. 2. pp. 1228-1235, 1985.

77 U. Keller, D. A. B. Miller, G. D. Boyd, T. H. Chiu, J. F. Ferguson and M. T. Asom, "Solid-state low-loss intracavity saturable absorber for Nd:YLF lasers: an antiresonant semiconductor Fabry-Perot saturable absorber", *Opt. Lett.*, vol. 17, pp. 505-507, 1992.

78 H. A. Haus, and Y. Silberberg, "Theory of mode locking of a laser diode with a multiple-quantum-well structure", *J. Opt. Soc. Am. B.*, vol. 2, pp. 1237-1243, 1985.

79 J. P. van der Ziel and R. A. Logan, "Dispersion of the group velocity refractive index in GaAs double heterostructure lasers", *IEEE J. Quantum. Electron.*, vol. 19, pp. 164-169, 1983.

80 P. P. Vasil'ev, *Ultrafast Diode Lasers, Fundamentals and Applications* (Artech House, Boston, 1995), section 4.7, pp. 143.

81 P. A. Morton, R. Helkey and J. E. Bowers, "Dynamic Detuning in Actively Mode-locked Semiconductor Lasers", *IEEE J. Quantum. Electron.*, vol. 25, pp. 2621-2633, 1989.

82 M. Schell, J. Yu, M. Tsuchiya and T. Kayima, "Chirp of passively and actively mode-locked semiconductor lasers", *Appl. Phys. Lett.*, vol. 67, pp. 1797-1799, 1995.
83 M. Schell, M. Tsuchiya and T. Kamiya, "Chirp and Stability of Mode-locked Semiconductor Lasers", *IEEE J. Quantum. Electron.*, vol. 32, pp. 1180-1190, 1996.
84 C. H. Henry, "Theory of the linewidth of semiconductor lasers", *IEEE J. Quantum. Electron.*, vol. 18, pp. 259-264, 1982.
85 G. P. Agrawal and C. M. Bowden, "Concept of Linewidth Enhancement Factor in Semiconductor Lasers: Its Usefulness and Limitations", *IEEE Photon. Tech. Lett.*, vol. 5, pp. 640-642, 1993.
86 C-F. Lin, B-L. Lee and P-C. Lin, "Broad-band Superluminescent Diodes Fabricated on a substrate with Asymmetric Dual Quantum Wells", *IEEE Photon. Tech. Lett.*, vol. 8, pp. 1456-1458, 1996.
87 C-F. Lin and B-L. Lee, "Extremely broadband AlGaAs/GaAs superluminescent diodes", *Appl. Phys. Lett.*, vol. 71, pp. 1598-1600, 1997.
88 X. Zhu, D. T. Cassidy, M. J. Hamp, D. A. Thompson, B. J. Robinson, Q. C. Zhao and M. Davies, "1.4-μm InGaAsP-InP Strained Multiple-Quantum-Well Laser for Broad-Wavelength Tunability", *IEEE Photon. Tech. Lett.*, vol. 9, pp. 1202-1204, 1997.
89 H. S. Gingrich, D. R. Chumney, S.-Z. Sun, S. D. Hersee, L. F. Lester and S. R. J. Brueck, "Broadly Tunable External Cavity Laser Diodes with Staggered Thickness Multiple Quantum Wells", *IEEE Photon. Tech. Lett.*, vol. 9, pp. 155- 157, 1997.
90 M. J. Hamp and D. T. Cassidy, "Critical Design Parameters for Engineering Broadly Tunable Asymmetric Multiple-Quantum-Well Lasers", *IEEE J. Quantum. Electron.*, vol. 36, pp. 978-983, 2000.
91 M. J. Hamp, *Asymmetric Quantum Well Lasers*, Ph. D. thesis, McMaster University, 2000.
92 S. C. Woodworth, D. T. Cassidy and M. J. Hamp, "Experimental Analysis of a Broadly Tunable InGaAsP Laser with Compositionally Varied Quantum Wells", *IEEE J. Quantum. Electron.*, vol. 39, pp. 426-430, 2003.
93 S. Adachi, "Material Parameters of $In_{1-x}Ga_xAs_yP_{1-y}$ and related binaries", *J. Appl. Phys.*, vol. 53, pp. 8775-8792, 1982.
94 R. E. Nahory, M. A. Pollack, W. D. Johnston Jr., and R. L. Barns, "Band Gap versus composition and demonstration of Vegard's law for $In_{1-x}Ga_xAs_yP_{1-y}$ lattice matched to InP", *Appl. Phys. Lett.*, vol. 33, pp. 659-661, 1978.
95 L. A. Coldren, and S. W. Corzine, *Diode Lasers and Photonic Integrated Circuits,* (Wiley-Interscience, New York, 1995), section 4.6, pp. 160-162.
96 J. W. Matthews and A. E. Blakeslee, "Defects in epitaxial multilayers I – Misfit dislocations", *J. Cryst. Growth*, vol. 27, pp. 118-125, 1974.
97 I. J. Fritz, T. Picraux, L. R. Dawson, T. J. Drummond, W. D. Laidig and N. G. Anderson, "Dependence of critical layer thickness on strain for InGaAs/GaAs strained-layer superlattices", *Appl. Phys. Lett.*, vol. 46, pp. 967-969, 1985.
98 T. G. Andersson, Z. G. Chen, V. D. Kulakovskii, A. Uddin and J. T. Vallin, "Variation of the critical layer thickness with In Content in Strained InGaAs-GaAs quantum wells grown by Molecular Beam Epitaxy", *Appl. Phys. Lett.*, vol. 51, pp. 752-754, 1987.
99 N. K. Dutta, W. S. Hobson, D. Vakhshoori, H. Han, P. N. Freeman, J. F. de Jong and J. Lopata, "Strain Compensated InGaAs-GaAsP-InGaP Laser", *IEEE Photon. Tech. Lett.*, vol. 8, pp. 852-854, 1996.
100 H. Han, P. N. Freeman, W. S. Hobson, N. K. Dutta, J. Lopata, J. D. Wynn, S. N. G. Chu, "High-speed Modulation of Strain-Compensated InGaAs-GaAsP-InGaP Multiple-Quantum-Well Lasers", *IEEE Photon. Tech. Lett.*, vol. 8, pp. 1133-1135, 1996.
101 W.-J. Choi, P. D. Dapkus, J. J. Jewell, "1.2 μm GaAsP/InGaAs Strain compensated single-quantum-well diode laser on GaAs using Metal-Organic Chemical Vapor Deposition", *IEEE Photon. Tech. Lett.*, vol. 11, pp. 1572-1574, 1999.

102 N. Tansu, L. J. Mawst, "High-performance strain compensated InGaAs-GaAsP-GaAs ($\lambda = 1.17$ μm) quantum-well diode lasers", *IEEE Photon. Tech. Lett.*, vol. 13, pp. 179-181, 2001.
103 F. Bugge, U. Zeimer, S. Gramlich, I. Rechenberg, J. Sebastian, G. Erbert and M. Weyers, "Effect of growth conditions and strain compensation on indium incorporation for diode lasers emitting above 1050 nm", *J. Cryst. Growth.*, vol. 221, pp. 496-502, 2000.
104 S. G. Wallace, "InGaAsP/GaAs Quantum Well Lasers: Material Properties, Laser Design and Fabrication, Ultrashort Pulse External Cavity Operation", Ph. D. thesis, McMaster University, 2000.
105 S. W. Corzine, R.-H. Yan and L. A. Coldren, in *Quantum Well Lasers, pp.17-96, Academic Press, 1993.*
106 H. Yamazaki, A. Tomita, M. Yamaguchi and Y. Sasaki, "Evidence of nonuniform carrier distribution in multiple quantum well lasers", *Appl. Phys. Lett.*, vol. 71, pp. 767-769, 1997.
107 M. J. Hamp, D. T. Cassidy, B. J. Robinson, Q. C. Zhao, D. A. Thompson and M. Davies, "Effect of Barrier Height on the Uneven Carrier Distribution in Asymmetric Multiple-Quantum-Well InGaAsP Lasers", *IEEE Photon. Tech. Lett.*, vol. 10, pp. 1380-1382, 1998.
108 M. J. Hamp, D. T. Cassidy, B. J. Robinson, Q. C. Zhao, and D. A. Thompson, "Nonuniform carrier distribution in asymmetric multiple-quantum-well InGaAsP laser structures with different numbers of quantum wells", *Appl. Phys. Lett.*, vol 74, pp. 744-746, 1999.
109 M. J. Hamp, and D. T. Cassidy, "Experimental and Theoretical Analysis of the Carrier Distribution in Asymmetric Multiple-Quantum-Well InGaAsP Lasers", *IEEE J. Quantum. Electron.*, vol. 37, pp. 92-99, 2001.
110 M. Asada, A. R. Adams, K. E. Stubkjaer, Y. Suematsu, Y. Itaya and S. Arai, "The Temperature Dependence of the Threshold Current of GaInAsP/InP DH Lasers", *IEEE J. Quantum. Electron.*, vol. 17, pp. 611-619, 1981.
111 S. R. Chinn, P. S. Zory, and A. R. Reisinger, "A Model for GRIN-SCH-SQW Diode Lasers", *IEEE J. Quantum. Electron.*, vol. 24, pp. 2291-2214, 1988.
112 M. Asada, "Intraband relaxation time in quantum-well lasers", *IEEE J. Quantum. Electron.*, vol. 25, pp. 2019-2026, 1989.
113 L. M. Walpita, "Solution for planar optical waveguide equations by selecting zero elements in a characteristic matrix", *J. Opt. Soc. Am. A*, vol. 2, pp. 595-602, 1985.
114 S. L. Chuang, *Physics of Optoelectronic Devices,* (Wiley-Interscience, New York, 1995), section 7.5, pp. 270-273.
115 X. Zeng and A. Naqwi, "Far-field distribution of double-heterostructure diode laser beams", *Applied Optics*, vol. 32, pp.4491-4494 (1993).
116 M. G. Boudreau, *SiON Waveguides deposited by electron cyclotron resonance chemical vapour deposition, Master's Thesis, McMaster University, 1993.*
117 B. W. Hakki and T. L. Paoli, "Gain spectra in GaAs double-heterostructure injection lasers", *J. Appl. Phys.*, vol. 46, pp. 1299-1306, 1975.
118 D. T. Cassidy, "Technique for measurement of the gain spectra of semiconductor diode lasers", *J. Appl. Phys.*, vol. 56, pp. 3096-3099, 1984.
119 C. Vassallo, "Rigorous and approximate calculations of antireflection layer parameters for traveling-wave diode-laser amplifiers", *Electron. Lett.*, vol. 21, pp. 333-334, 1985.
120 C. Vassallo, "Reflectivity of multidielectric coatings deposited on the end facet of a weakly guiding dielectric slab wave-guide", *J. Opt. Soc. Am.*, vol. 5, pp. 1918-1928, 1988.
121 M. Boudreau, implementation of the Vassallo algorithm in Turbo C.
122 P. Sewell, M. Reed, T. M. Benson, P. C.Kendall, "Full vector analysis of two-dimensional angled and coated optical waveguide facets", *IEEE J. Quantum. Electron.*, vol. 33, pp. 2311-2318, 1997.
123 A. T. Semenov, V. R. Shidlovski and S. A. Safin, "Wide spectrum single quantum well superluminescent diodes at 0.8 μm with bent optical waveguides", *Electron. Lett.*, vol. 29, pp. 854-855, 1993.

124 C.-F. Lin and C.-S. Juang, "Superluminescent diodes with bent waveguide", *IEEE Photon. Tech. Lett.*, vol. 8, pp. 206-208, 1996.
125 H. Hillmer, K. Magari and Y. Suzuki, "Chirped gratings for DFB laser diodes using bent waveguides", *IEEE Photon. Tech. Lett.*, vol. 5, pp. 10-12, 1993.
126 R. Helkey, W. Zou, A. Mar, D. B. Young and J. Bowers, "Curved and Tapered Waveguide Mode-locked InGaAs/AlGaAs Semiconductor Lasers Fabricated by Impurity Induced Disordering", *IEEE Trans. Electron Devices*, vol. 40, pp. 2107, 1993.
127 C. A. Williamson, M. J. Adams, A. D. Ellis and A. Borghesani, "Mode locking of semiconductor laser with curved waveguide and passive mode expander", *Appl. Phys. Lett.*, vol. 82, pp. 322-324, 2003.
128 O. E. Martinez, "3000 times grating compressor with positive group velocity dispersion: Application to fiber compensation in 1.3-1.6 μm region", *IEEE J. Quantum. Electron.*, vol. 23, pp. 59-64, 1987.
129 J. P. Curtis, J. E. Carroll, "Autocorrelation systems for the measurement of picosecond pulses from injection-lasers", *Int. J. Electron.*, vol. 60, pp. 87-111, 1986.
130 M.J. Brennan, J.N. Milgram, P. Mascher and H.K. Haugen, "Wavelength Tunable ultrashort pulse generation from a passively mode-locked asymmetric-quantum-well semiconductor laser", *Appl. Phys. Lett.*, vol. 81, pp. 2502-2504, 2002.
131 M.J. Brennan, A. J. Budz, B. J. Robinson, P. Mascher and H. K. Haugen, "Ultrashort optical pulse generation with a mode-locked long wavelength (1075 nm – 1085 nm) InGaAs/GaAs semiconductor laser", *accepted for publication IEEE Photon. Tech. Lett., August issue 2004.*
132 G. Eisenstein, U. Koren, G. Raybon, T. L. Koch, J. M. Wiesenfeld, M. Wegener, R. S. Tucker, and B. I. Miller, "Large- and small-signal gain characteristics of 1.5 μm multiple quantum well optical amplifiers", *Appl. Phys. Lett.*, vol. 56, pp. 1201-1203, 1990.
133 J. L. Pleumeekers, M. Kauer, K. Dreyer, C. Burrus, A. G. Dentai, S. Shunk, J. Leuthold, C. H. Joyner, "Acceleration of gain recovery in semiconductor optical amplifiers by optical injection near transparency wavelength", *IEEE Photon. Tech. Lett.*, vol. 14, pp. 12-14, 2002.
134 J. L. A. Dubbeldam, J. A. Leegwater and D. Lenstra, "Theory of mode-locked semiconductor lasers with finite absorber relaxation times", *Appl. Phys. Lett.*, vol. 70, pp. 1938-1940, 1997.
135 J. N. Milgram, *Picosecond Pulse Generation Using Mode-locked Diode Lasers and Semiconductor Optical Amplifiers*, Masters thesis, McMaster University, 2002.
136 J. N. Milgram, M. J. Brennan, H. F. Tiedje and H. K. Haugen, "Picosecond pulses from mode-locked quantum well semiconductor lasers", *OPTO Canada: SPIE Regional Meeting on Optoelectronics, Photonics and Imaging*, SPIE vol. TD01, pp. 21-23, 2002.
137 M. J. Brennan, J. Milgram, A. Budz, P. Mascher and H. Haugen, "Generation and amplification of wavelength tunable short optical pulses from asymmetric quantum well semiconductor devices", *Conference for Lasers and Electro-Optics*, June 2003, paper #CThM10.
138 A. J. Budz, M. J. Brennan and H. K. Haugen, "Generation and amplification of ultra-short optical pulses from a mode-locked long-wavelength (1075 nm – 1085 nm) InGaAs/GaAs quantum well laser", *Conference for Lasers and Electro-Optics*, accepted for presentation May 2004.
139 M. J. Brennan, A. J. Budz, B. J. Robinson, P. Mascher, and H. K. Haugen, "Ultrashort optical pulse generation with a mode-locked long wavelength (1075 nm – 1085 nm) InGaAs/GaAs semiconductor laser", *submitted for publication to IEEE Photon. Tech. Lett.*
140 D. J. Derickson, P. A. Morton, and J. E. Bowers, "Comparison of timing jitter in external and monolithic cavity mode-locked semiconductor lasers", *Appl. Phys. Lett.*, vol. 59, pp. 3372-3374, 1991.
141 D. J. Derickson, R. J. Helkey, A. Mar, J. R. Karin, J. E. Bowers and R. L. Thornton, "Suppression of multiple pulse formation in external-cavity mode-locked semiconductor lasers using intrawaveguide saturable absorbers", *IEEE Photon. Tech. Lett.*, vol. 4, pp. 333-335, 1992.
142 K. Smith and J. K. Lucek, "All-optical clock recovery using a mode-locked laser", *Electron. Lett.*, vol. 28, pp. 1814-1816, 1992.

143 P. E. Barnsley, H. J. Wickes, G. E. Wickens, and D. Spirit, "All-optical clock recovery from 5 Gb/s RZ data using a self-pulsating 1.56 μm laser diode", *IEEE Photon. Tech. Lett.*, pp. 942-945, 1991.
144 D. J. Jones, K. W. Holman, M. Notcutt, J. Ye, J. Chandalia, L. A. Jiang, E. P. Ippen and H. Yokoyama, "Ultralow-jitter, 1550-nm mode-locked semiconductor laser synchronized to a visible optical frequency standard", *Opt. Lett.*, vol. 28, pp. 813-815, 2003.
145 M. J. Brennan, H. F. Tiedje and H. K. Haugen, "Passively modelocked semiconductor laser synchronisation and pulse cross-correlation with Ti : sapphire laser", *Electron. Lett.*, vol. 38, pp. 713-714, 2002.
146 W. L. Gans, "The measurement and deconvolution of time jitter in equivalent-time waveform samplers", IEEE Trans. Instrum. Meas., vol. 32, pp. 126-133, 1983.
147 D. von der Linde, "Characterization of the noise in continuously operating mode-locked lasers", *Appl. Phys. B.*, vol. 39, pp. 201-217, 1986.
148 P. Langlois, D. Gay, N. McCarthy and M. Piché, "Noise reduction in a mode-locked semiconductor laser by coherent photon seeding", *Opt. Lett.*, vol. 23, pp. 114-116, 1998.
149 H. Tsuchida, "Pulse timing-jitter reduction by incoherent addition", *Opt. Lett.*, vol. 28, pp. 474-476, 2003.
150 J. B. Georges, L. Buckman, D. Vassilovski, J. Park, M.-H. Kiang, O. Solgaard and K. L. Lau, "Stable picosecond pulse generation at 46GHz by modelocking of a semiconductor laser operating in an optoelectronic phaselocked loop", *Electron. Lett.*, vol. 30, pp. 69-71, 1994.
151 S. Arahira, S. Kutsuzawa, and Y. Ogawa, "Extreme timing jitter reduction of a passively mode-locked laser diode by optical pulse injection", *IEEE J. Quantum. Electron.*, vol. 35, pp. 1805-1811, 1999.
152 S. Arahira, Y. Katoh and Y. Ogawa, "Generation and stabilization of ultrafast optical pulse trains with monolithic mode-locked laser diodes", *Optical and Quantum Electronics,* vol. 33, pp. 691-707, 2001.
153 R. W. Gerchberg and W. O. Saxton, "A practical algorithm for the determination of phase from image and diffraction plane pictures", *Optik,* vol. 35, pp. 237-246, 1972.
154 R. A. Gonsalves, "Phase retrieval from modulus data", *J. Opt. Soc. Am.*, vol. 66, pp. 961-963, 1976.
155 V. B. Khalfin, J. M. Arnold and J. H. Marsh, "A theoretical model of synchronization of a mode-locked semiconductor laser with an external pulse stream", *IEEE J. Sel. Topics Quantum. Electron.*, vol. 1, pp. 523-527, 1995.
156 G. P. Agrawal and N. A. Olsson, "Self-phase modulation and spectral broadening of optical pulses in semiconductor laser amplifiers", *IEEE J. Quantum. Electron.*, vol. 25, pp. 2297-2306, 1989.
157 G. P. Agrawal, "Effect of Gain Dispersion on Ultrashort Pulse Amplification in Semiconductor Laser Amplifiers", *IEEE J. Quantum. Electron.*, vol. 27, pp. 1843-1849, 1991.
158 M. Hofmann, M. Kock, H.-J. Heinrich, G. Weiser, J. Feldmann, W. Elsaber, E. O. Gobel, W. W. Chow and S. W. Koch, "Temporal and spectra gain dynamics in an actively modelocked semiconductor laser", *IEE Proc.-Optoelectron.*, vol. 141, pp. 127-132, 1994.
159 X. Wang, H. Yokoyama and T. Shimizu, "Synchronized Harmonic Frequency Mode-Locking with laser diodes through optical pulse train injection", *IEEE Photon. Tech. Lett.*, vol. 8, pp. 617-619, 1996.
160 H. Kurita, T. Shimizu and H. Yokoyama, "Experimental investigations of harmonic synchronization conditions and mechanisms of mode-locked laser diodes induced by optical-pulse injection", *IEEE J. Sel. Topics Quantum. Electron.*, vol. 2, pp. 508-513, 1996.
161 B. Lakshmi, D. T. Cassidy, B. J. Robinson, "Quantum-well strain and thickness characterization by degree of polarization", *J. Appl. Phys.*, vol. 79, pp. 7640-7645, 1996.
162 S. Gee, G. A. Alphonse, J. C. Connolly, C. Barty, P. J. Delfyett , "Ultrashort pulse generation by intracavity spectral shaping and phase compensation of external-cavity modelocked semiconductor lasers", *IEEE J. Quantum. Electron.*, vol. 36, pp. 1035-1040, 2000.
163 B. Resan, L. Archundia, and P. J. Delfyett, "Dispersion-managed semiconductor mode-locked ring laser", *Opt. Lett.*, vol. 28, pp. 1371-1373, 2003.

164 R. Trebino, D. J. Kane, "Using phase retrieval to measure the intensity and phase of ultrashort pulses: frequency-resolved optical gating", *J. Opt. Soc. Am. A*, vol. 10, pp. 1101-1111, 1993.
165 P. J. Delfyett, H. Shi, S. Gee, I. Nitta, J. C. Connolly, G. A. Alphonse, "Joint time-frequency measurements of mode-locked semiconductor diode lasers and dynamics using frequency-resolved optical gating", *IEEE J. Quantum. Electron.*, vol. 35, pp. 487-500, 1999.
166 Budz, A. J., private communication